OFFICE OF
RIVER PROTECTION
United States Department of Energy

DISTINCTIVE 3rd Annual Meeting
6 April, 2017 York, U.K.

Hanford; The Creation and Remediation of the Legacy

ORP-60691

Presented by: Albert A. Kruger, Glass Scientist, US Department of Energy

Presentation Outline & Key Messages

- Background, Hanford Waste Generation
- Challenges and Approaches for Hanford Vitrification
- Advanced LAW glass formulations allow the additional flexibility to reconsider feed vectors to the WTP.
- Performance enhancements through improved glass formulations are essentially transparent to the engineered facility.
- Next Steps

Background

- **1943-1964: 149 single-shell tanks constructed**
  - 67 presumed to have leaked
- **1968-1986: 28 double-shell tanks constructed**
  - 1 leaking, waste contained within annulus

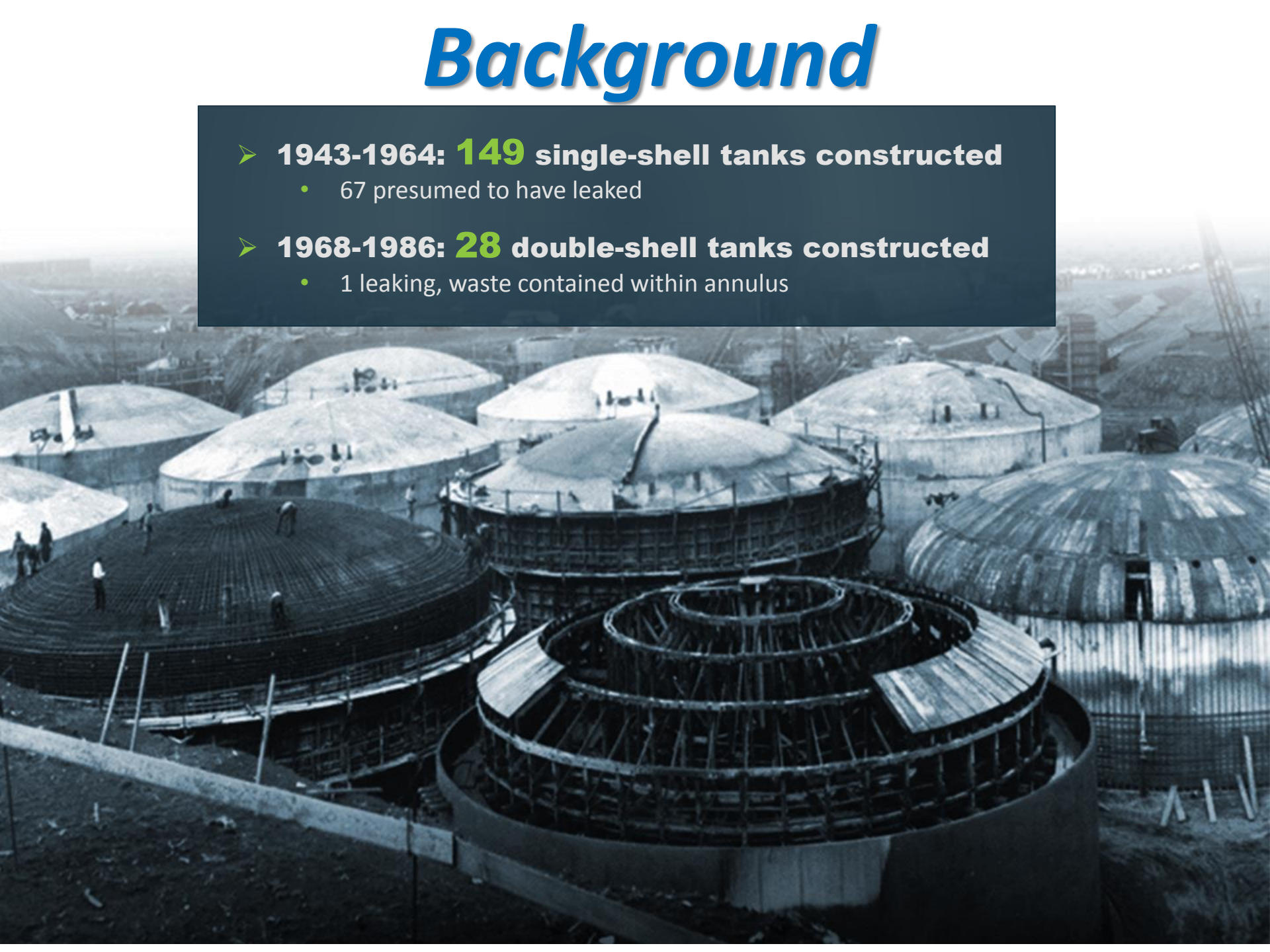

Historical Overview of the Hanford Site

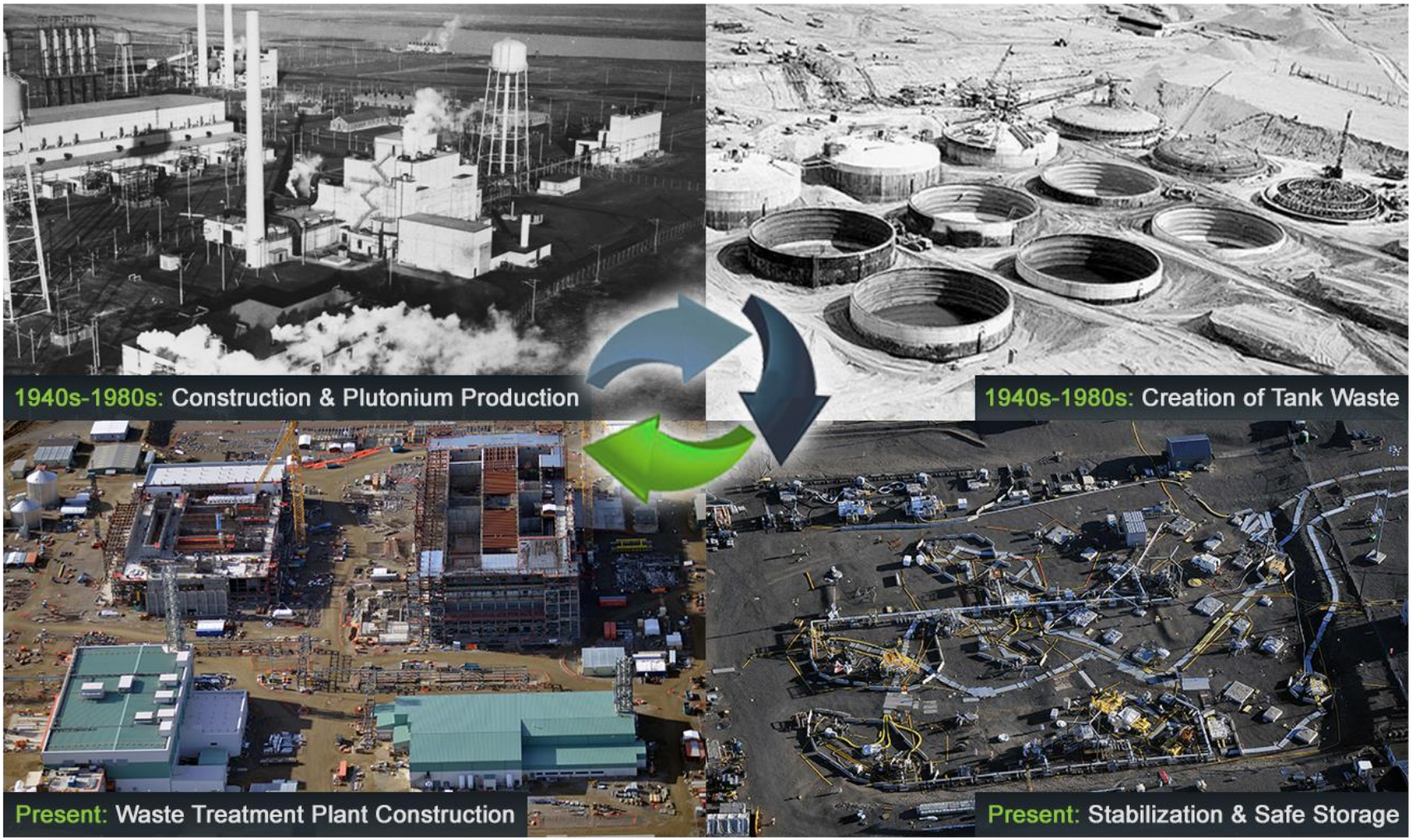

Generation of Hanford Tank Wastes

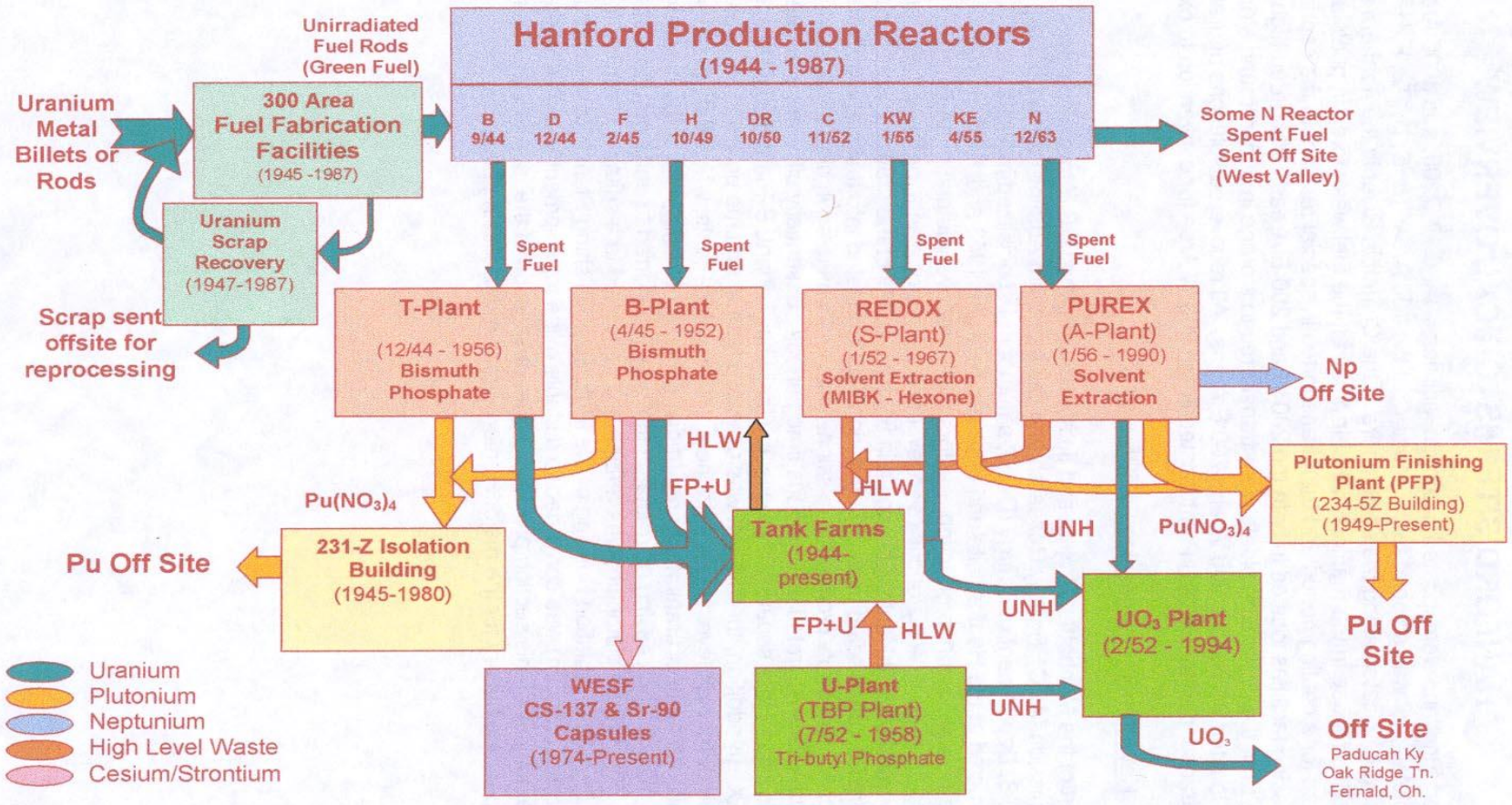

9 Reactors; 4 Fuel Reprocessing Flowsheets; 100,000 MT Fuel Processed

Chemical Processes and Resulting Waste

- Al Cladding Removal
  - rich in Na, **Al**, **Si**, OH
- Zr Cladding Removal
  - rich in **Zr**, **F**, Na
- Fuel Dissolution
  - rich in **NO_3**
- $BiPO_4$ carrier ppt
  - rich in **Bi**, **P**, **Ca**, Mn, La, F, Fe, K, U, **S, Cr**
- REDOX SX
  - rich in **Al**, **Cr**, **S**, F, **Mn**, Fe
- PUREX SX
  - rich in **Fe**, **S**
- THOREX SX
  - rich in **Th**, P
- U Recovery
  - rich in **FeCN**, K, **Ni**, CO_3
- Cs/Sr Recovery
  - rich in P, Ca, S, organics
- Waste Neutralization/ Corrosion Control
  - rich in **Na**, **OH**, **NO_2**, Cr
- Other
  - Atm. absorption (**CO_3**, -OH)
  - Solvent washes (Na, K, Mn, CO_3)
  - Chemical impurities (**Cl**)
  - Radiolysis (NO_2)
  - Dash-5 (**Pu**, F)
  - Diatomaceous earth (Si)
  - Corrosion (Fe, **Ni**, Cr)

Hanford History

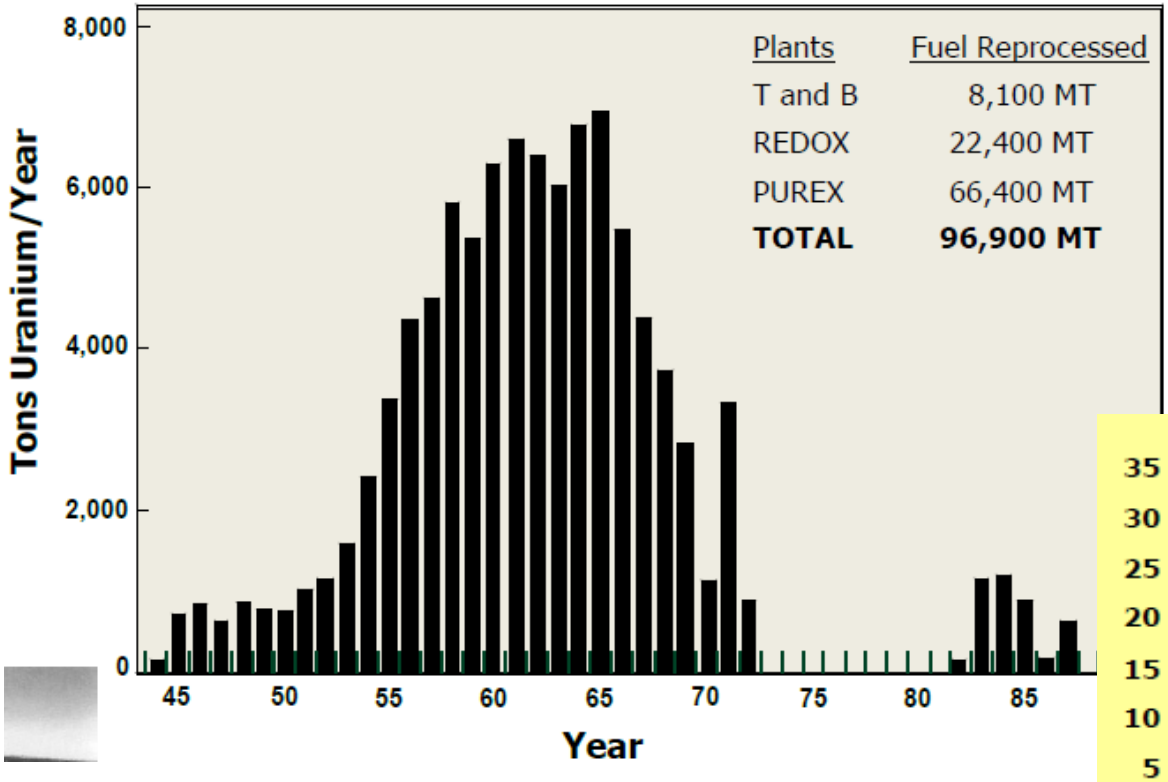

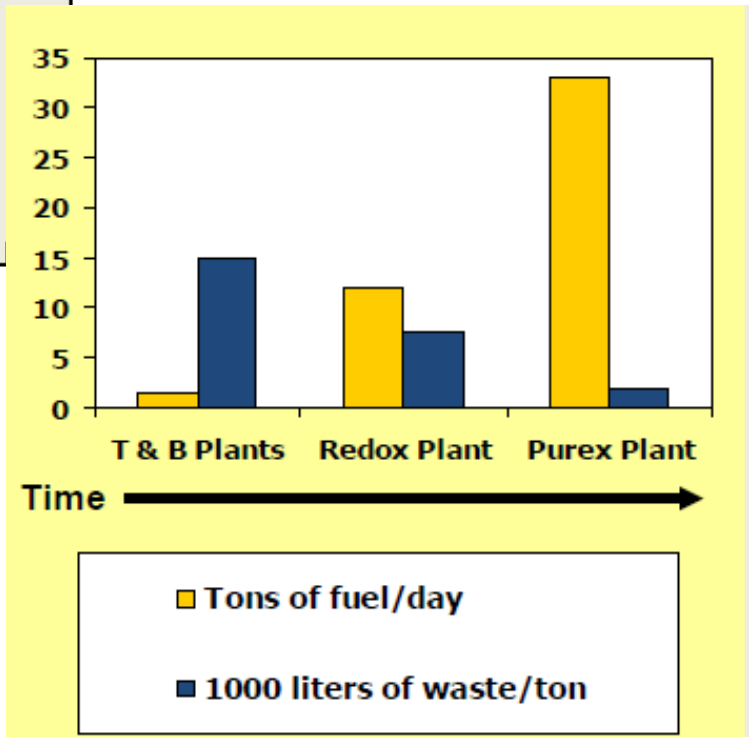

Hanford History, cont.

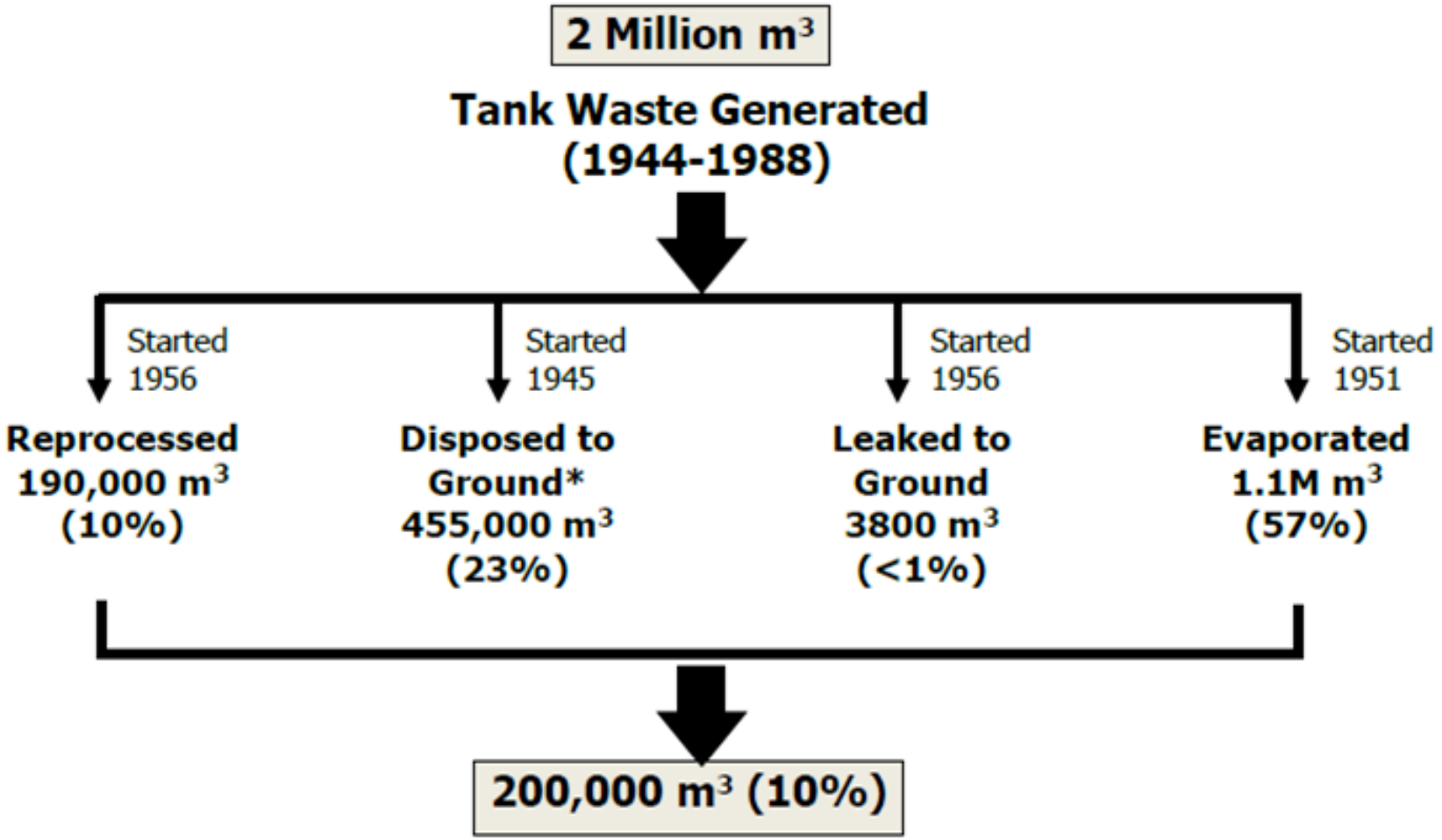

Overall Tank Composition

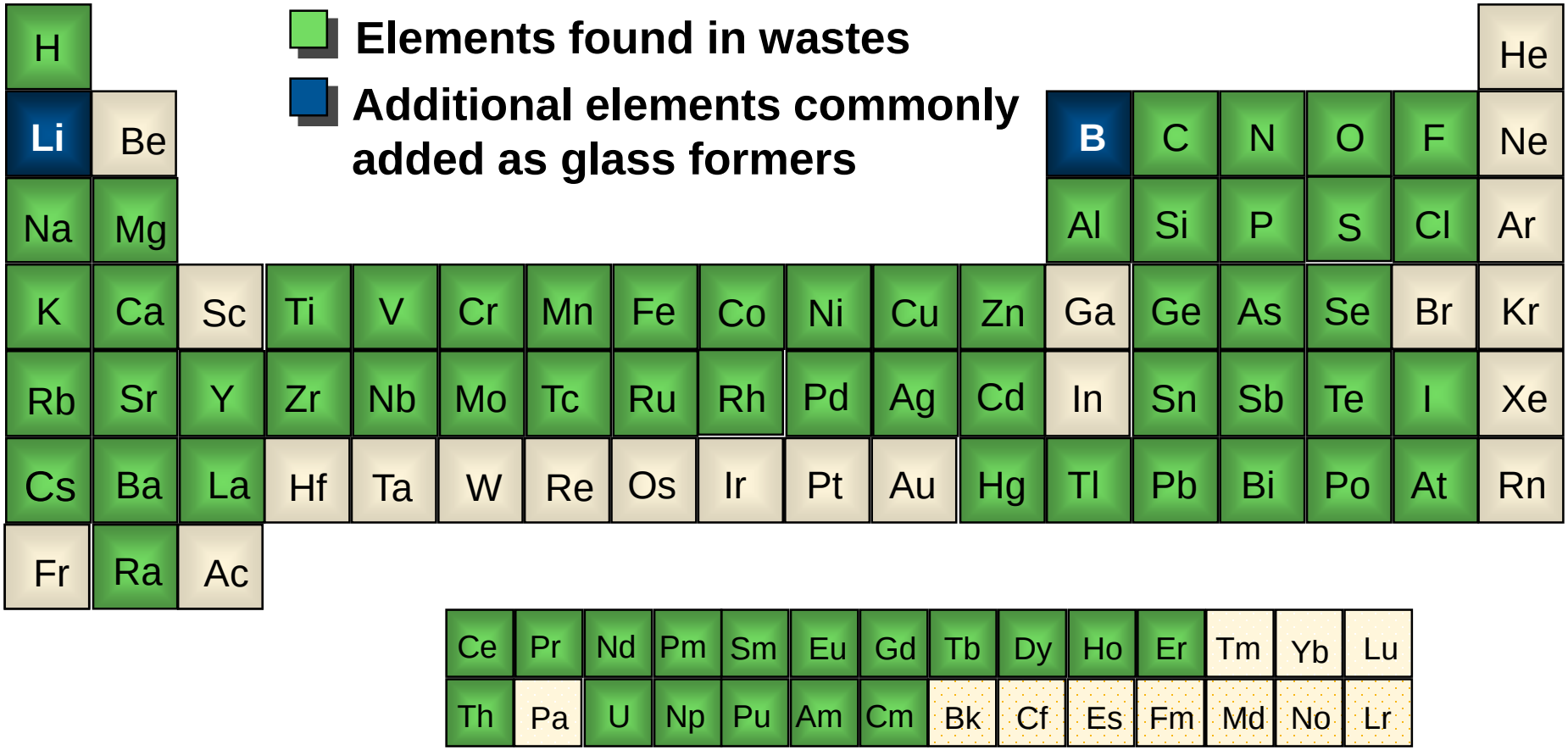

Hanford Tank Waste

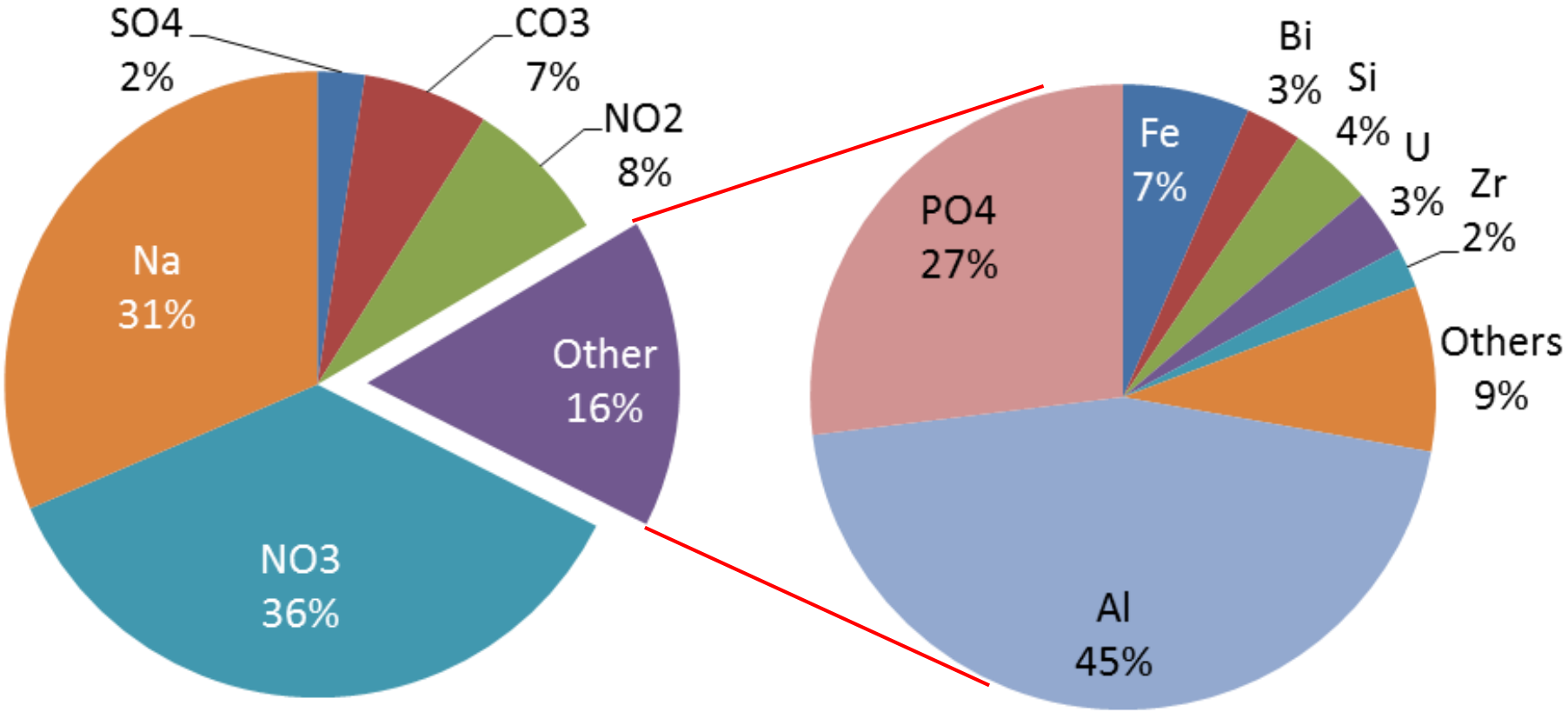

Best Basis Inventory, 2014

Chemical Inventory

BBI, Jan. 2008

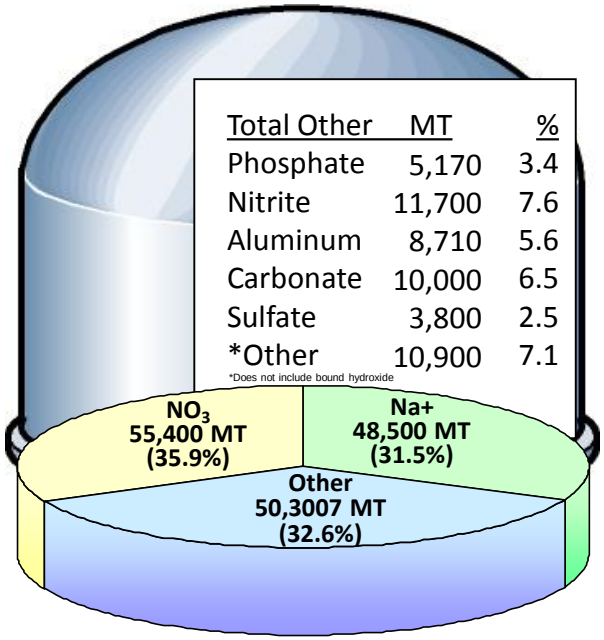

Total in All Tanks
154,000 Metric Tons

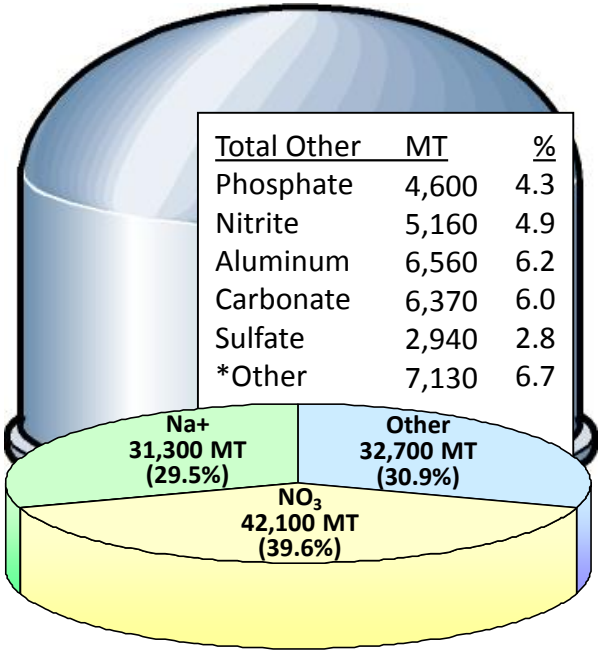

Single-Shell Tanks
106,000 Metric Tons

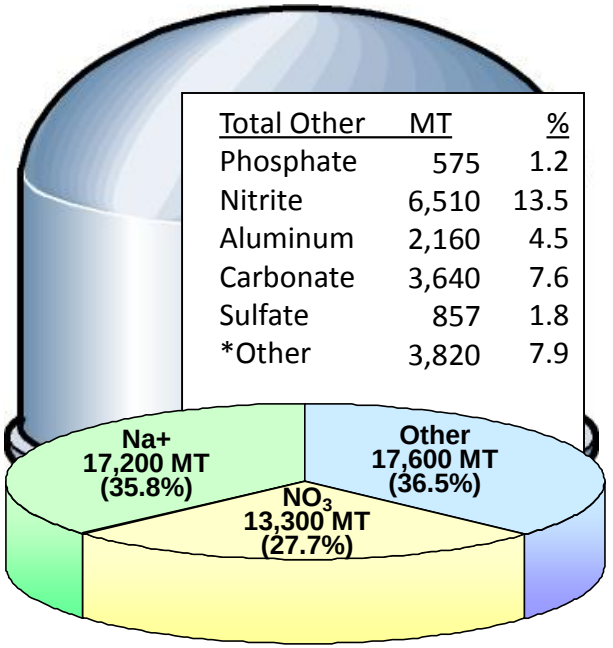

Double-Shell Tanks
48,100 Metric Tons

Herting and Barton 2008

Radionuclide Inventory

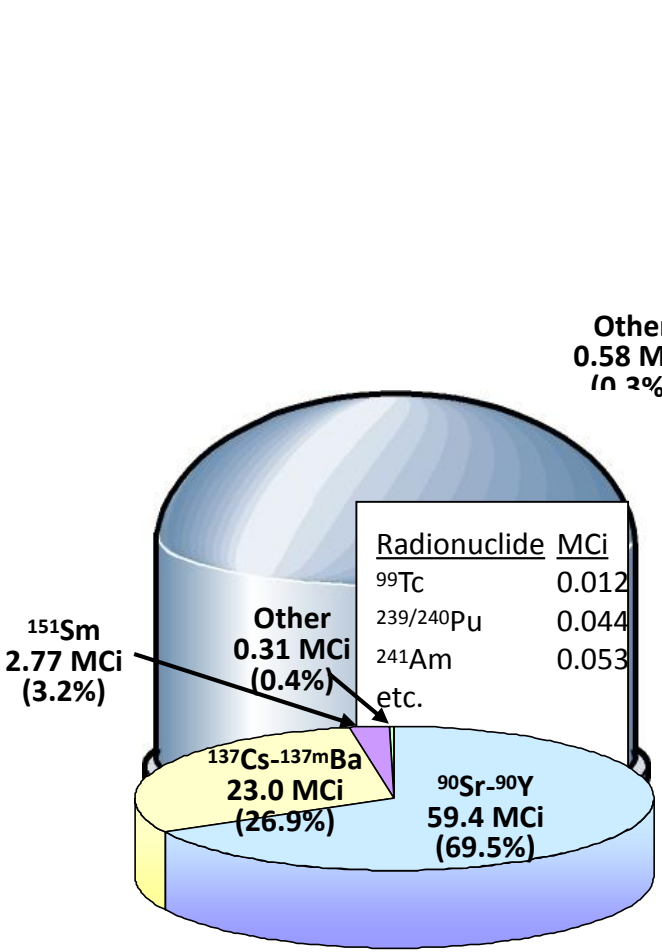

Single-Shell Tanks
85.5 MCi

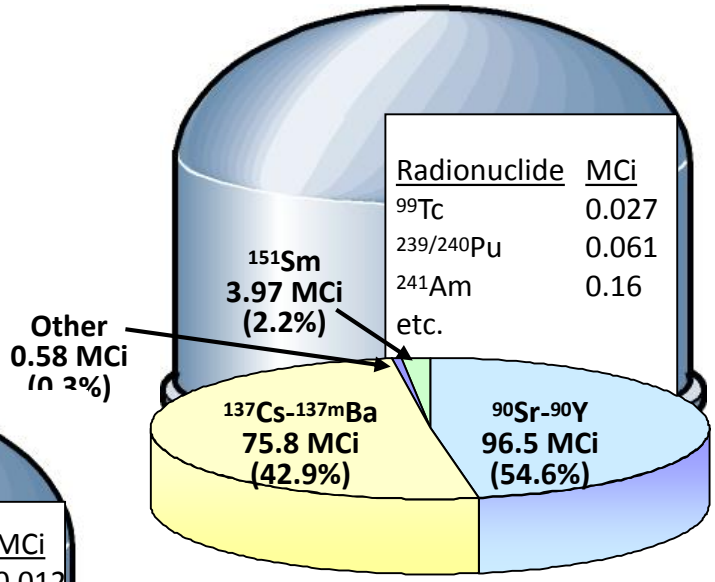

Total in All Tanks
177 MCi

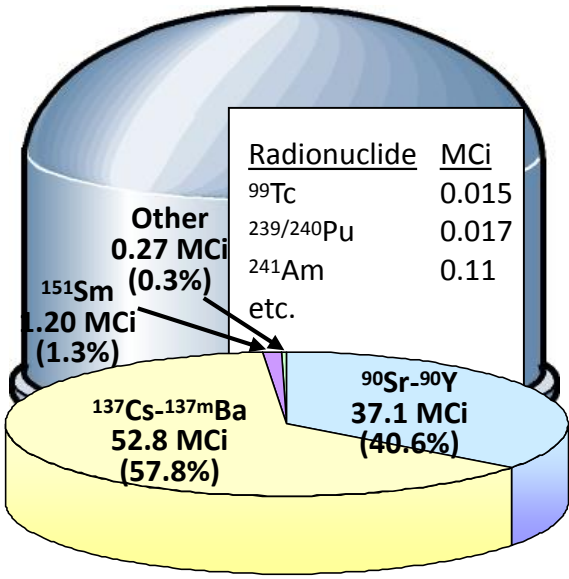

Double-Shell Tanks
91.3 MCi

Decayed to January 1, 2008

From: Herting and Barton 2008

Tank Waste Characterization/Feed Control to WTP

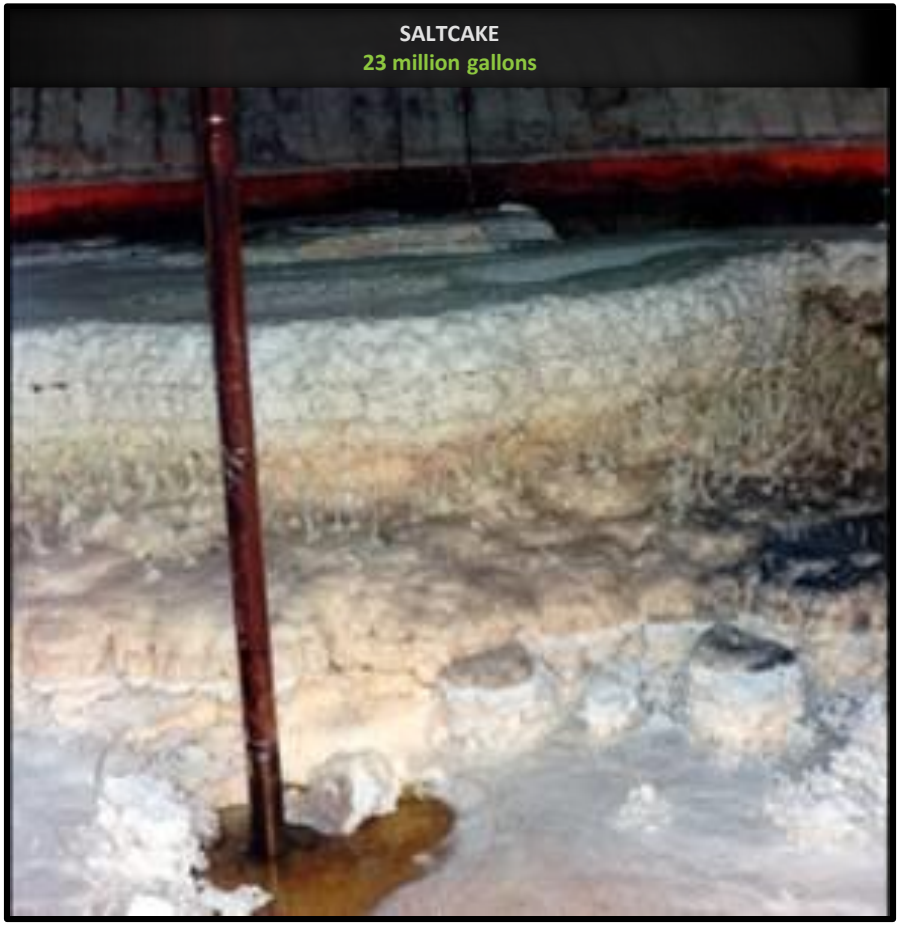

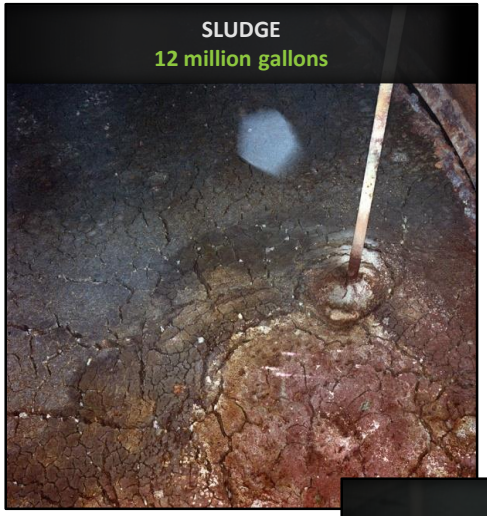

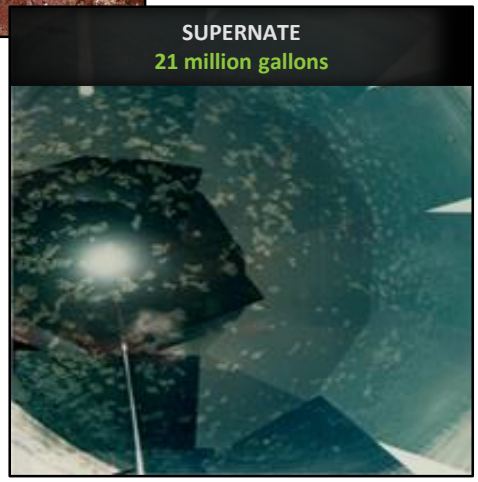

Saltcake

- Water-soluble
- White to black (usu. light brown)
- 10-50% H_2O
- High in Na, Al, anions, ^{137}Cs

Herting and Barton Tank Chemical and Radionuclide Inventories: Source, Occurrence, and Speciation, 2008

U-104

U-104

Sludge

- Wet mud
- Water-insoluble
- White to black (usu. dark brown)
- 50-80% H_2O
- High in Fe, Al, Si Mn, ^{90}Sr, TRU

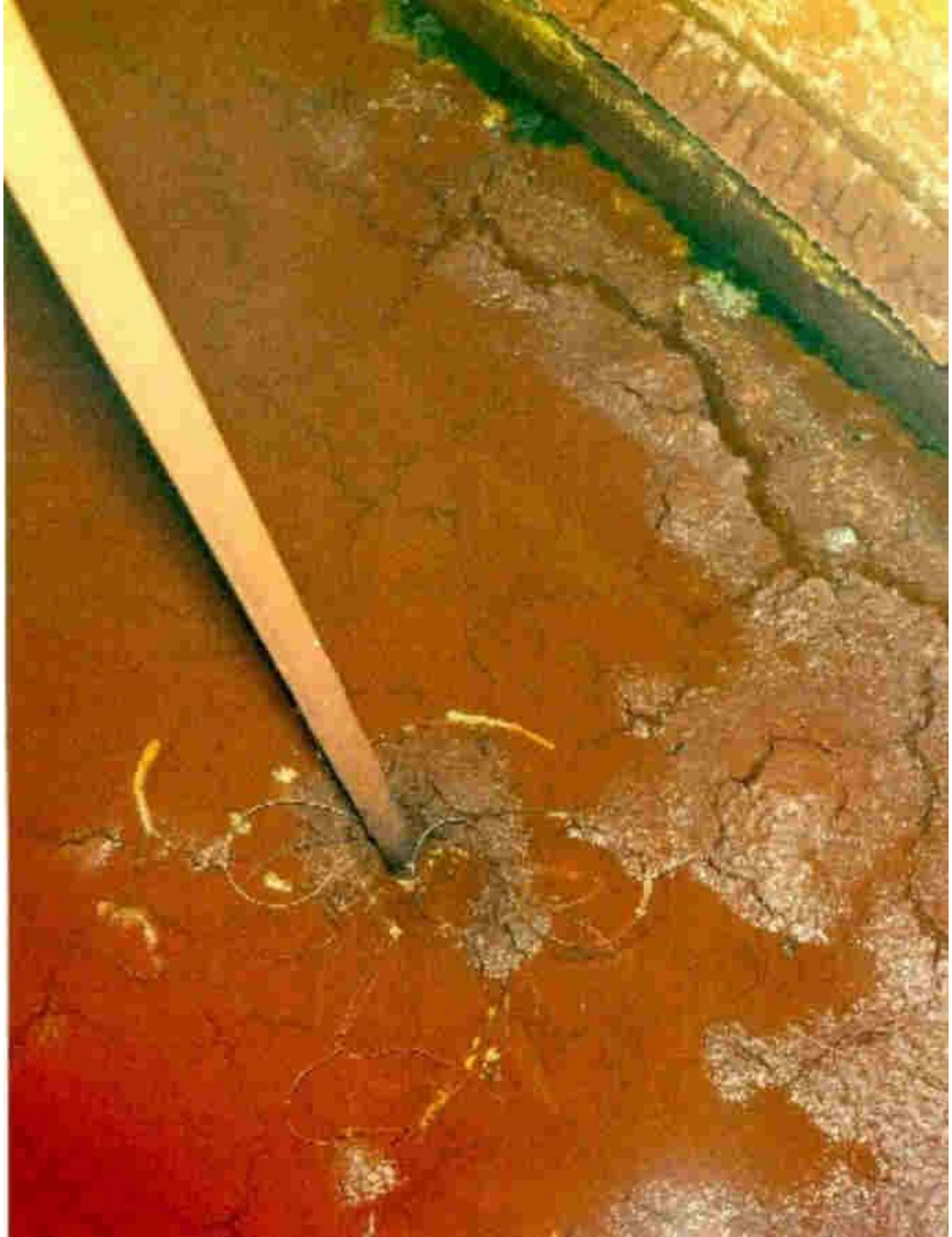

Herting and Barton 2008

Tank T-111

Tank S-112

Tank SX-114 1987 (8701219-

Supernatant Liquid

- Pale yellow or green to coffee-colored
  (usually bright yellow)
- 50 – 90% H_2O
- Na^+ 10 M
  NO_3^- 3 M
  NO_2^- 2 M
  OH^- 1 M
  $Al(OH)_4^-$ 0.5 M
  (all with wide variations)

Herting and Barton 2008

River Protection Project Flowsheet

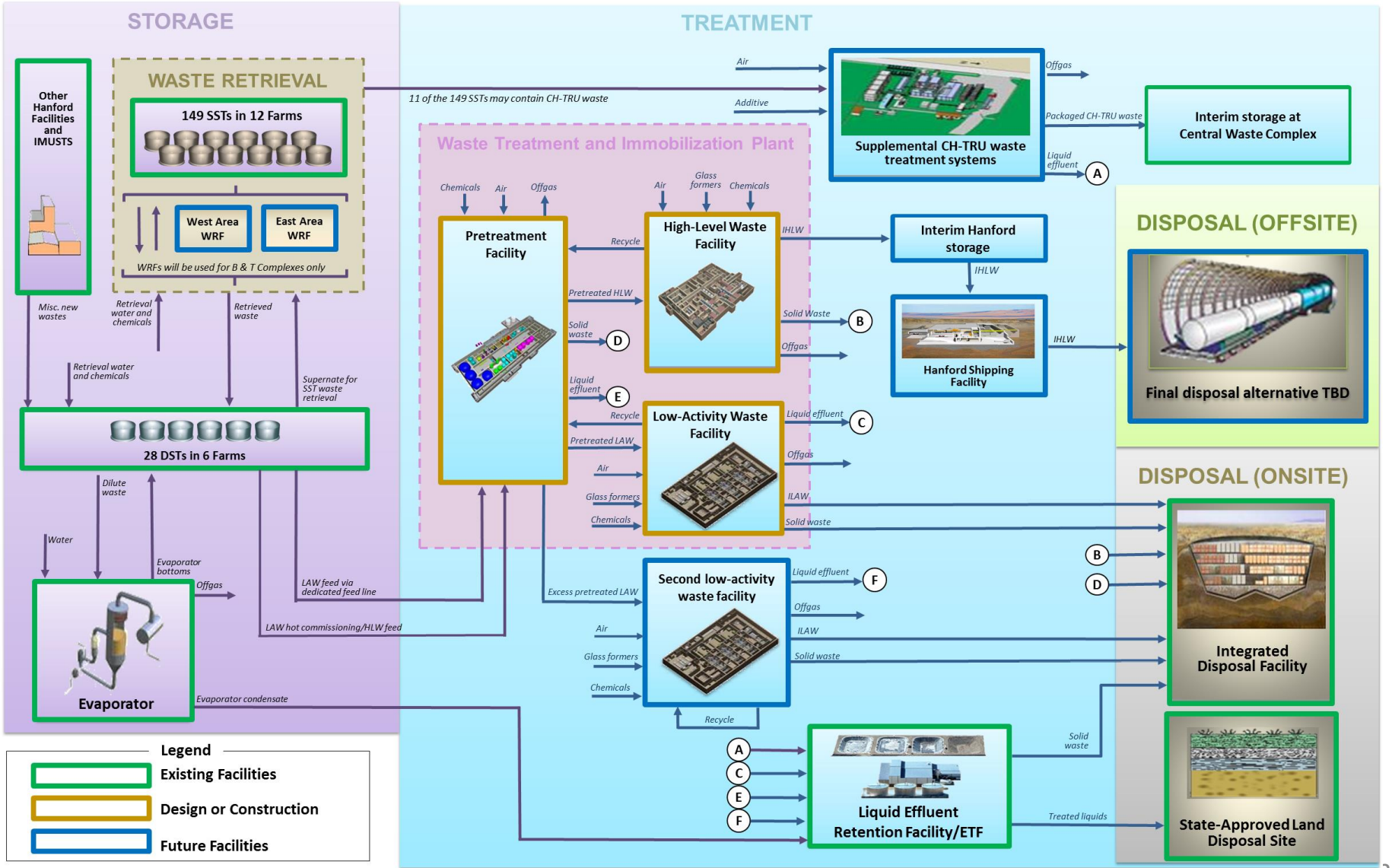

What Happens in the WTP?

- Waste is received from PT (or LAWPS & EMF)
- Waste is sampled & analyzed for chemical/rad composition
- Waste is mixed with glass forming chemicals (GFCs) to target a compliant and processable glass
- Melter feed is fed to the melter, melted, and cast into cans to solidify into alkali-alumino-borosilicate glass waste form
- Canisters/containers are stored/cooled, sealed, decontaminated, and prepared for shipment out of the facility
- Off-gas is treated to meet release requirements
- Liquid and solid secondary wastes are managed and prepared for shipment out of the facility

Waste Treatment and Immobilization Plant

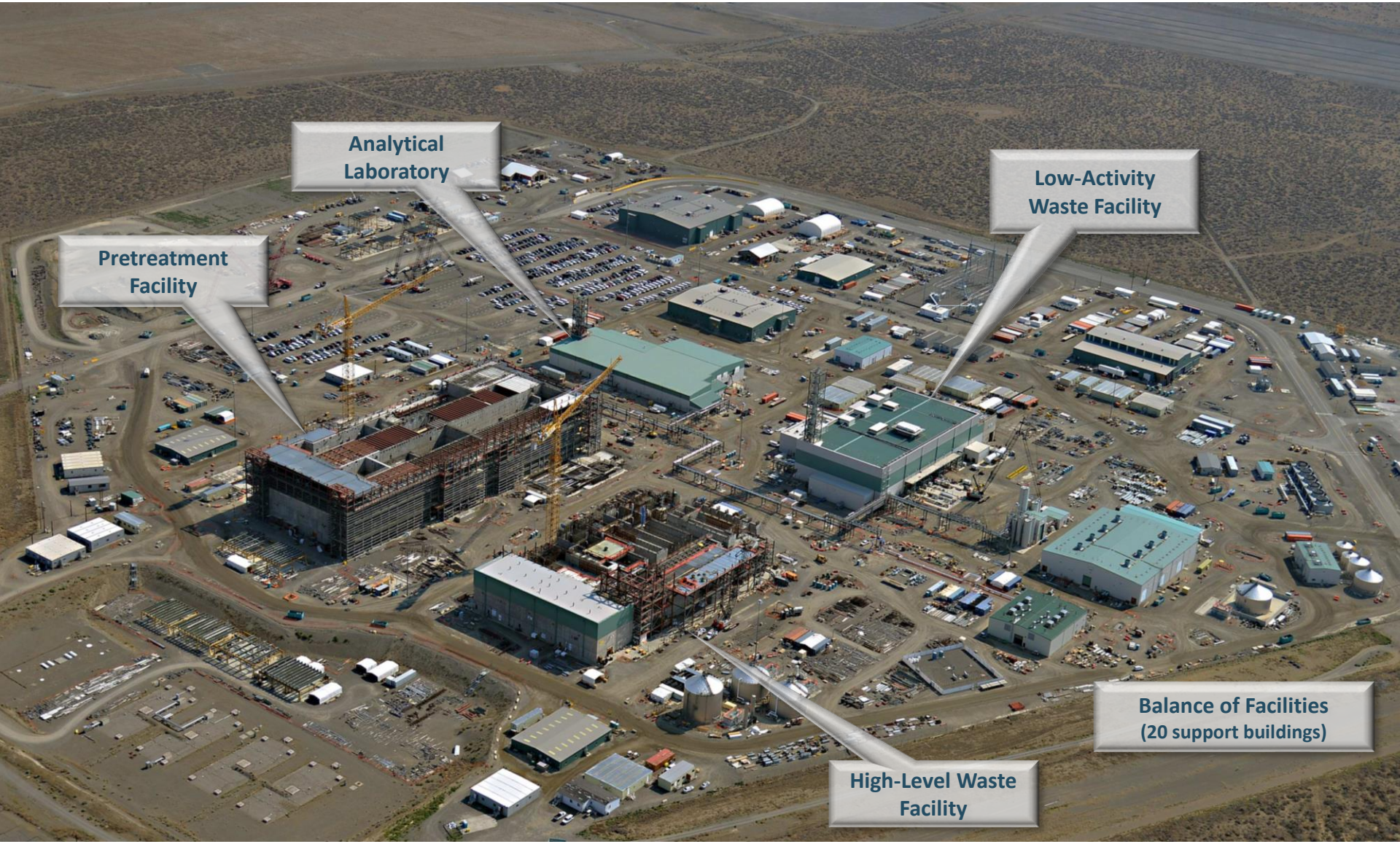

ORP Baseline Glass Formulation for HLW & LAW Treatment

- Current estimates (SP7: ORP-11242) project that ORP will produce 10,214 HLW canisters (30,845 MT glass). The *ca.* 79,056 MT of sodium (LAW processing basis) will produce 127,753 LAW containers (687,187 MT ILAW glass).
- The current glass formulation efforts have been conservative in terms of achievable waste loadings (WTP baseline).
- These formulations have been specified to ensure the glasses are homogenous, preclude secondary phases (sulfate-based salts or crystalline phases), are processable in joule-heated, ceramic-lined melters and meet WTP Contract terms.

Formulating Glass

$$g_i = Ww_i + (1-W)a_i$$

$$P = \widehat{P}_T(g_1, g_2, \ldots, gn)$$

For a given waste composition (w_i),
determine mineral addition (a_i),
to obtain glass composition (g_i),
with optimized properties (P),
and maximized waste loading (W)
The selection of properties to be optimized depends on melter technology and glass acceptability criteria

Process Optimization – HLW and LAW Vitrification Process Enhancements

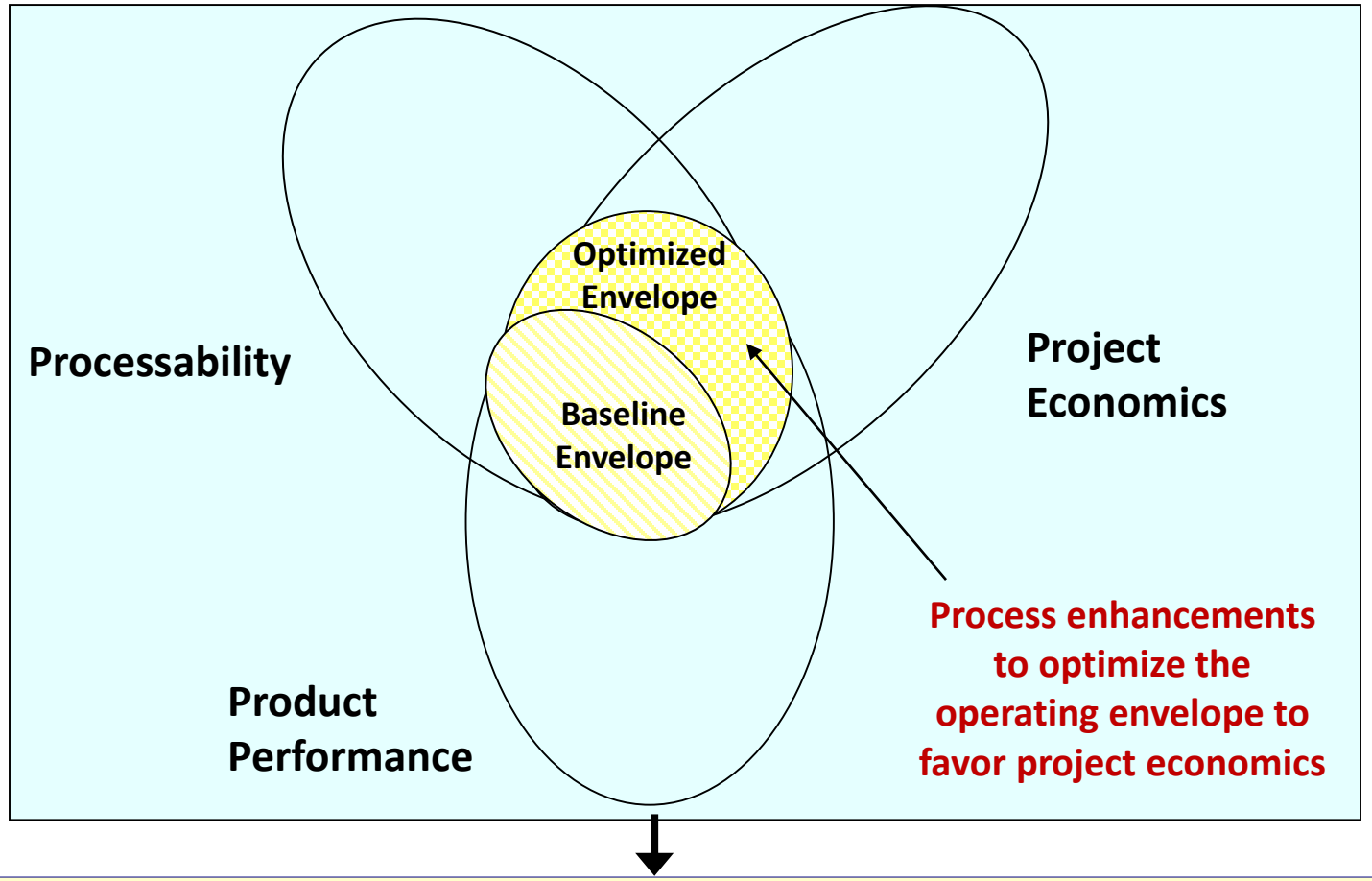

Integration of glass formulation with melter engineering is crucial

Vitrification

Heat transfer

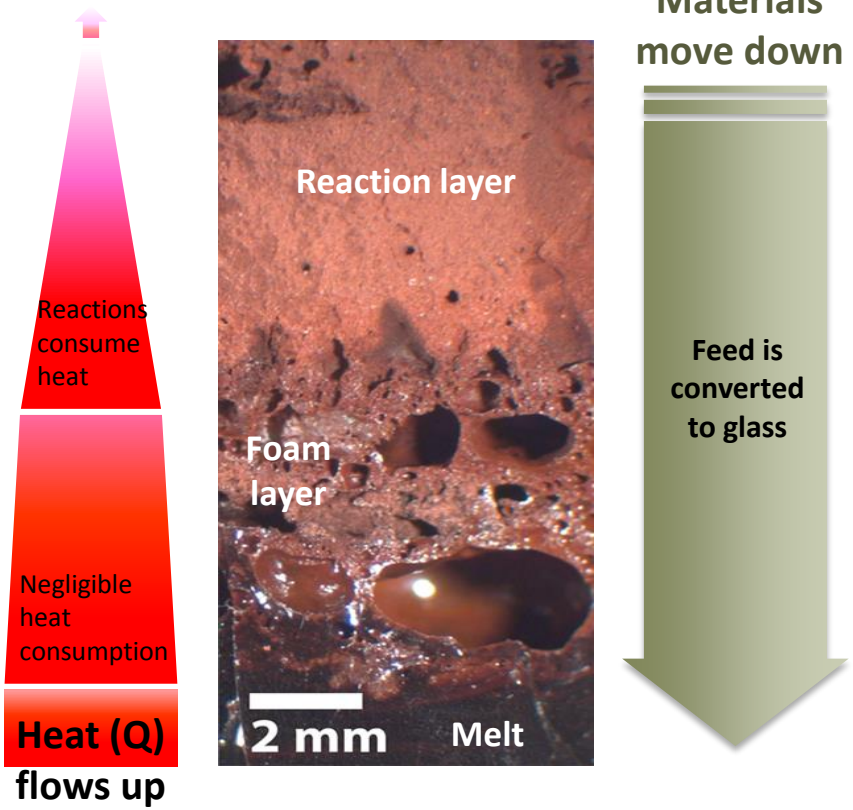

The feed-to-glass conversion heat is related to the rate of melting:

$$Q = (\Delta H + c_P \Delta T) j$$

Q is delivered through the cold-cap bottom and is transferred through the foam layer.

Q	conversion heat flux
ΔH	reaction heat
C_P	heat capacity
ΔT	cold cap temperature difference
j	melting rate

Enhanced heat flux by bubbling

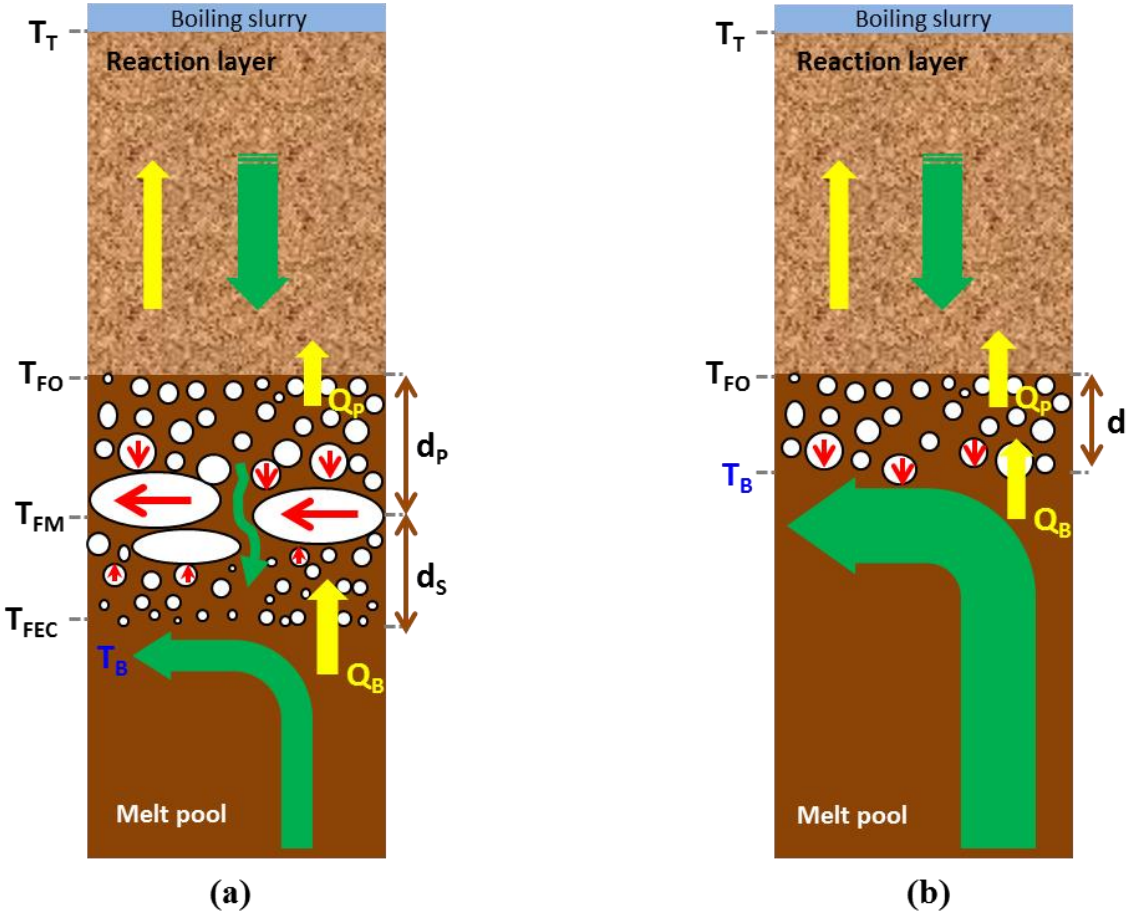

- Primary foam related to CO_2 gas goes down, grows, coalesces, and creates a cavity in the foam layer.
- Secondary foam related to O_2 gas goes up and accumulates under the cavity (or some foam maybe burst into the cavity) in the bottom of the cold cap.
- Gases in the cavity tends to move to the side of the cold cap and burst to atmosphere.

Melter Scale Comparison

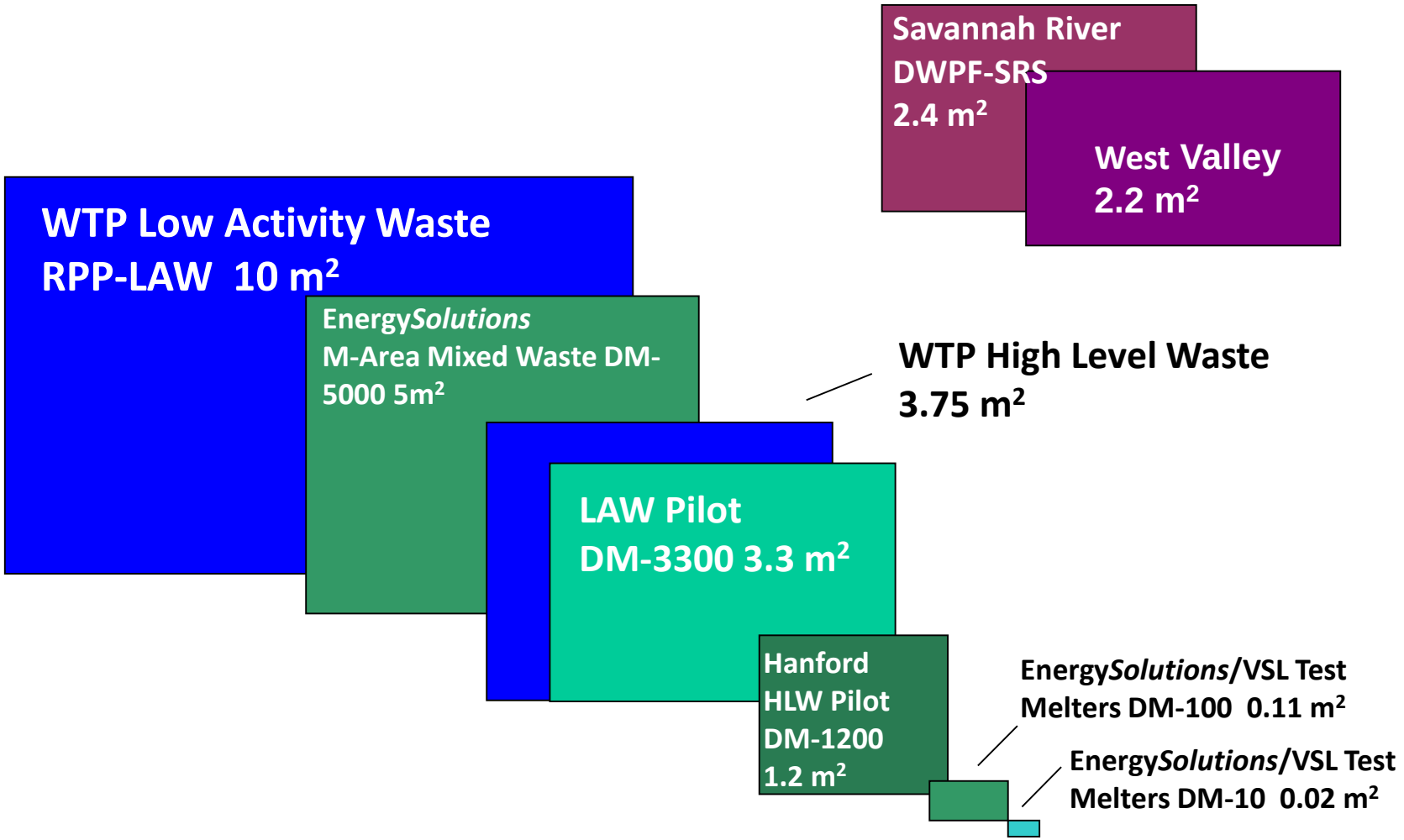

LAW Vitrification

Selected Pellet Pictures

AN-102

625°C

675°C

725°C

775°C

AZ-102

820°C

860°C

AN-102

AZ-102

LAW Glass Property Constraints

- Processing
  - AB constraints on rad: Cs-137 < 0.3 Ci/m^3(glass)
  - Viscosity: 20 to 80 P at 1150°C
  - Electrical Conductivity: 0.1 to 0.7 S/cm at 1100 to 1200°C
  - No salt accumulation on melt surface
  - Acceptable corrosion of glass contact materials
  - Process rate: >30 MTG/d instantaneous, > 70% TOE
- Product Acceptance
  - Contract waste loading limit: waste Na_2O >14, 3, 10 wt%
  - Rad content: <Class C, <20 Ci/m^3 Sr-90, <3 Ci/m^3 Cs-137
  - Surface dose: < 500 mrem/h
  - Durability: < 2 g/m^2 PCT, <50 g/m^2/d VHT (predictable)
  - Phase stability: avoid phase changes or understand impacts on durability/regulatory compliance

Sulfur and Alkali Limits

- The factors limiting LAW glasses are:
  - chemical durability as measured by PCT and VHT for high Alk:SO_3 wastes
  - salt accumulation for low Alk:SO_3 wastes and high halide wastes

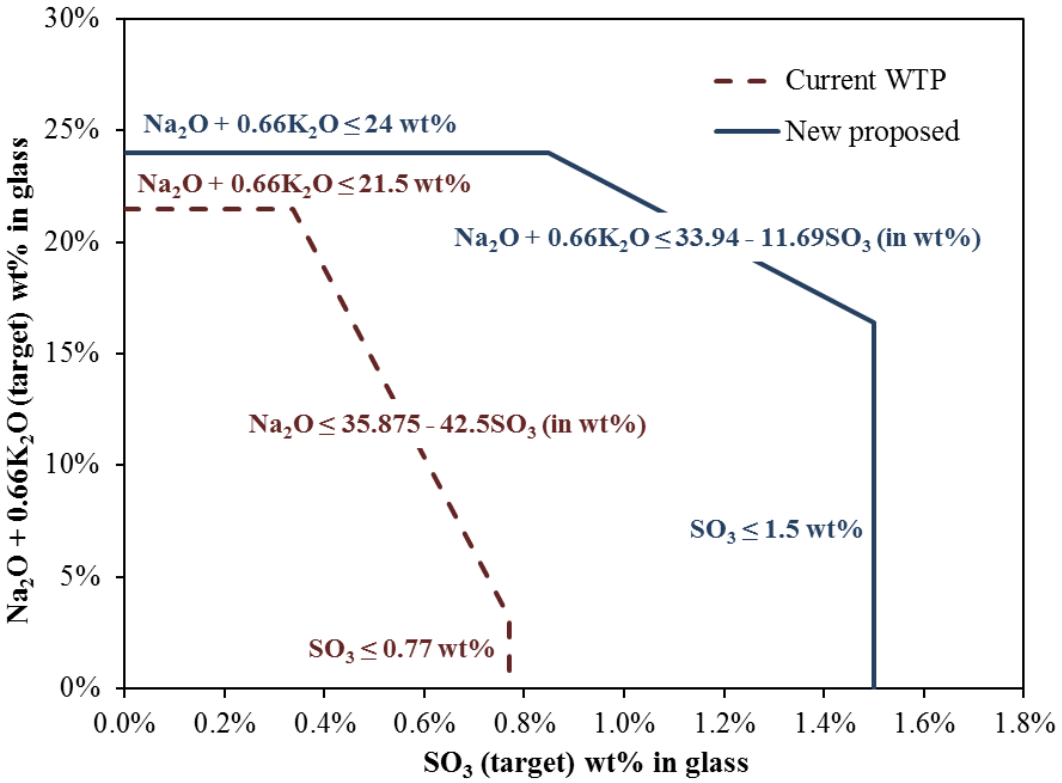

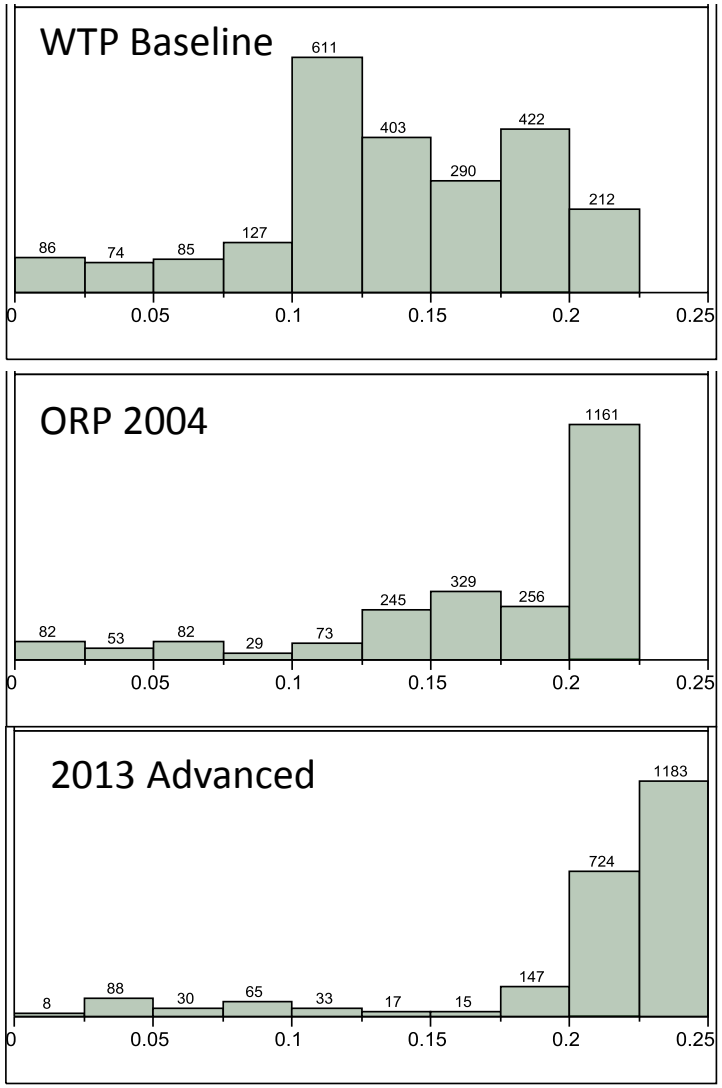

Composition Effects

Oxide	Al_2O_3	B_2O_3	CaO	Cr_2O_3	Fe_2O_3	K_2O	Li_2O	MgO	Na_2O	SiO_2	ZnO	ZrO_2	Other
Viscosity	↑	↓	↓	↔	↔	↓	↓	↓	↓	↑	↔	↑	
EC	↔	↔	↔	↔	↔	↑	↑	↔	↑	↓	↔	↔	
T_L, C_T (sp)	↑	↓	↓	↑	↑	↓	↓	↔	↓	↓	↑	↑	NiO, MnO↑
PCT	↓↑	↓↑	↔	↔	↔	↑	↑	↑	↑	↓	↔	↓	
VHT	↓↑	↓↔	↔	↔	↔	↑	↑	↔↑	↑	↓	↔	↓	
Nepheline	↑	↓	↑	↔	↔	↑	↑	↔	↑	↓	↔	↔	
Salt	↑	↓	↓	↑	↔	↓	↓	↔	↓	↑	↔	↔	SO_3, Cl ↑, V_2O_5↓
TCLP	↓	↑	↔	↔	↔	↑	↑	↔	↑	↓	↑	↓	MnO↑
Corrosion	↓	↔	↔	↓	↓	↑	↑	↔	↑	↓	↓	↓	NiO↓

↑ - Increase property
↓ - Decrease property
↔ - Small effect on property
multiple arrows are for non-linear effects, first is for lower concentrations

'Significant' Waste Constituents

- Na, S, K: base waste loading/formulation
- NO_3, NO_2, TOC: reductant addition
- Cl, Cr, P: salt formation rules (impacts waste loading)
- Al: Alumina addition requirements
- Any other element with >0.5 wt% in glass: reporting
- Tc-99, I-129: IDF reporting
- Cs-137, Sr-90, class-C limits, TRU, total β/γ: AB, waste classification, reporting

Selection of Feeds

Based on Re and ^{99m}Tc Retention Data from small-scale melter (DM10) Tests by Vitreous State Laboratory (VSL)

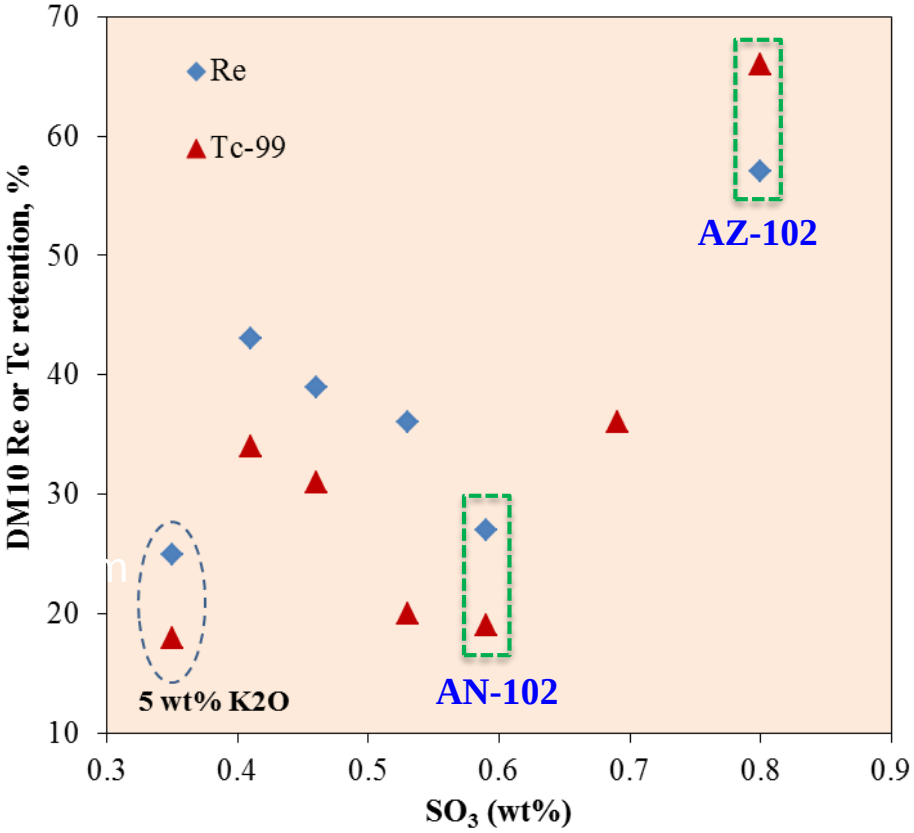

"$Na_2O + K_2O$" wt% versus SO_3 wt% for 7 representative LAW feeds (WTP LAW glass formulation rules)

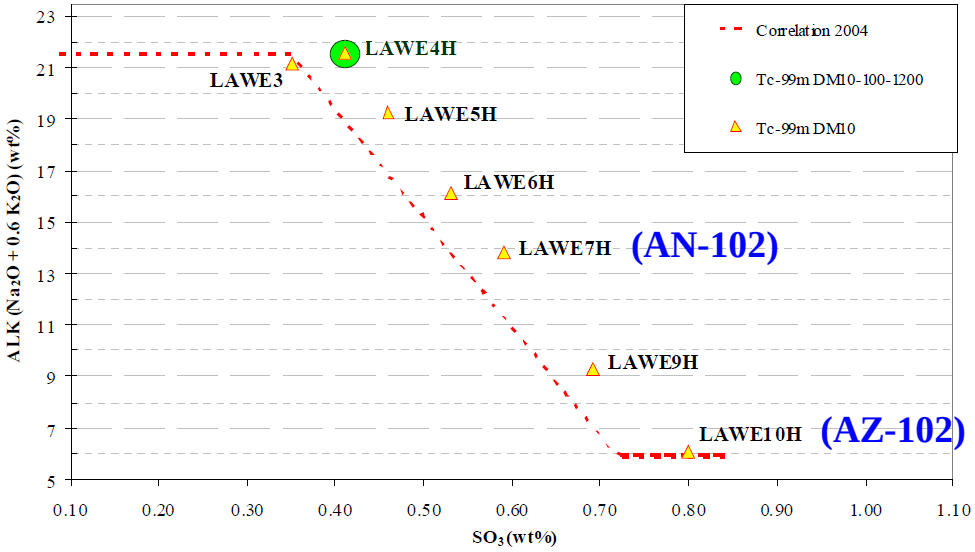

AN-102 and AZ-102 feeds with large difference in Re/Tc retention from DM10 tests were selected for initial set of crucible tests

- **AN-102: medium sulfur, high nitrates**
- **AZ-102: high sulfur, low nitrates**

Data and plot from VSL-11R2260-1, Rev 0

LAW Off-Gas Treatment

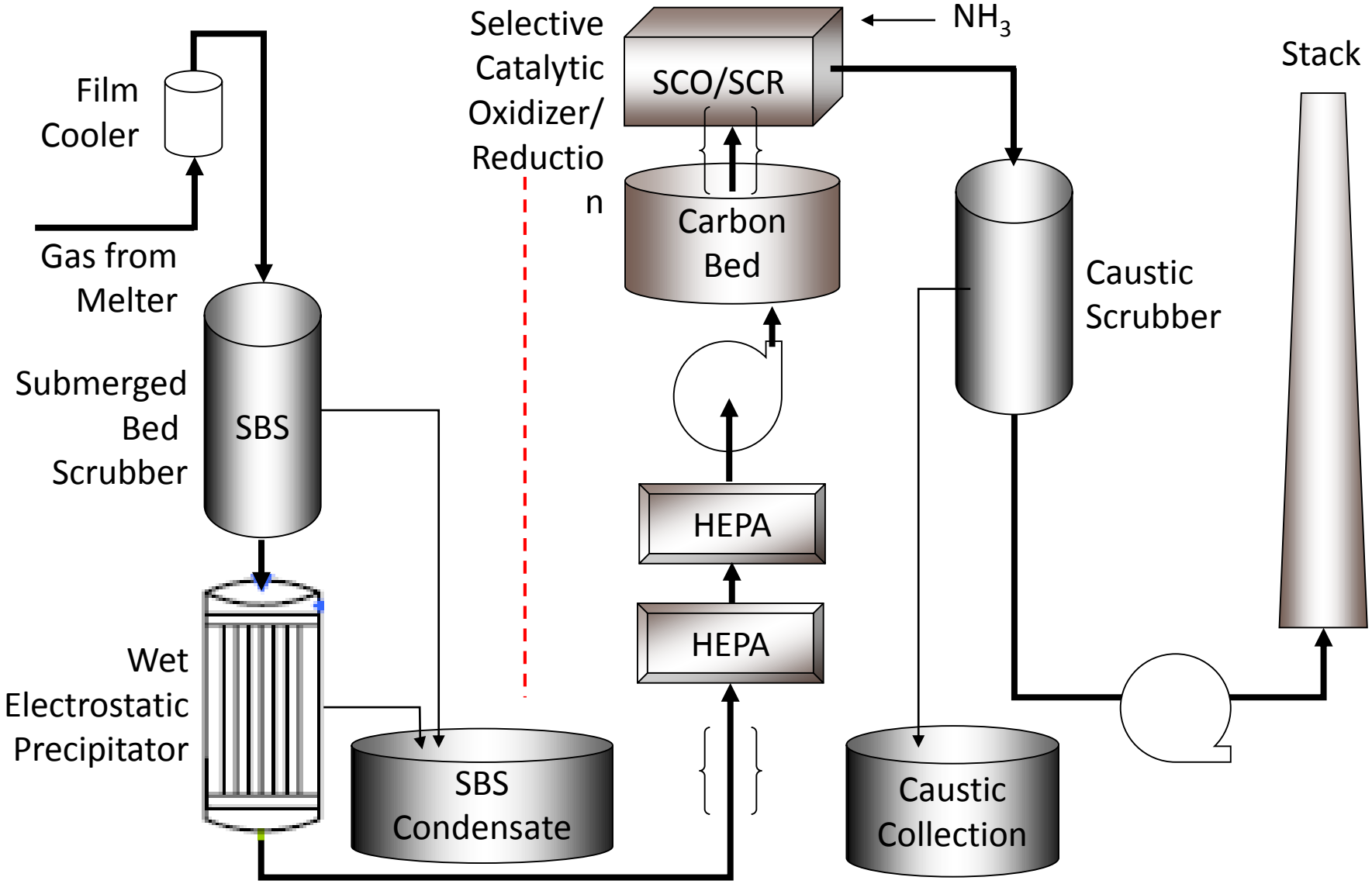

Kim and Vienna *Preliminary ILAW Formulation Algorithm Description*: 24590-LAW-RPT-RT-04-0003, Rev. 1, ORP-56321, 2012

HLW Vitrification

HLW Glass Property Constraints

- Processing
  - Viscosity: 20 to 80 P at 1150°C
  - Electrical Conductivity: 0.1 to 0.7 S/cm at 1100 to 1200°C
  - Acceptable crystal accumulation in the melter
  - No salt accumulation or phosphate scum on melt surface
  - Process rate: >7.5 MTG/d instantaneous, > 70% TOE
- Product Acceptance
  - Contract waste loading limit: Contract TS-1.1
  - Durability: PCT < DWPF EA glass (predictable)
  - Regulatory acceptability: CdO < 0.1 wt% or TCLP Cd < 0.48 mg/L and Tl_2O < 0.465 wt%
  - Phase stability: avoid phase changes or understand impacts on durability/regulatory compliance

Composition Effects

Oxide	Al_2O_3	B_2O_3	CaO	Cr_2O_3	Fe_2O_3	K_2O	Li_2O	MgO	Na_2O	SiO_2	ZnO	ZrO_2	Other
Viscosity	↑	↓	↓	↔	↔	↓	↓	↓	↓	↑	↔	↑	
EC	↔	↔	↔	↔	↔	↑	↑	↔	↑	↓	↔	↔	
T_L, C_T (sp)	↑	↓	↓	↑	↑	↓	↓	↔	↓	↓	↑	↑	NiO, MnO↑
PCT	↓↑	↓↑	↔	↔	↔	↑	↑	↑	↑	↓	↔	↓	
VHT	↓↑	↓↔	↔	↔	↔	↑	↑	↔↑	↑	↓	↔	↓	
Nepheline	↑	↓	↑	↔	↔	↑	↑	↔	↑	↓	↔	↔	
Salt	↑	↓	↓	↑	↔	↓	↓	↔	↓	↑	↔	↔	SO_3, Cl ↑, V_2O_5↓
TCLP	↓	↑	↔	↔	↔	↑	↑	↔	↑	↓	↑	↓	MnO↑
Corrosion	↓	↔	↔	↓	↓	↑	↑	↔	↑	↓	↓	↓	NiO↓

↑ - Increase property
↓ - Decrease property
↔ - Small effect on property
multiple arrows are for non-linear effects, first is for lower concentrations

Small-Scale Melt Rate Screening Results: ORP HLW Glasses with 24 wt% Al_2O_3

30 min

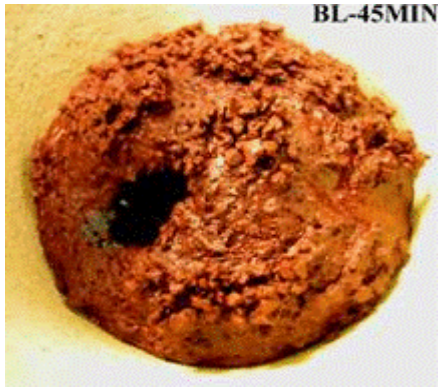

45 min

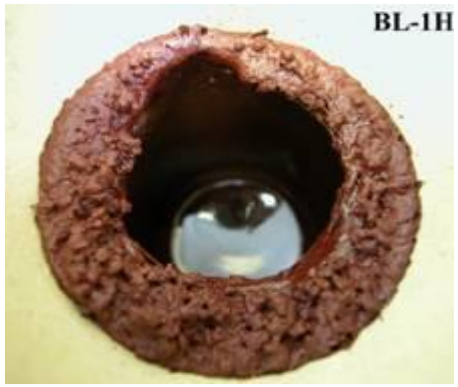

60 min

Initial Formulation

Reaction Time

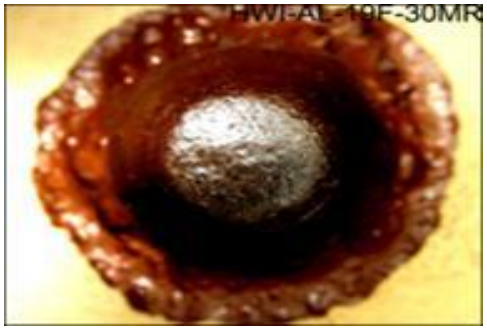

30 min

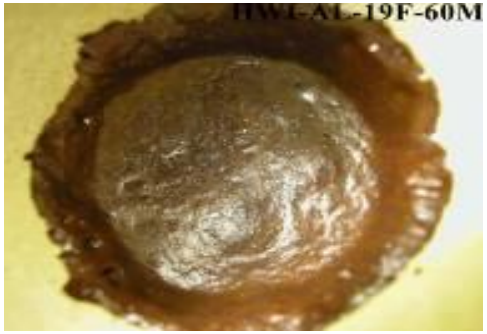

60 min

Improved Formulation

Improvements confirmed in one-third scale pilot melter tests

VSL-08R1360-1, Rev.0; VSL-10R1690-1, Rev. 0

EGA and O_2 partial pressure by RAPIDOX

The melt is highly oversaturated with oxygen. Such a high oversaturation is not likely to arise solely from the iron redox equilibrium, but also from the oxygen "stored" in the feed from earlier batch decomposition reactions (mostly nitrates).

Foaming Curve & Secondary Foam

- **Detected CO_2 in the foam layer as a residual gas from the feed reaction and involved in the primary foam.**
- **Detected O_2 gas was from iron redox reaction and involved in the secondary foam.**
- **Influence of Gibbsite, Boehmite and Corundum**

Foaming in High Bi-P HLW Glass Melts

Results were used to modify glass formulations to mitigate melt foaming

Melt Rate & Loading in High Fe Glasses

Improved formulations have been developed with both high melt rates and high waste loadings

Nepheline Precipitation

- Many attempts have been made to predict Nepheline ($NaAlSiO_4$) formation
  - the most successful was the Li et al. 1997[13] Nepheline discriminator:

$$ND = \frac{g_{SiO_2}}{g_{SiO_2} + g_{Na_2O} + g_{Al_2O_3}}$$

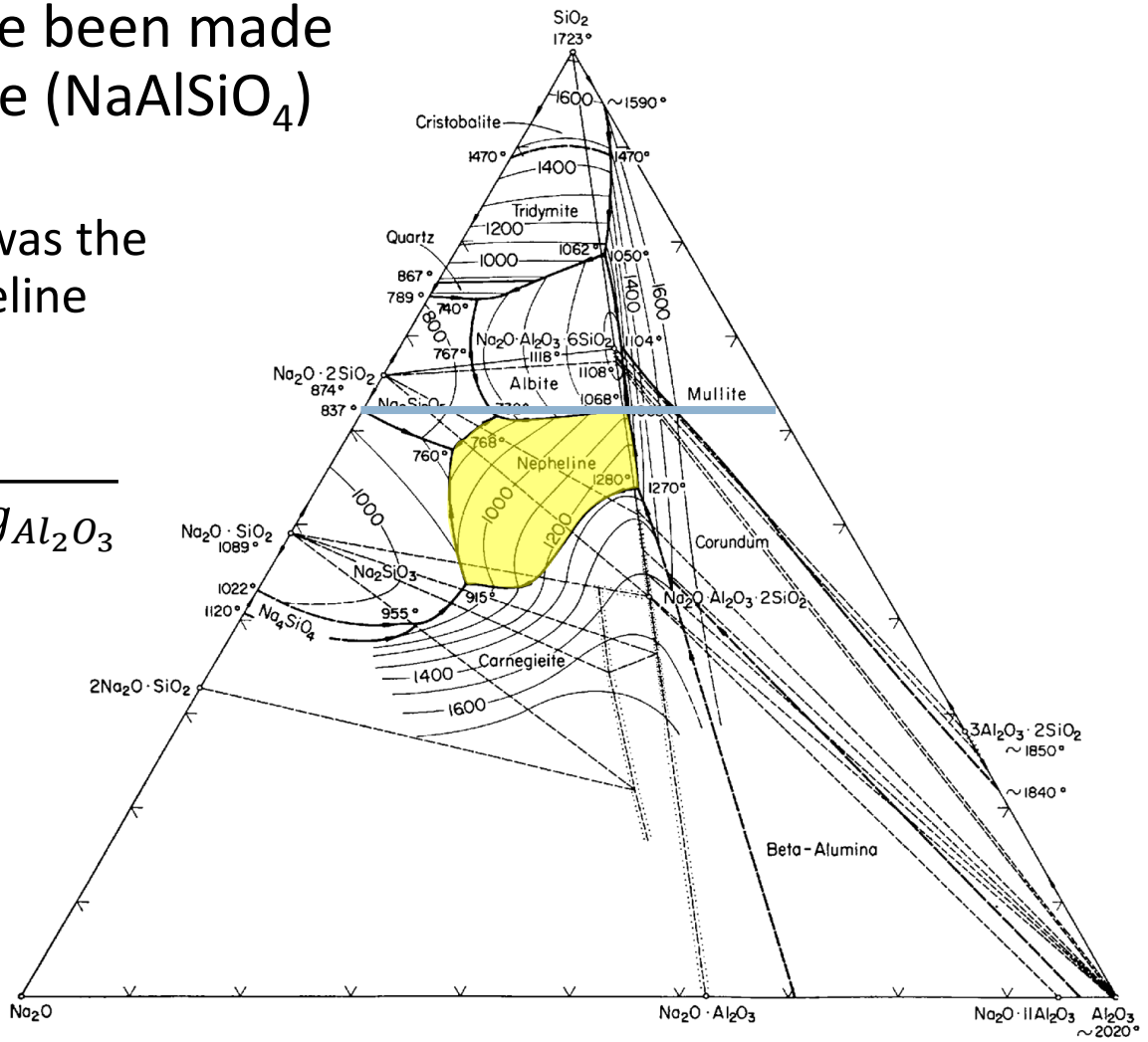

Sulfur Tolerance in HLW Glass

- At concentrations above the sulfur tolerance limit, a sulfate containing salt accumulates on the melt surface
- About 22% of the projected HLW feed batches to the WTP are expected to be limited by sulfate (WTP Contract Minimum 0.5%)

Crystal Tolerance

- Two approaches considered
  1. Matyas et al. 2013 model for predicting the accumulation rate of spinel in the pour-spout riser at 850°C
  2. Limit the crystal fraction in the melt

Spinel $[Fe,Zn,Mn][Fe,Cr,Mn,Al]_2O_4$

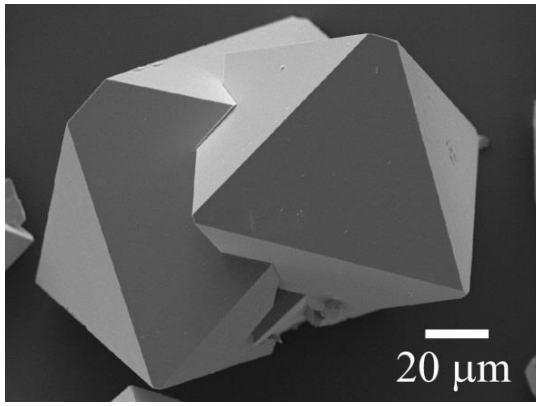

Eskolaite Cr_2O_3

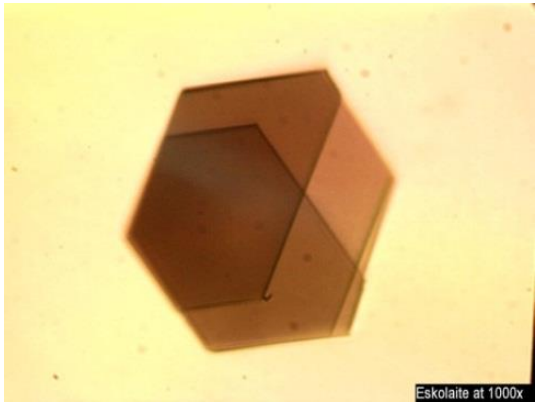

'Significant' Waste Constituents

- Al, Ca, Cr, Fe, K, Mg, Mn, Na, Ni, P, S, Si, Th, U, Zr: base waste loading/formulation
- Any other element with >0.5 wt% in glass: comp. reporting
- NO_3, NO_2, TOC: reductant addition
- > 0.05% of the total radioactive inventory indexed to the years 2015 and 3115: rad. reporting

HLW Off-Gas Treatment

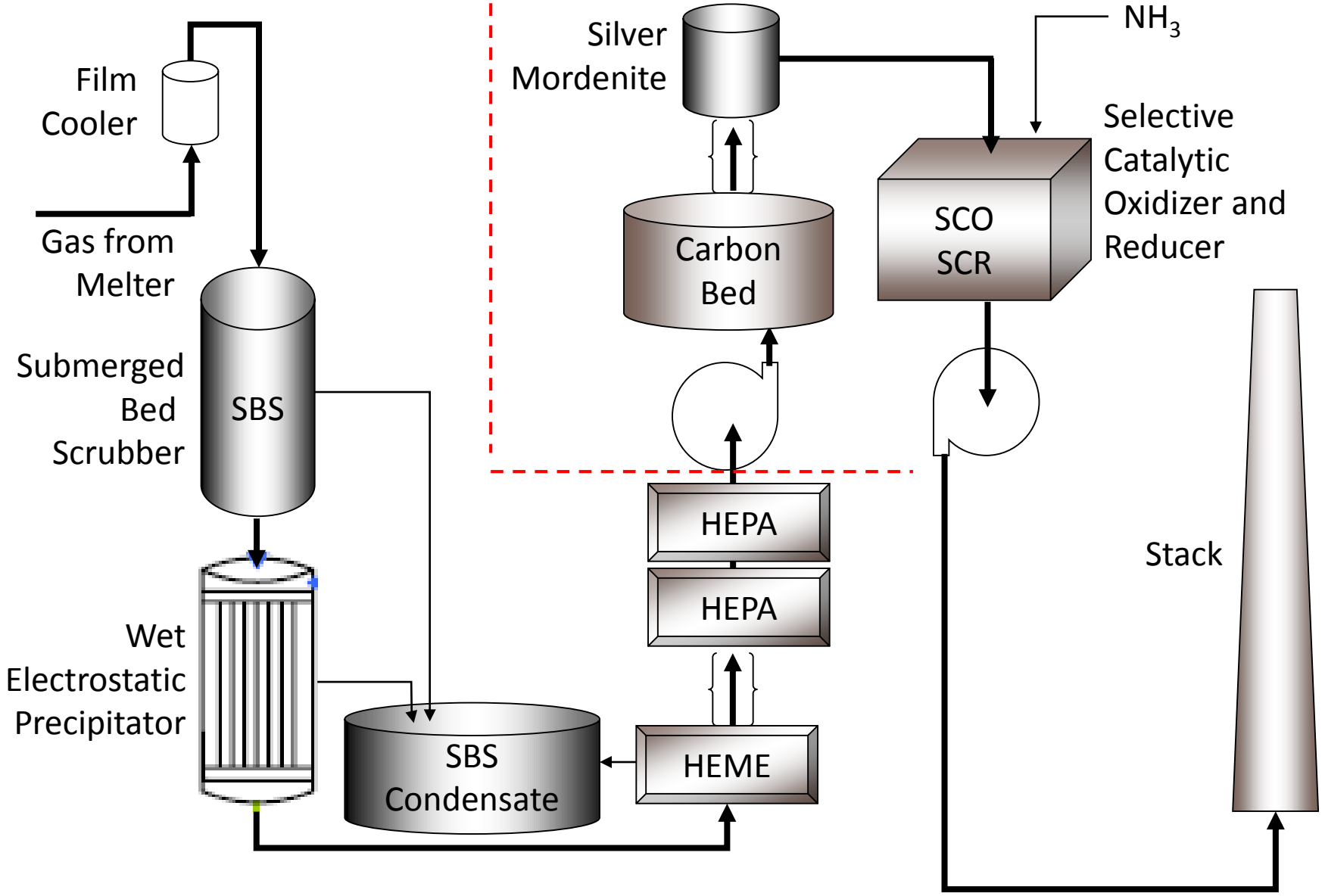

Vienna and Kim *Preliminary IHLW Formulation Algorithm Description*, 24590-HLW-RPT-RT-05-001, Rev. 1, 2014

Schematic of Processing Window

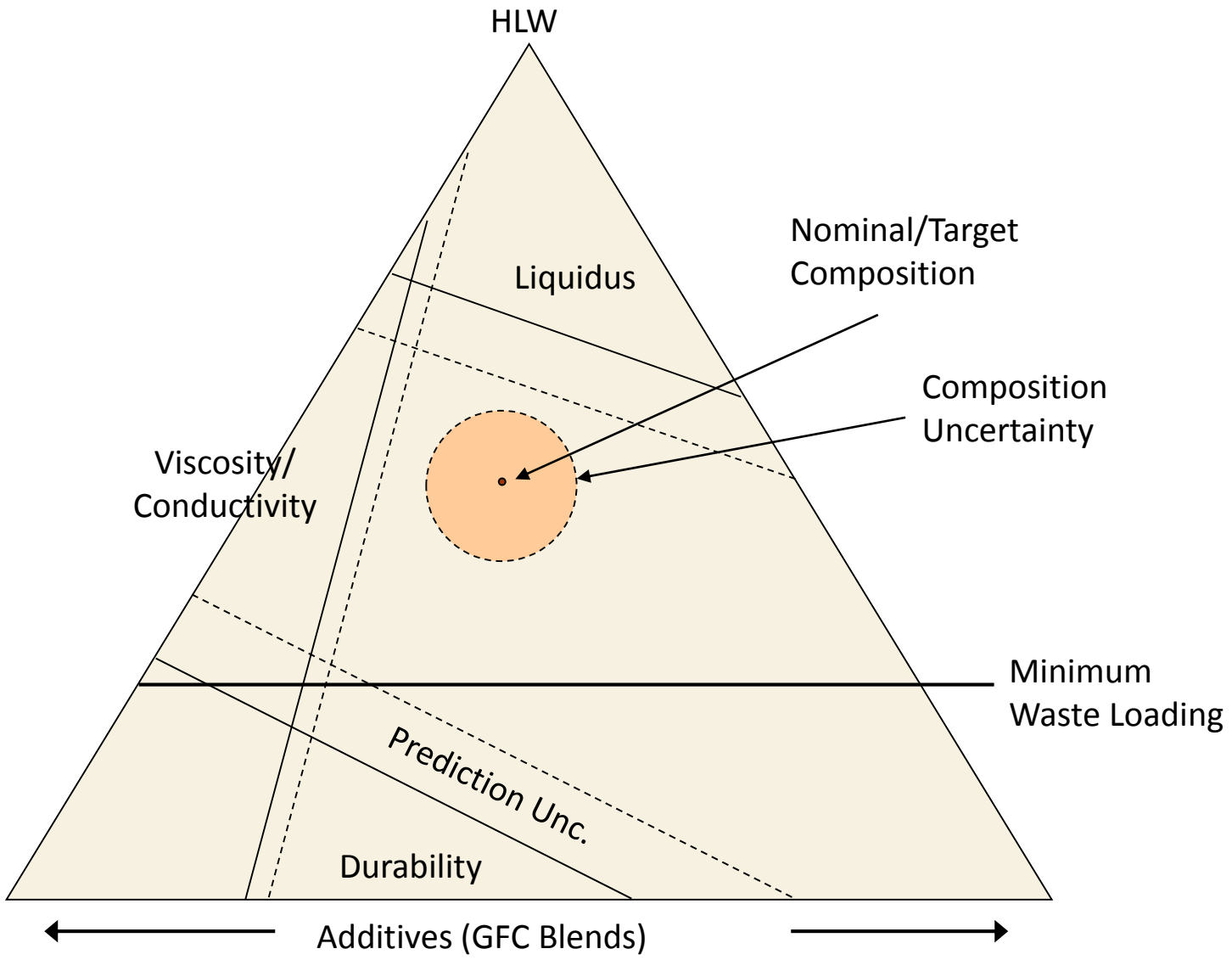

Composition Uncertainty

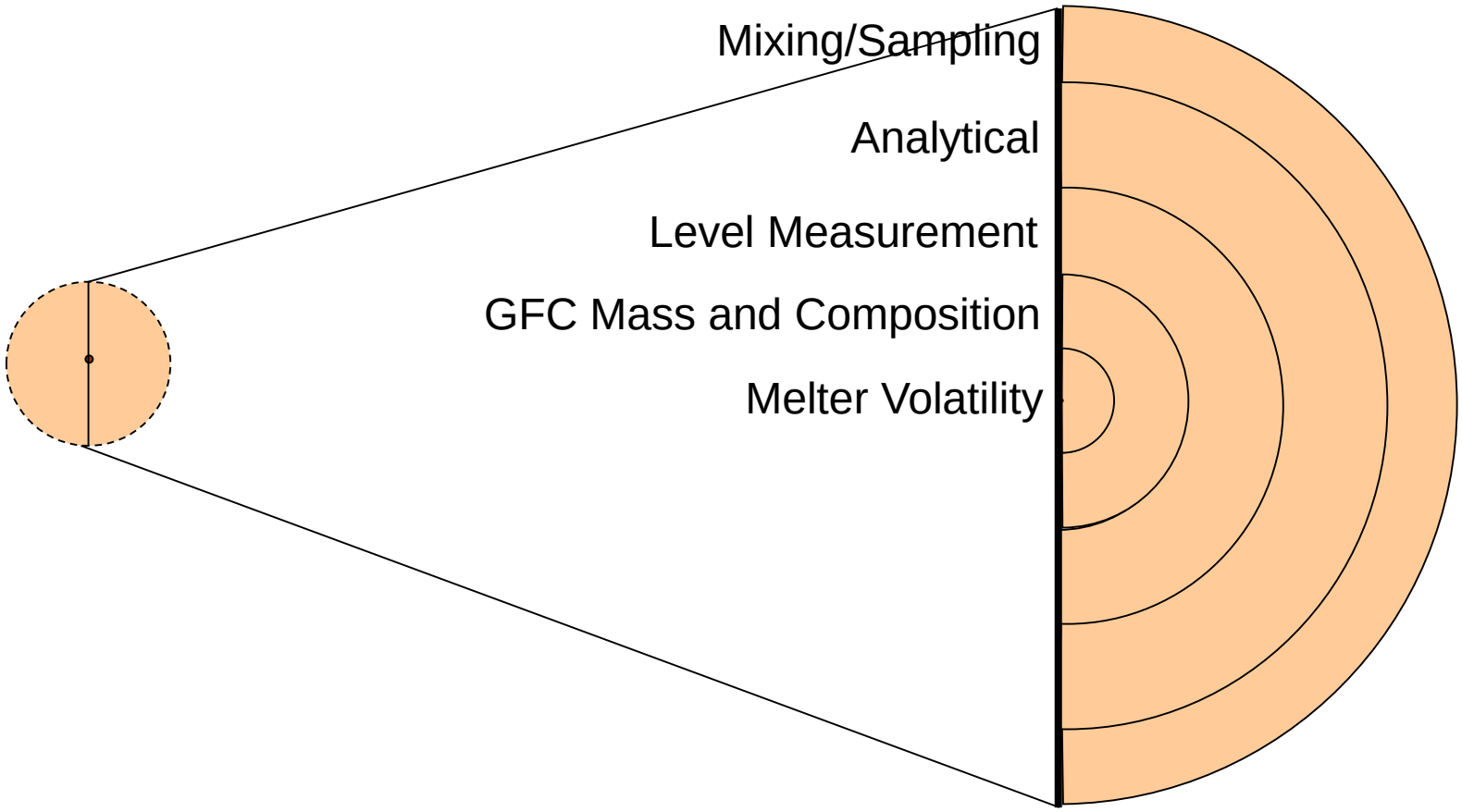

Enhanced Glass Models & the Impact on the Treatment Mission

Treatment Mission Projections

	BNI/WTP Baseline Models	2008 TUA* Baseline	2013 TUA Baseline	2013 TUA w/ caustic and oxidative leaching eliminated
HLW Canisters	18,400	14,838	8,223	13,534
LAW Containers	145,000	91,400	79,465	65,151
Total Canisters & Containers	163,000	106,238	87,688	78,685

* The “2008 models” were altered in anticipation of our work

24590-WTP-RPT-PE-13-003, Rev 0, 2013 Tank Utilization Assessment (TUA) Part 1: Potential Impact of Advanced Glass Models on the WTP, 3 December 2013

Lessons Learned and New Data, LAW

- Significantly new LAW PCT data available → fit new LAW PCT model
- Neural network VHT model was very difficult to implement and not sufficiently predictive of new data → find different form of models that are easier to apply and more predictive
- LAW Viscosity model was not refit in 2013 but significant new data available since 2007 → fit new LAW viscosity model
- 29 new melter test data with LAW sulfate solubility validated this model well → no change in LAW sulfate model
- Need for refractory corrosion constraint with high loaded LAW glasses → VSL recently published preliminary K3 corrosion model
- Halide rules split between conservative and optimistic approach added confusion and new data added, suggesting the need for a new approach → new halide/chromium rules added based on optimization

Lessons Learned and New Data, HLW

- The spinel c_T under-predicts new data at the higher spinel fraction → refit model without combined c and T (e.g., c_{950} or $T_{2\%}$)
- Neural network nepheline model was very difficult to implement and not sufficiently predictive of new data → find different form of models that are easier to apply and more predictive
- New HLW sulfate solubility data (13 glasses) showed the combined LAW + HLW model significantly under-predicted new data → fit separate HLW sulfate solubility model
- New HLW PCT data showed that the previous PCT model was not sufficiently predictive of PCT responses for glasses with Al_2O_3 concentrations > 25 wt% → fit new HLW PCT model trying new methods of accounting for non-linear effects of Al_2O_3
- HLW Viscosity model was not refit in 2013 but significant new data available since 2009 → fit new HLW viscosity model

Acknowledgements

Acknowledgements

I am forever indebted to Professor Pavel Hrma for his guidance, profound understanding of glass chemistry and humble but erudite manner.

and

I am grateful to the management of US Department of Energy for recognizing the value and acting in the best interest of the taxpayers.

Acknowledgements

Rutgers, State University of New Jersey

Professor Ashutosh Goel - PI

- Pr. Jincheng Du (University of North Texas), Prof. David Bryce (University of Ottawa, Canada), Pr. Paul Bingham (Sheffield Hallam University, UK), Pr. Hellmut Eckert (University of Sao Paulo, Brazil)

Dr. Mohamed Naji, Yaqoot Shaharyar Charles Cao, Ambar Deshkar, Nicholas Stone Weiss, Hrishikesh Kamat, Steven Cheng, Edmund Han, Nikhil Jani

Washington State University Pullman

Prof. John McCloy – PI (WSU & PNNL)

- Pr. Steven Martin (Iowa Sate University), Dr. Joerg Neuefeind (Oak Ridge National Laboratory, Pr. Joshua Feinberg (University of Minnesota, Institute for Rock Magnetism), Pr. Neill Owen (Washington State University), Dr. Joseph Ryan (PNNL)

Jamie Weaver, Mostafa Ahmadzadeh, José Marcial, Joseph Osborn, Mahmood Abusamha

Acknowledgements

Idaho National Laboratory

Dr. Donna Guillen - PI

Alexander Abboud, Benjamin Parruzot,, Alex Scrimshire, William H. Harris, Lisa E. Mitchell, Joseph Cambareri, Igor Bolotnov, & Clyde Beers

Savannah River National Laboratory

Dr. Kevin Fox - PI

Dr. Jake Amoroso, Madison Caldwell, Dr. Tommy Edwards, Andy Foreman, Mark Fowley, Devon McClane, Whitney Riley, & Dr. Charles Crawford

Lawrence Berkeley National Laboratory

Dr. Wayne W. Lukens

University of Chemistry and Technology Prague

The Institute of Rock Structure and Mechanics

Dr. Richard Pokorny

Pr. Jaroslav Klouzek & Miroslava Hujova

Acknowledgements

Vitreous State Laboratory of the Catholic University of America

Pr. Ian Pegg - PI

Dr. Keith Matlack, Dr. Wing Kot, Dr. Isabelle Muller, Dr. Hao Gan, Dr. Marek Brandys, Howard Abramowitz, Dr. Konstantin Gilbo, Dr. Adonia Papathanassiu, & Dr.Malabika Chaudhuri

Atkins

Brad Bowan, Dr. Innocent Joseph, Glenn Diener, & Eric Smith

University of Sheffield

Dr. Claire L. Corkhill - PI

Pr. Neil C. Hyatt, Dr. Clare L. Thorpe, & Pr. Russell J. Hand

Tokyo Institute of Technology

Department of Chemistry and Materials Science,

Pr. Tetsuji Yano - PI

Takuma Naito, Yukihiro Yoshida, & Tetsuo Kishi

Vanderbilt University

Pr. David S. Kosson - PI

Acknowledgements

PNNL

Management, QA, etc.: Michael J. Schweiger – PI & Program Manager
Laura M. Buchanan, Mona G. Champion, Teresa Schott, and Kirsten M. Meier

Cold Cap Reactions: Pavel R. Hrma - Lead
Carissa J. Humrickhouse, J. Adam Moody, Rachel M. Tate, Timothy T. Rainsdon, Nathan E. Tegrotenhuis, Benjamin M. Arrigoni, Carmen P. Rodriguez, Benjamin H. Tincher, Samuel H. Henager, David A. Pierce, Jarrett A. Rice, Brian J. Riley, Rachel M. Tate, Jaehun Chun, Dong-Sang Kim, Chul-Woo Chung, Jesse B. Lang, Abigail E. Winschell, Derek R. Dixon, Tzuhan Tsui, Jarrod V. Crum, Steven A. Luksic, Kai Xu, & Carolyn I. Pearce

Tc in Glass: Dong-Sang Kim - Lead
Brian J. Riley, Martin Liezers, Michael J. Schweiger, Jamie George, Carmen P. Rodriguez, Pavel R. Hrma, Charles F. Windisch Jr, Chuck Z Soderquist, Mark Bowden, Ryan M Covert, Abigail E Winschell, Chulwoo Chung, Jarrod V Crum, Steven A Luksic, Carolyn Pearce, Tongan Jin, Edgar C Buck, Cristian Lovin, Paul L Gassman, Ravi Kukkadapu, Andy Lipton, Brigitte Weese and Lori P. Darnell

Acknowledgements

PNNL Cont'd

Crystal Tolerant Glass: Josef Matyas, Charmayne Lonergan, Carmen P. Rodriguez, Jesse B. Lang, Jarrod V. Crum, Michael J. Schweiger, James E Amonette, Antoinette T Owen, Danielle P Jansik, Timothy A White, Alyssa Kimura, Micah J. Schaible, Rachel M. Tate, and Benjamin M. Arrigoni

Glass Property Modeling: John D. Vienna - Lead
Dong-sang Kim, Pavel R. Hrma, Gary J. Sevigny, Josef Matyas, Greg F. Piepel, Scott K. Cooley, John S. Hardy, Rich P. Pires, Carmen P. Rodriguez, James M. Davis, Michael J. Schweiger, William C. Buchmiller, Mac R Zumhoff, Christopher M. Fisher, Donald E. Rinehart, Lori P. Darnell, Nathan L. Canfield, Charlie C. Bonham, Daniel C. Skorski, Derek R. Dixon, Jarrod V. Crum, Brian J. Riley, Jaehun Chun, Jesse B. Lang, Paul L. Gassman, Nancy Washton

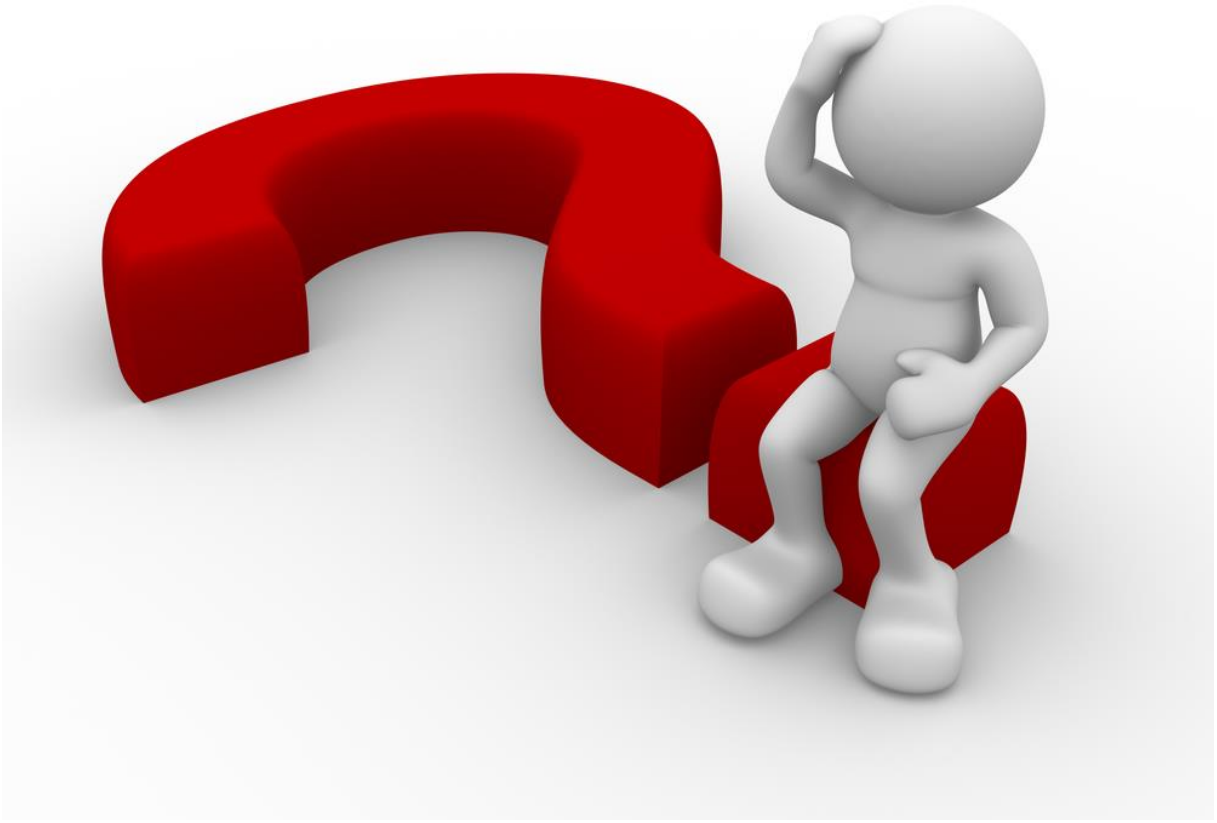

Back Up Slides

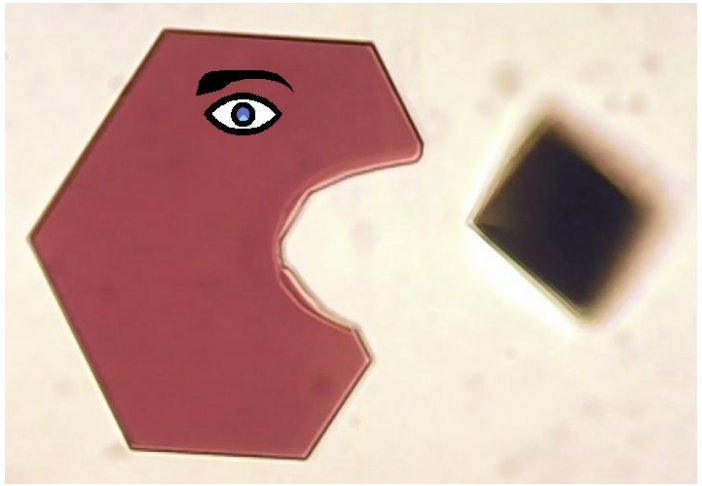

Oxide Compositions of Limiting HLW Streams (wt%)

Waste Component	Bi Limited	Cr Limited	Al Limited	Al and Na Limited
Al_2O_3	22.45%	25.53%	49.21%	43.30%
B_2O_3	0.58%	0.53%	0.39%	0.74%
CaO	1.61%	2.47%	2.21%	1.47%
Fe_2O_3	13.40%	13.13%	12.11%	5.71%
Li_2O	0.31%	0.36%	0.35%	0.15%
MgO	0.82%	0.16%	0.24%	0.44%
Na_2O	12.97%	20.09%	7.35%	25.79%
SiO_2	12.04%	10.56%	10.05%	6.22%
TiO_2	0.30%	0.01%	0.02%	0.35%
ZnO	0.31%	0.25%	0.17%	0.36%
ZrO_2	0.40%	0.11%	0.81%	0.25%
SO_3	0.91%	1.52%	0.41%	0.44%
Bi_2O_3	12.91%	7.29%	2.35%	2.35%
ThO_2	0.25%	0.04%	0.37%	0.04%
Cr_2O_3	1.00%	3.07%	1.07%	1.44%
K_2O	0.89%	0.37%	0.29%	1.34%
U_3O_8	3.48%	7.59%	7.25%	4.58%
BaO	0.02%	0.03%	0.11%	0.06%
CdO	0.00%	0.01%	0.05%	0.02%
NiO	3.71%	1.06%	0.82%	0.20%
PbO	0.48%	0.48%	0.84%	0.18%
P_2O_5	9.60%	3.34%	2.16%	4.10%
F-	1.58%	2.00%	1.37%	0.46%
Total	100.00%	100.00%	100.00%	100.00%

Table TS-8.3 High-Level Waste Feed Unwashed Solids Maximum Radionuclide Composition (Curies per 100 grams non-volatile waste oxides)

Isotope	Maximum (Ci / 100 grams waste oxides)	Isotope	Maximum (Ci / 100 grams waste oxides)	Isotope	Maximum (Ci / 100 grams waste oxides)
^{3}H	6.5E-05	^{129}I	2.9E-07	^{237}Np	7.4E-05
^{14}C	6.5E-06	^{137}Cs	1.5E00	^{238}Pu	3.5E-04
^{60}Co	1E-02	^{152}Eu	4.8E-04	^{239}Pu	3.1E-03
^{90}Sr	1E+01	^{154}Eu	5.2E-02	^{241}Pu	2.2E-02
^{99}Tc	1.5E-02			^{241}Am	9.0E-02
^{125}Sb	3.2E-02	^{233}U	4.5E-06 (all tanks except AY-101/C-104)(2.0E-04 for AY-101/C-104 only)	$^{243+244}Cm$	3.0E-03
^{126}Sn	1.5E-04	^{235}U	2.5E-07		

Table TS-7.1 Low-Activity Waste Chemical Composition, Soluble Fraction Only

Maximum Ratio, analyte (mole) to sodium (mole)			
Chemical Analyte	Envelope A	Envelope B	Envelope C[3]
Al	2.5E-01	2.5E-01	2.5E-01
Ba	1.0E-04	1.0E-04	1.0E-04
Ca	4.0E-02	4.0E-02	4.0E-02
Cd	4.0E-03	4.0E-03	4.0E-03
Cl	3.7E-02	8.9E-02	3.7E-02
Cr	6.9E-03	2.0E-02	6.9E-03
F	9.1E-02	2.0E-01	9.1E-02
Fe	1.0E-02	1.0E-02	1.0E-02
Hg	1.4E-05	1.4E-05	1.4E-05
K	1.8E-01	1.8E-01	1.8E-01
La	8.3E-05	8.3E-05	8.3E-05
Ni	3.0E-03	3.0E-03	3.0E-03
NO_2	3.8E-01	3.8E-01	3.8E-01
NO_3	8.0E-01	8.0E-01	8.0E-01
Pb	6.8E-04	6.8E-04	6.8E-04
PO_4	3.8E-02	1.3E-01	3.8E-02
SO_4	1.0E-02	7.0E-02	2.0E-02
TIC[1]	3.0E-01	3.0E-01	3.0E-01
TOC[2]	5.0E-01	5.0E-01	5.0E-01
U	1.2E-03	1.2E-03	1.2E-03

Notes:
1. Mole of inorganic carbon atoms/mole sodium.
2. Mole of organic carbon atoms/mole sodium.
3. Envelope C LAW is limited to complexed tank wastes from Hanford tanks AN-102 and AN-107.

Table TS-7.2 Low-Activity Waste Radionuclide Content, Soluble Fraction Only Maximum Ratio, radionuclide to sodium (mole)

Radionuclide	Envelope A		Envelope B		Envelope C	
	Bq	uCi	Bq	uCi	Bq	uCi
TRU	4.80E+05	1.30E+01	4.80E+05	1.30E+01	3.00E+06	8.11E+01
^{137}Cs	4.30E+09	1.16E+05	2.00E+10	5.41E+05	4.30E+09	1.16E+05
^{90}SR	4.40E+07	1.19E+03	4.40E+07	1.19E+03	8.00E+08	2.16E+04
^{99}Tc	7.10E+06	1.92E+02	7.10E+06	1.92E+02	7.10E+06	1.92E+02
^{60}Co	6.10E+04	1.65E+00	6.10E+04	1.65E+00	3.70E+05	1.00E+01
^{154}Eu	6.00E+05	1.62E+01	6.00E+05	1.62E+01	4.30E+06	1.16E+02

Notes:

1. The activity limit shall apply to the feed certification date.
2. TRU is defined as: Alpha-emitting radionuclides with an atomic number greater than 92 with half-life greater than 20 years.

Some radionuclides, such as ^{90}Sr and ^{137}Cs, have daughters with relatively short half-lives. These daughters have not been listed in this table. However, they are present in concentrations associated with the normal decay chains of the radionuclides.
1Bq = 2.703 e-5 uCi

Summary of HLW Melt and Glass Constraints

Constraint Description	Value/Range
Product Consistency Test (PCT) normalized B release	rB < 16.70 (g/L)
PCT normalized Li release	rLi < 9.57 (g/L)
PCT normalized Na release	rNa < 13.35 (g/L)
Nepheline rule	$g\mathrm{SiO_2}/(\ g\mathrm{Al2O3} + g\mathrm{Na_2O} + g\mathrm{SiO_2}) \geq 0.62$
CdO concentration in glass or Toxicity Characteristic Leaching Procedure (TCLP) Cd concentration	gCdO ≤ 0.1 (wt%) or cCd < 0.48 (mg/L)
Tl_2O concentration in glass	gTl2O ≤ 0.465 (wt%)
Temperature at 1 vol% crystal	T1% ≤ 950 (°C)
Non spinel phase rule	$g\mathrm{Al_2O_3} + g\mathrm{ThO_2} + g\mathrm{ZrO_2} < 18$ (wt%) $g\mathrm{ThO_2} + g\mathrm{ZrO_2} < 13$ (wt%) $g\mathrm{ZrO_2} < 9.5$ (wt%)
Viscosity at 1150°C	20 (P) ≤ η1150 ≤ 80 (P)
Viscosity at 1100°C	η1100 ≤ 150 (P)[(a)]
Electrical conductivity at 1100°C	0.1 (S/cm) ≤ ε1100
Electrical conductivity at 1200°C	ε1200 ≤ 0.7 (S/cm)
SO_3 concentration in glass (target)[(b)]	$g\mathrm{SO_3} \leq 0.44$ (wt%)

(a) Note that the lower limit of 10 Poise on η1100 is unnecessary given the lower limit of 20 Poise on η1150. This is because viscosity decreases with increasing temperature.
(b) The concentration before applying retention factors to account for losses during vitrification process is used. For all other constraints, the concentration values obtained after applying retention factors are used.

EGA and O_2 partial pressure by RAPIDOX

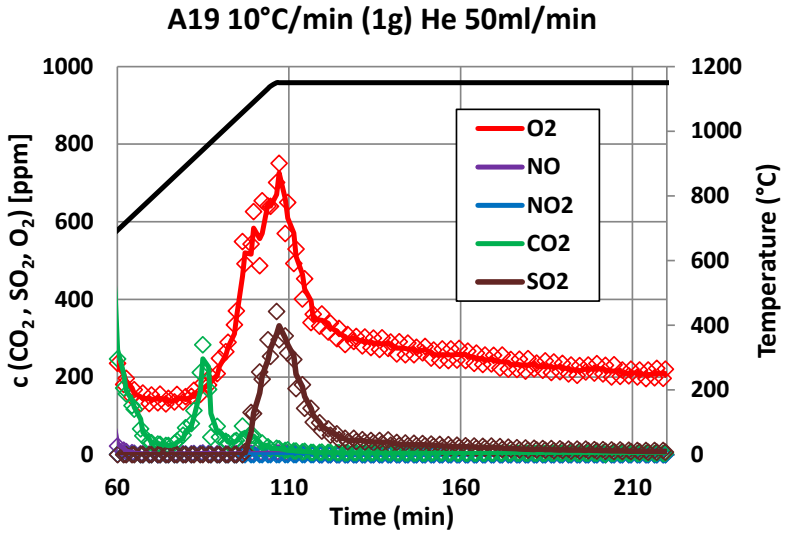

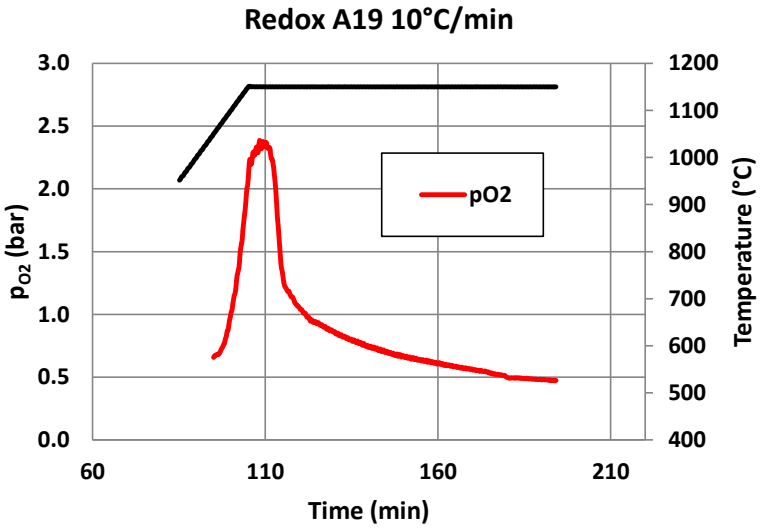

The evolved gas analysis, and the Rapidox analysis of pO_2 during the melting of A19 feed.

The black solid lines in both graphs show the temperature profile.

The melt is highly oversaturated with oxygen. Such a high oversaturation is not likely to arise solely from the iron redox equilibrium, but also from the oxygen "stored" in the feed from earlier batch decomposition reactions (mostly nitrates).

Foaming Curve & Secondary Foam

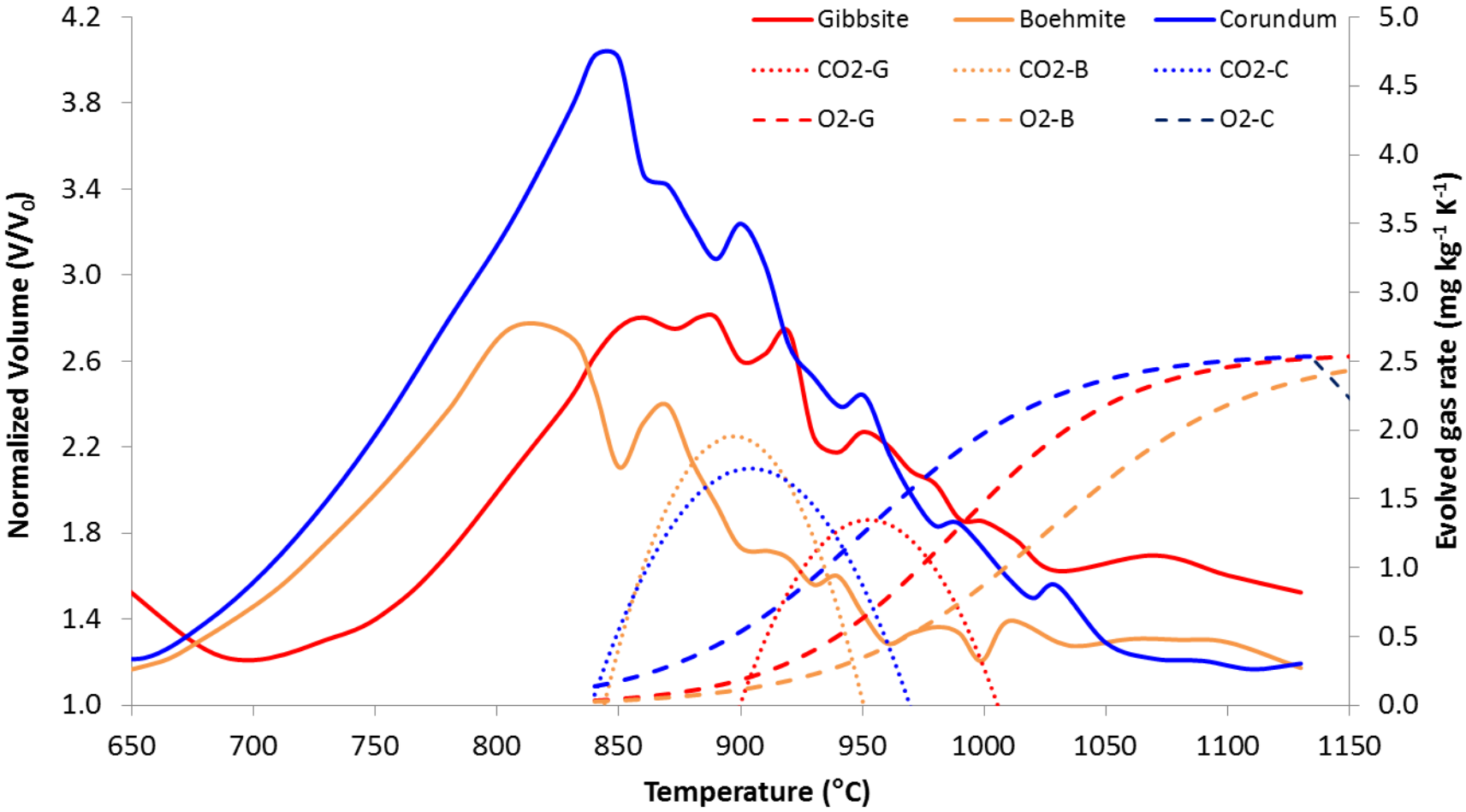

- Detected CO_2 gas in the foam layer was a residual gas remaining from the feed reaction and involved in the primary foam.
- Following detected O_2 gas was from iron redox reaction and involved in the secondary foam.

Nepheline Precipitation

- Many attempts have been made to predict Nepheline ($NaAlSiO_4$) formation
  - the most successful was the Li et al. 1997[13] Nepheline discriminator:

$$ND = \frac{g_{SiO_2}}{g_{SiO_2} + g_{Na_2O} + g_{Al_2O_3}}$$

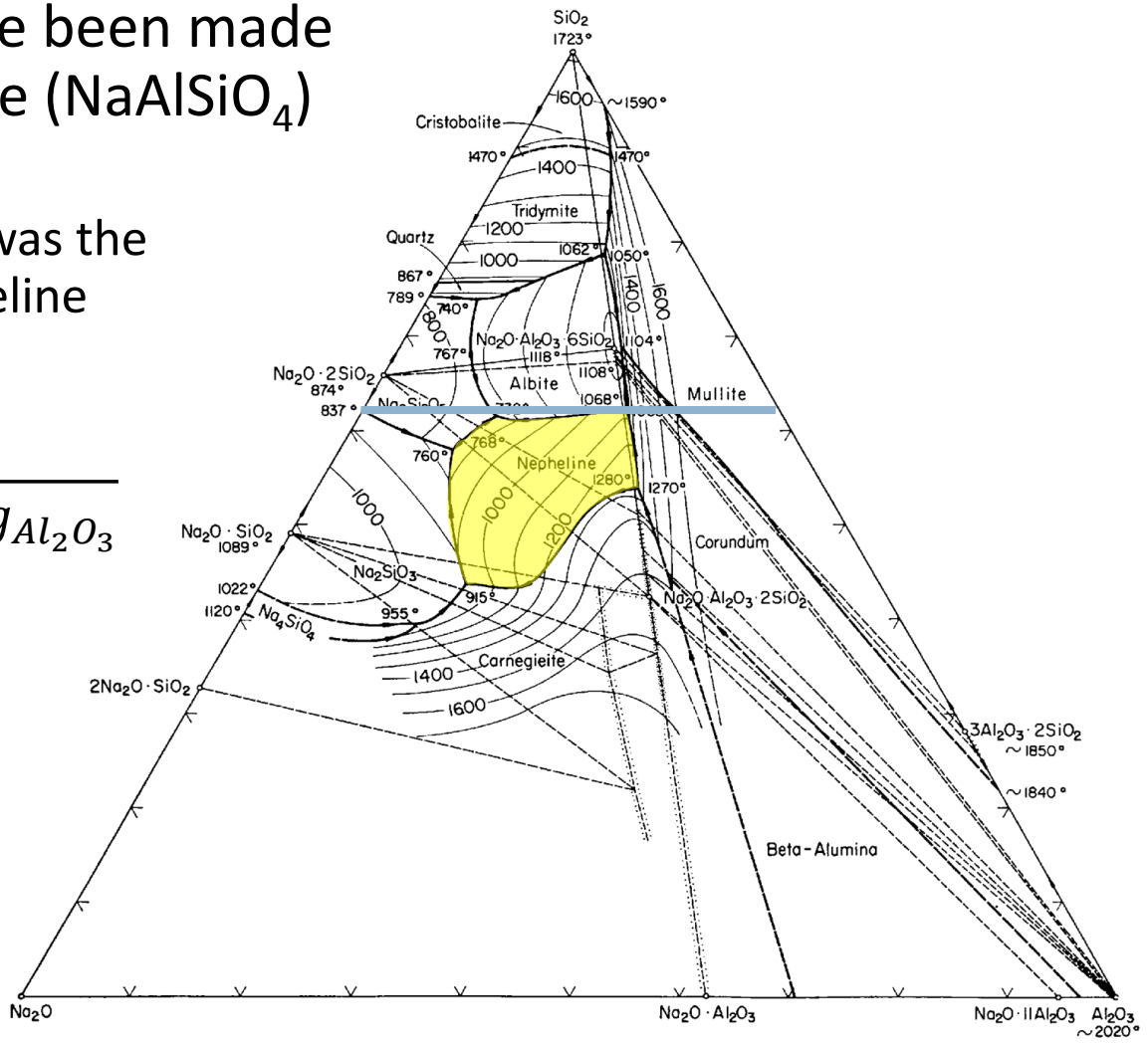

Foaming in High Bi-P HLW Glass Melts

Glass melts with high loadings of Bi-P wastes were found to exhibit foaming of the melt during cooling

- Potential risk of overflow during HLW canister cooling

Testing was performed to determine the foaming mechanism

- Stabilization of hexavalent Cr in phospho-chromate environments in the melt; auto-reduction to trivalent Cr on cooling as a result of its higher stability in spinels

Results were used to modify glass formulations to mitigate melt foaming

- Increased Al content to compete with Cr in phosphorus environments

Confirmed in one-third scale DM1200 pilot melter tests

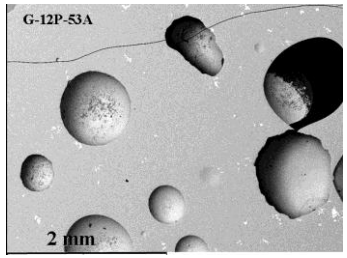

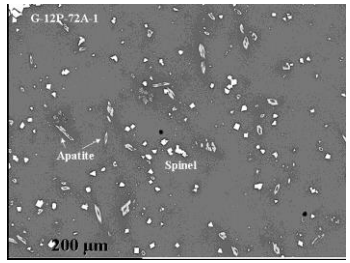

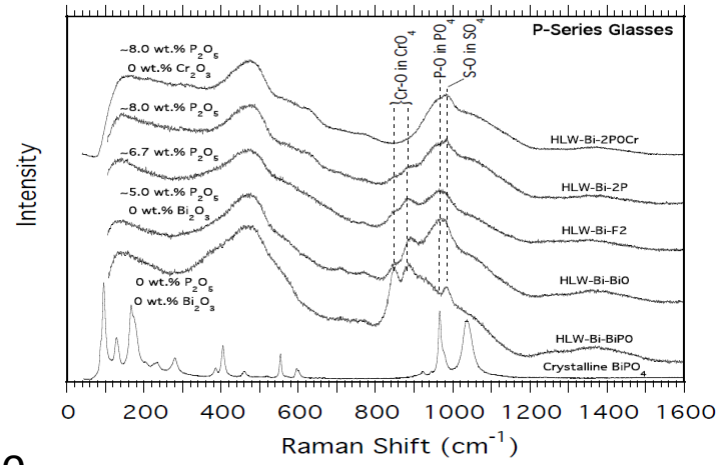

VSL-07R1010-1, Rev. 0; VSL-10R1780-1, Rev.0

Melt Rate and Waste Loading in High Bi-P HLW Glasses

- Glass formulations developed with very high waste loading (50 wt% waste oxides) for high Bi-P HLW streams
- However, slow melt rates were observed in scaled melter tests
- Melt rate screening tests were used to develop improved formulations with increased melt rate while retaining the same high waste loadings

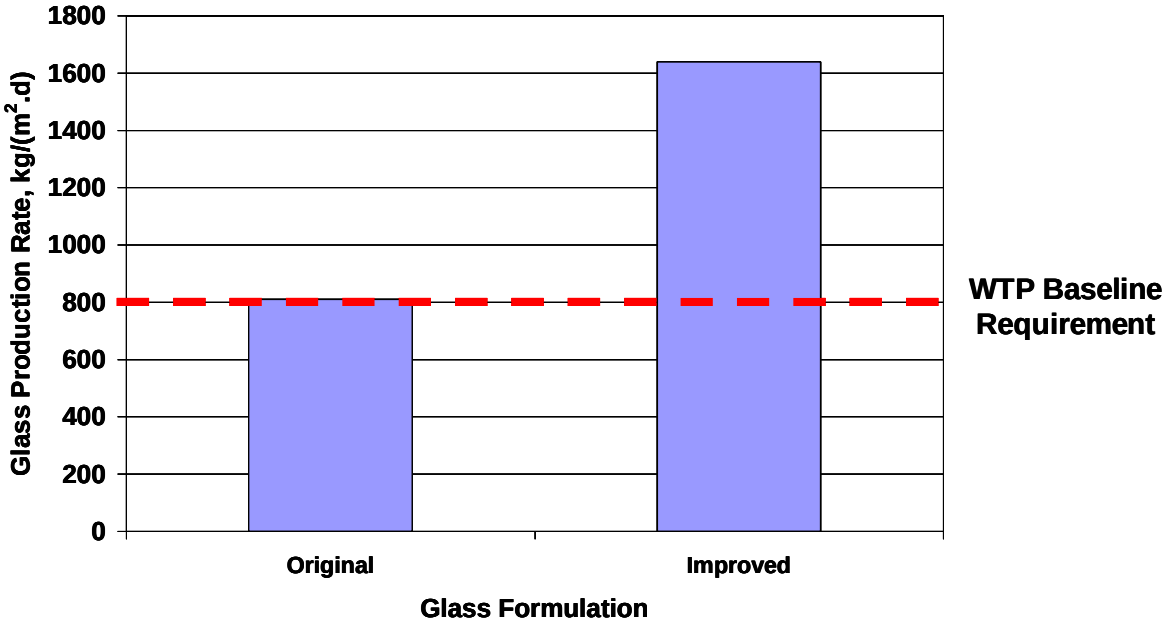

VSL-07R1010-1, Rev. 0; VSL-10R1780-1, Rev.0; VSL-12T2770-1, Rev. 0

Melt Rate and Waste Loading in High Fe HLW Glasses

Waste loading in typical high-Fe HLW stream is limited by spinel crystallization

Higher waste loadings often result in lower processing rates

Improved formulations have been developed with both high melt rates and high waste loadings

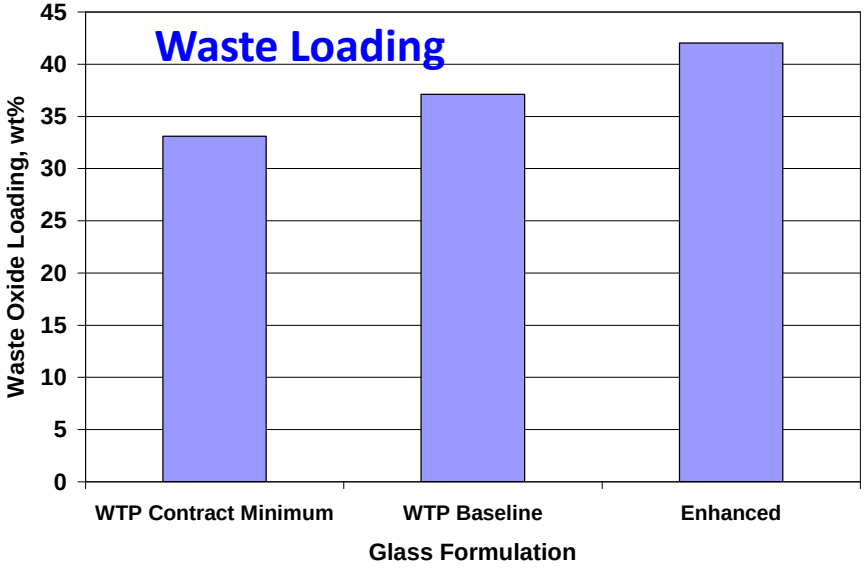

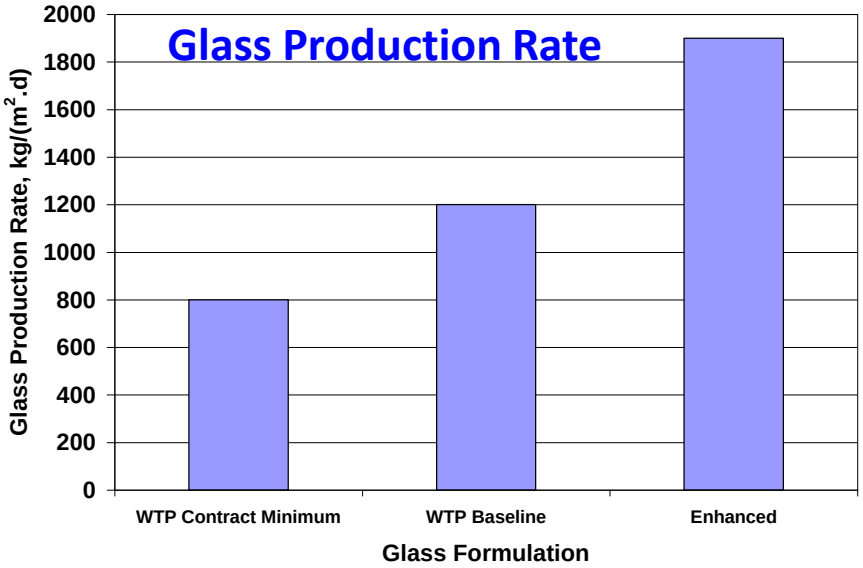

VSL-12R2490-1, Rev. 0

Sulfur Tolerance in HLW Glass

- At concentrations above the sulfur tolerance limit, a sulfate containing salt accumulates on the melt surface
- Limited melter tests suggest that sulfur tolerance is related to both Fe_2O_3 concentration and measured solubility in crucible melts

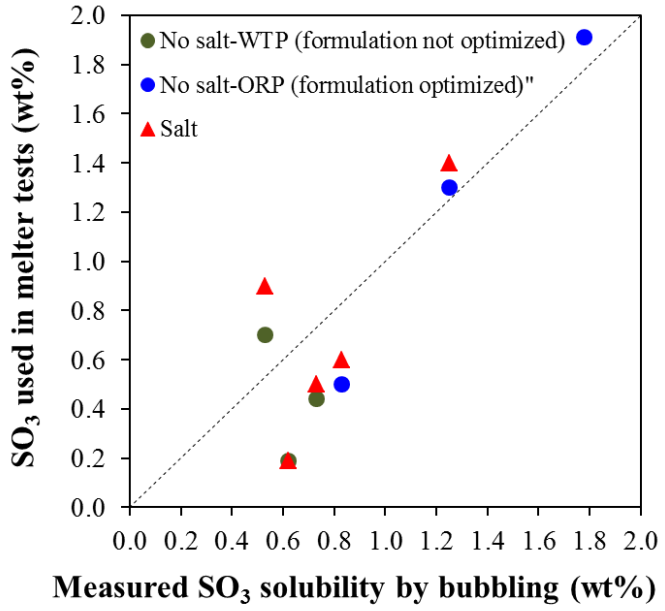

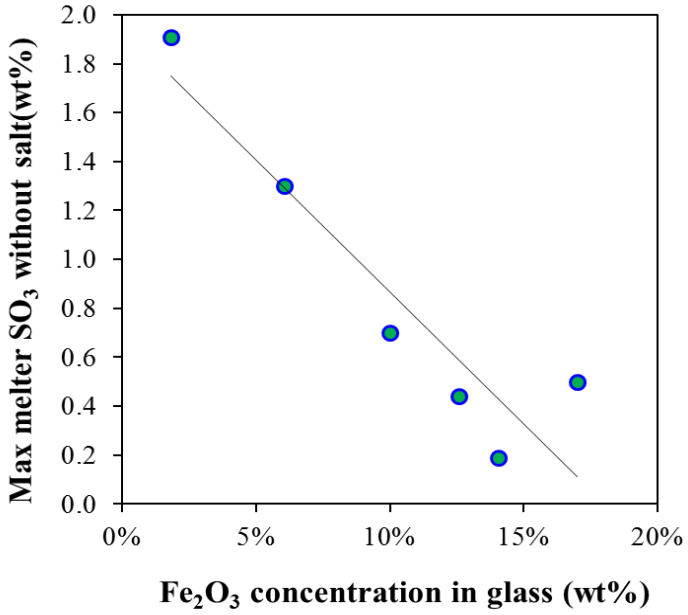

Waste Loading in High Sulfur HLW Glasses

About 22% of the projected HLW feed batches to the WTP are expected to be limited by sulfate

The sulfate content in the HLW fraction is dependent on the washing performance in pretreatment

High sulfate feeds pose the risk of molten salt formation in the melter

HLW glass formulations with high sulfate solubility have been developed to address this risk

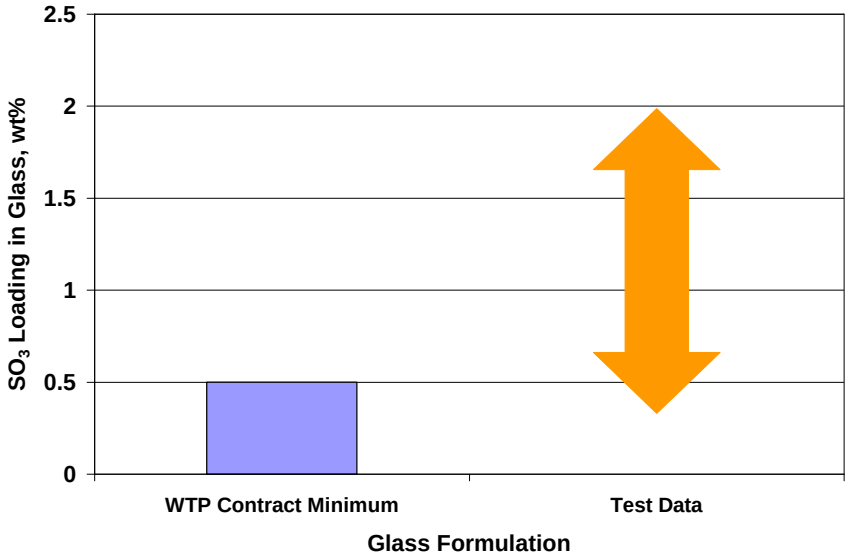

Effect of Glass Sulfate Capacity on Amount of Sulfate-Limited HLW Glass

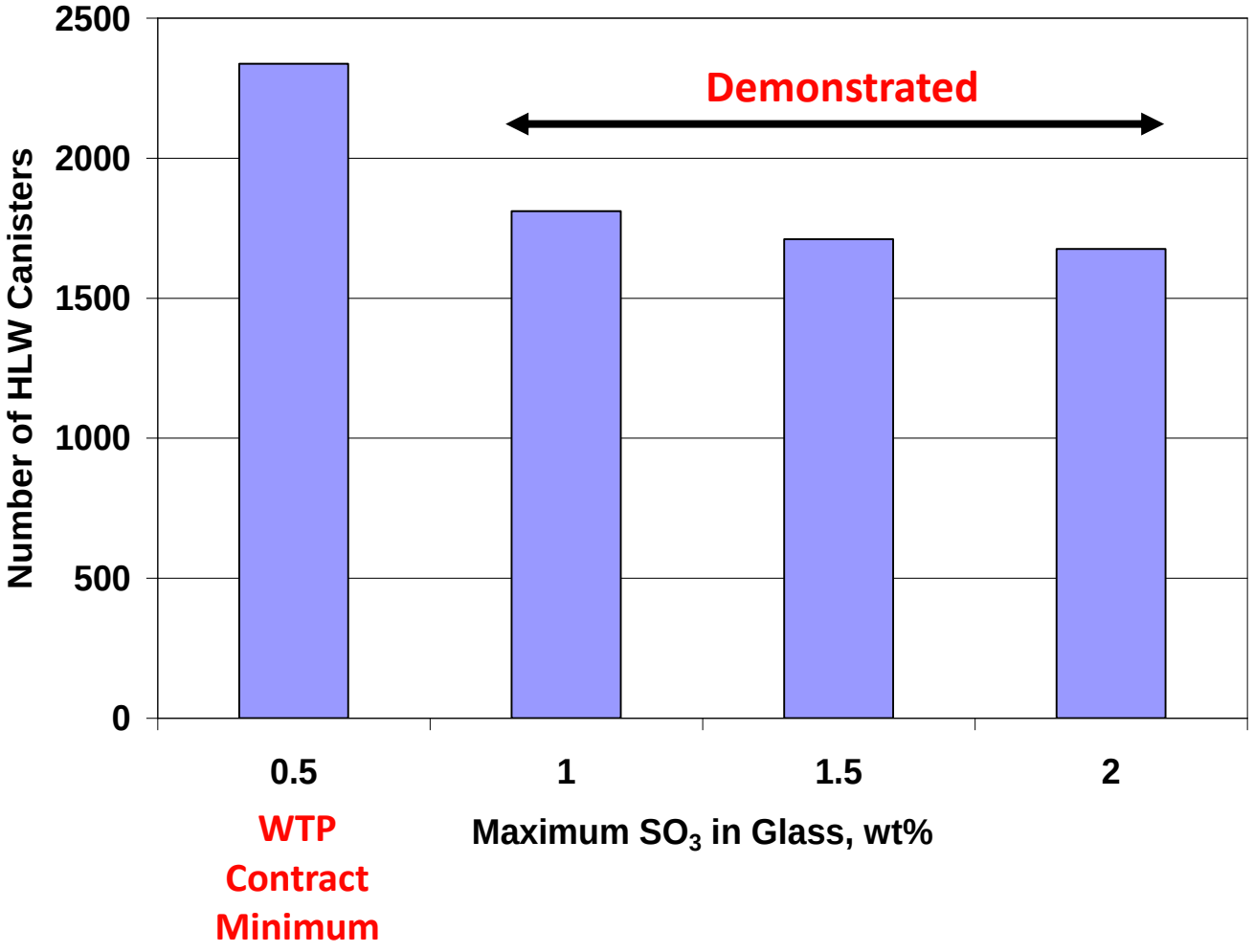

Crystal Tolerance

Spinel $[Fe,Zn,Mn][Fe,Cr,Mn,Al]_2O_4$

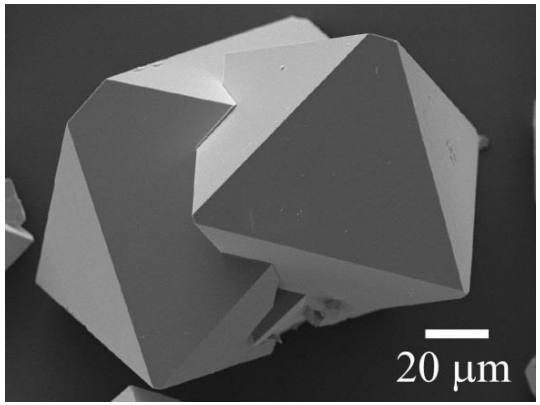

Eskolaite Cr_2O_3

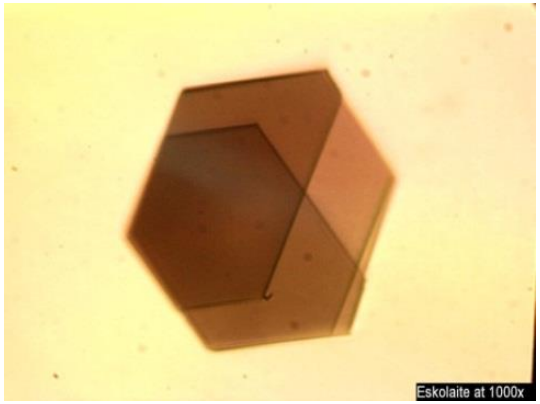

- Two approaches considered
  1. Matyas et al. 2013[4] model for predicting the accumulation rate of spinel in the pour-spout riser at 850°C
  2. Limit the crystal fraction in the melt

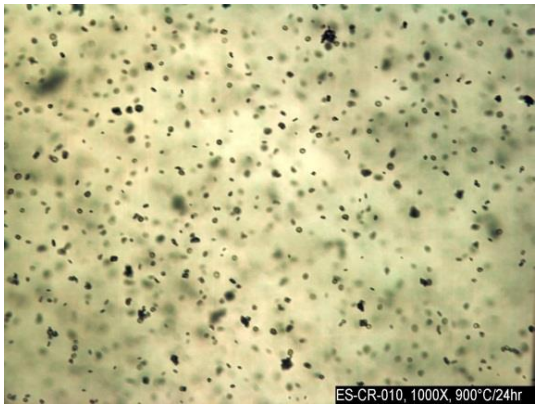

University of BRISTOL

Raman Probe Development:

An Investigation into Active Sludge Components

K.Wyness, S.Rennie & R.Springell

Interface Analysis Centre, University of Bristol, Bristol, BS8 1TL, UK.

Research Councils UK Energy For a Low Carbon Future

Sellafield Ltd

DISTINCTIVE

Motivation

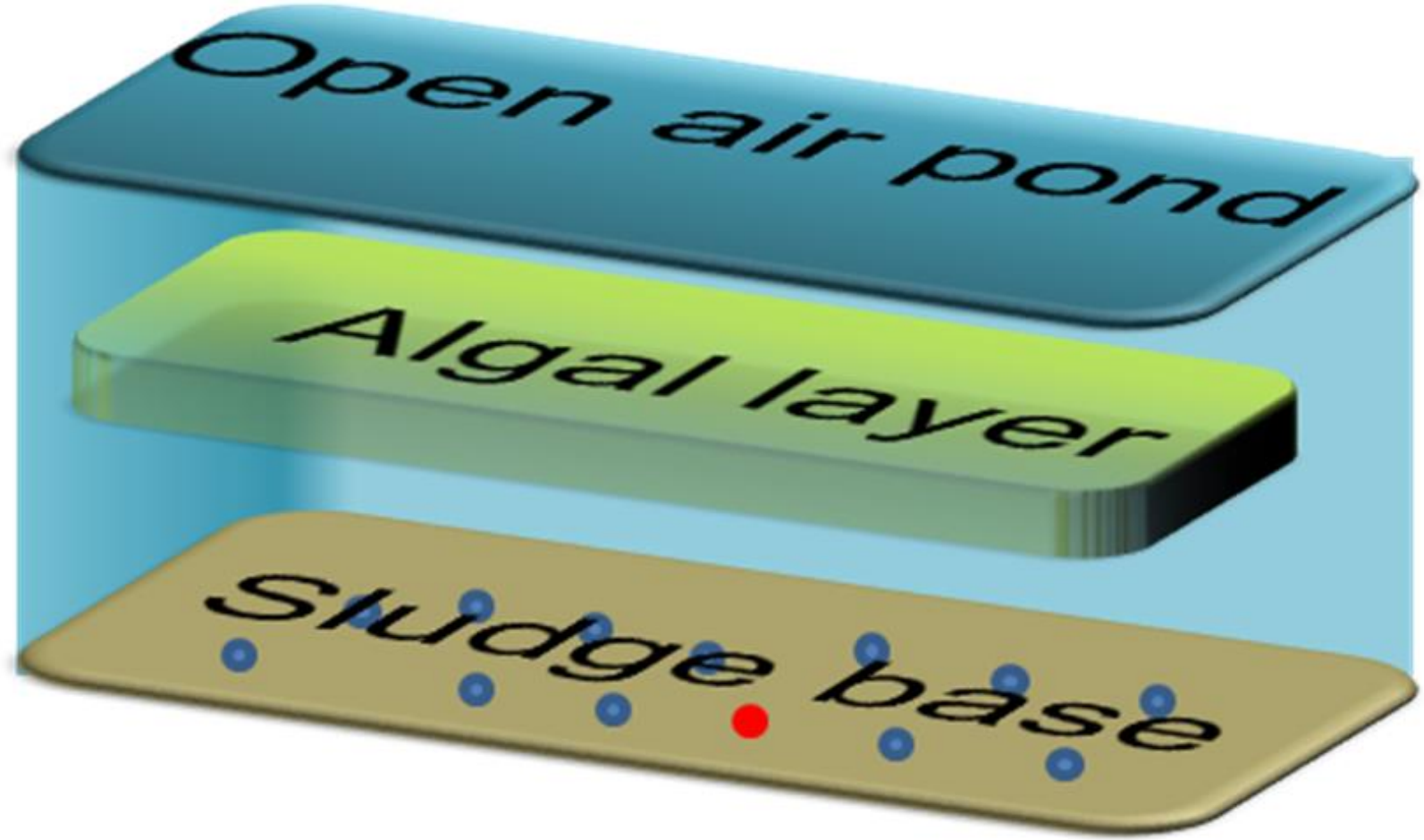

Research Councils UK Energy For a Low Carbon Future

DISTINCTIVE

Project Goals

Long term goal:

- Develop a stand off Raman probe to chemically characterise radioactive sludge.

Short term goals:

- Build a sample library of sludge component materials
- Optimise Raman optics for sample characterisation

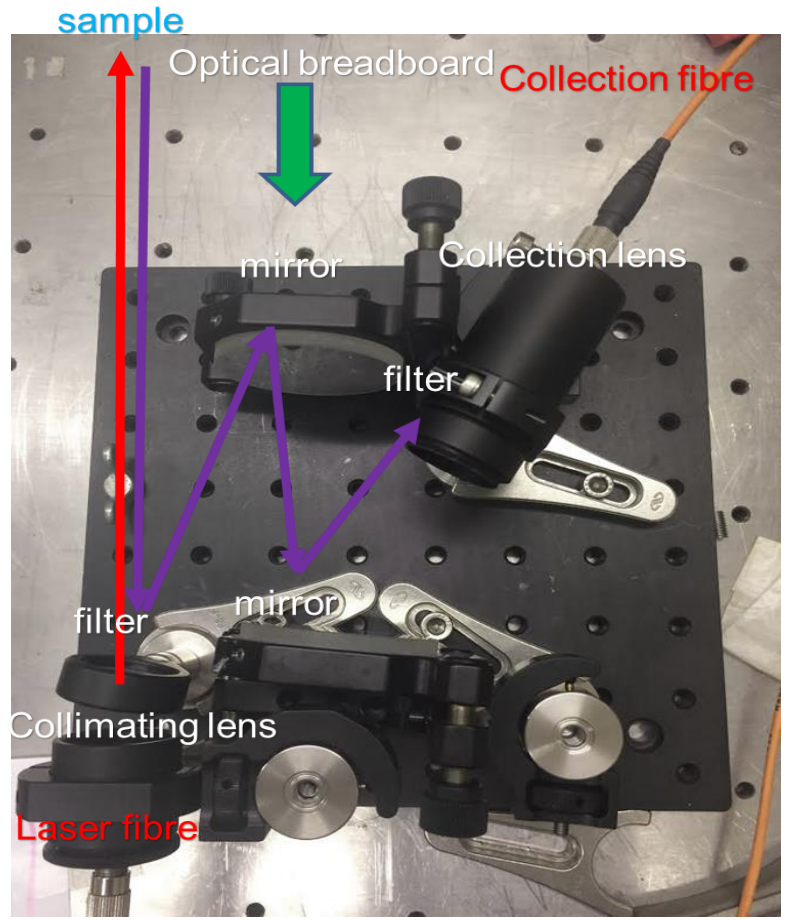

Research Councils UK Energy For a Low Carbon Future

DISTINCTIVE

Reference Library

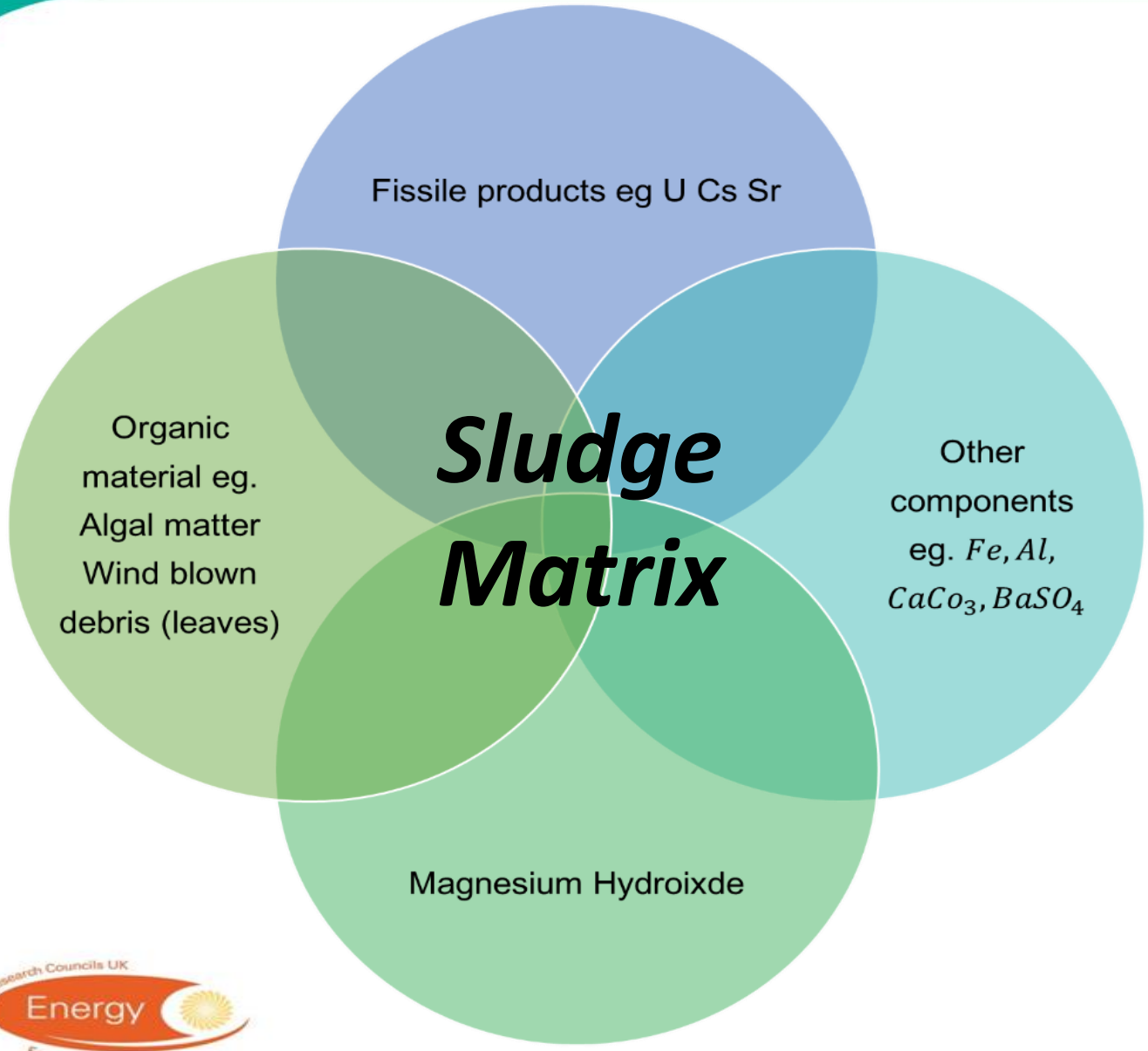

Corroded Magnox Sludge composition (most abundant only).

Element	Approximate composition (%) (UK National Nuclear Laboratory)
O	71.8
Mg	12.9
H	7.84
U	4.28
Al	0.63
Na	0.61
Fe	0.49
Ba	0.28
Zn	0.24
Ca	0.18
B	0.14
Cu	0.14
Si	0.11

N.B. Oxygen and hydrogen components make up water in wet sludge.

Research Councils UK Energy For a Low Carbon Future

DISTINCTIVE

Uranium oxides

$$UO_2 \leftrightarrow UO_{2+x} \leftrightarrow U_4O_9 \leftrightarrow U_3O_7 \leftrightarrow U_3O_8 \leftrightarrow UO_3$$

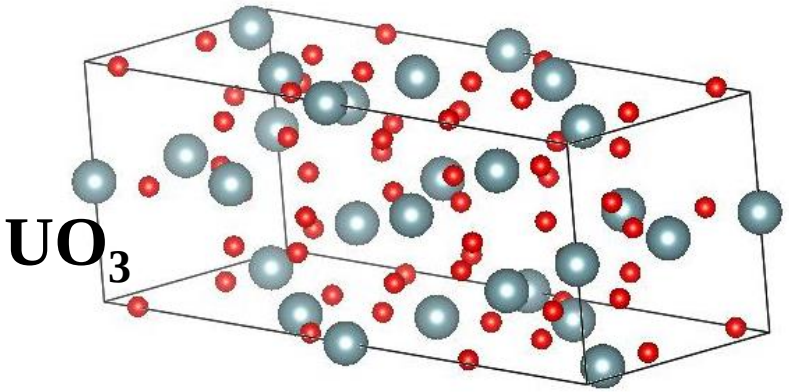

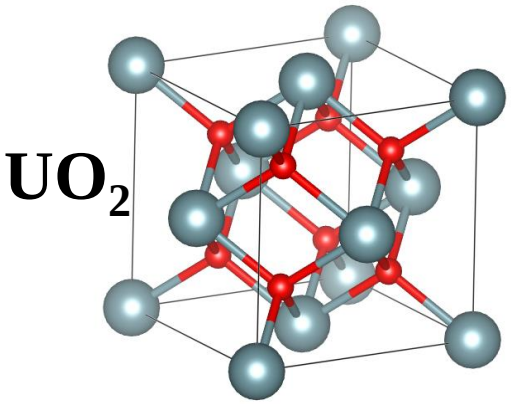

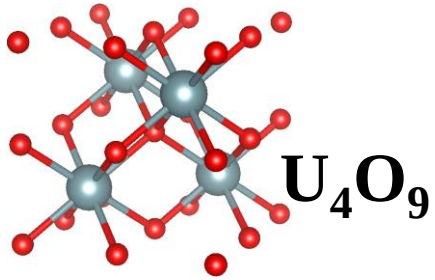

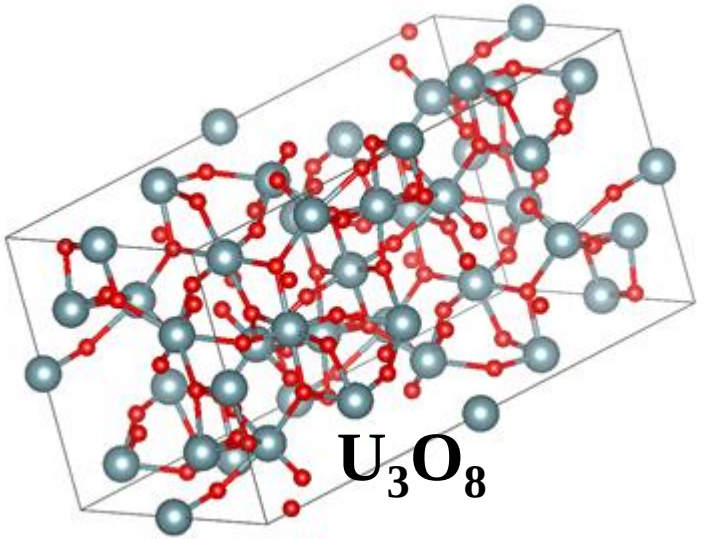

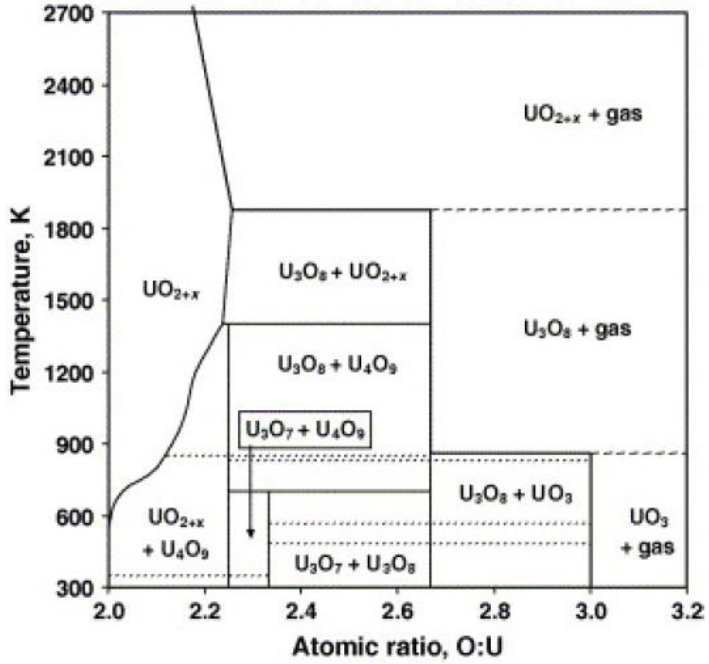

Research Councils UK Energy For a Low Carbon Future

DISTINCTIVE

Synthesis of uranium oxides

Sample name	Material
367AB	$UO_2(NO$
367EA	UO_3
367EB	UO_2
367EC	UO_2

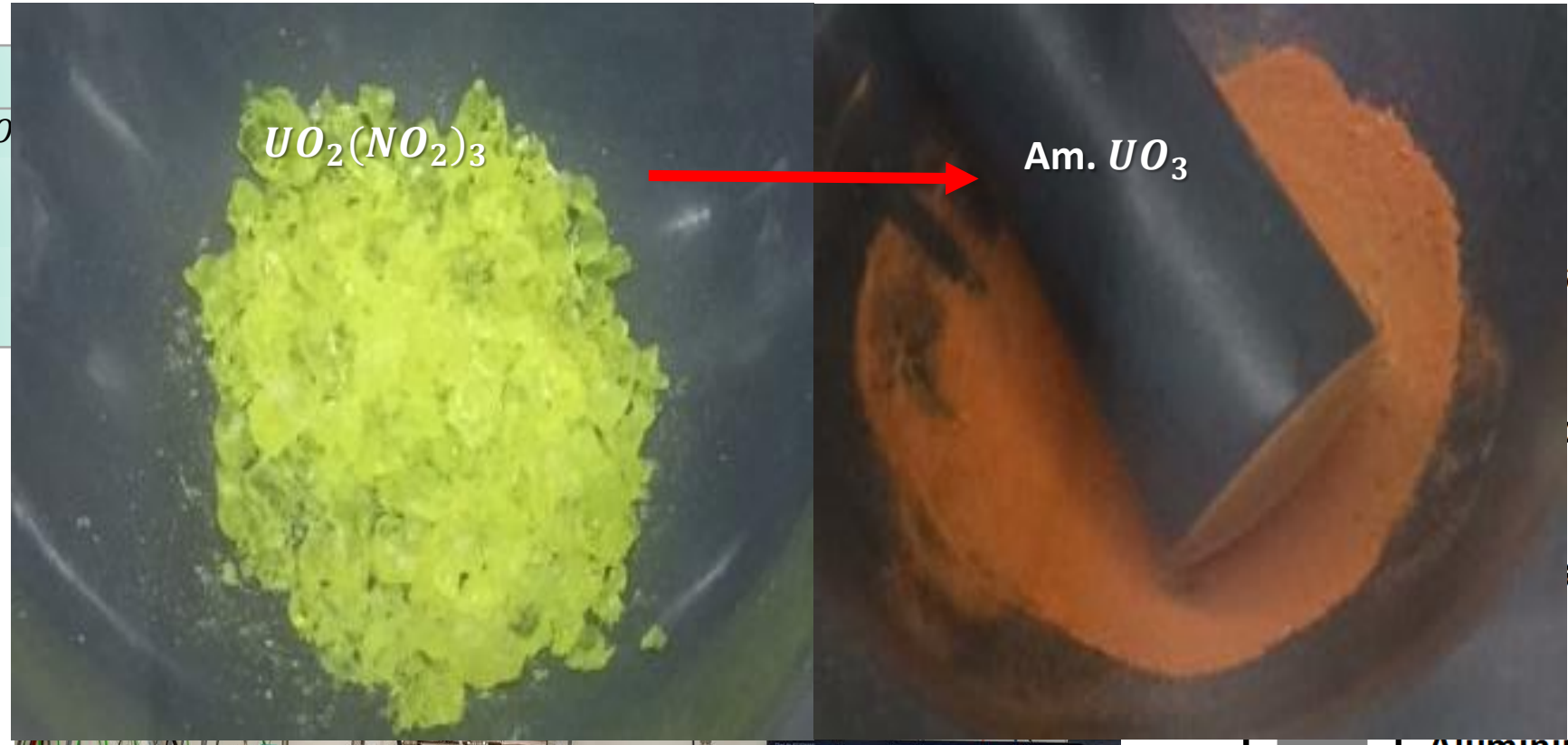

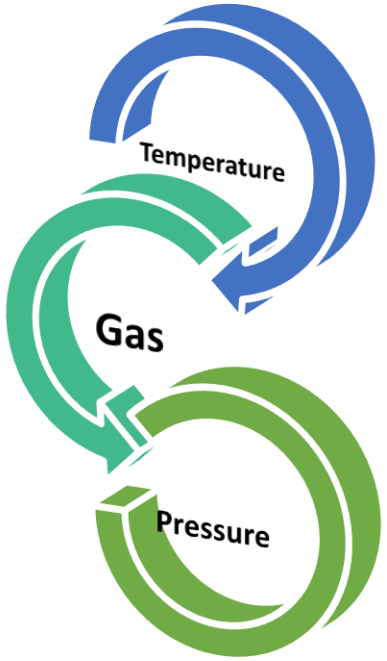

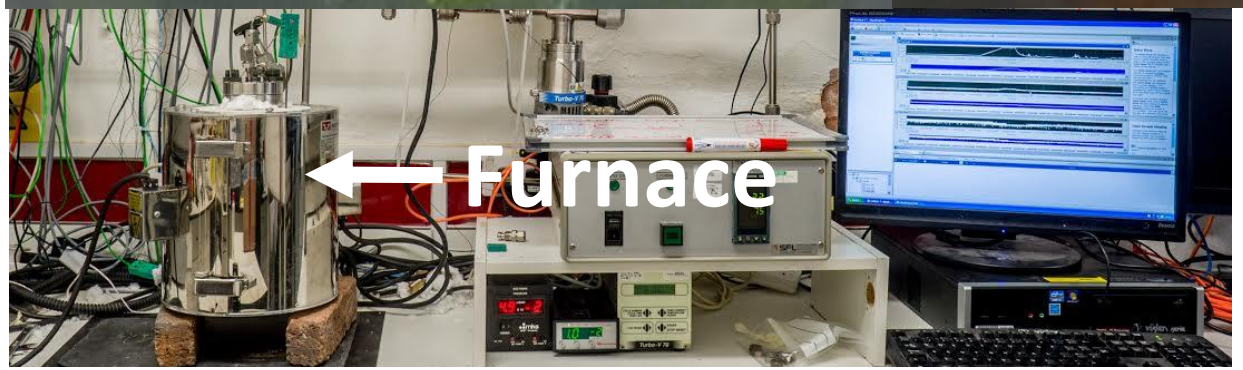

alve

er gasket seal

ss Steel

Aluminium Shell

Research Councils UK Energy For a Low Carbon Future

DISTINCTIVE

X-ray Diffraction

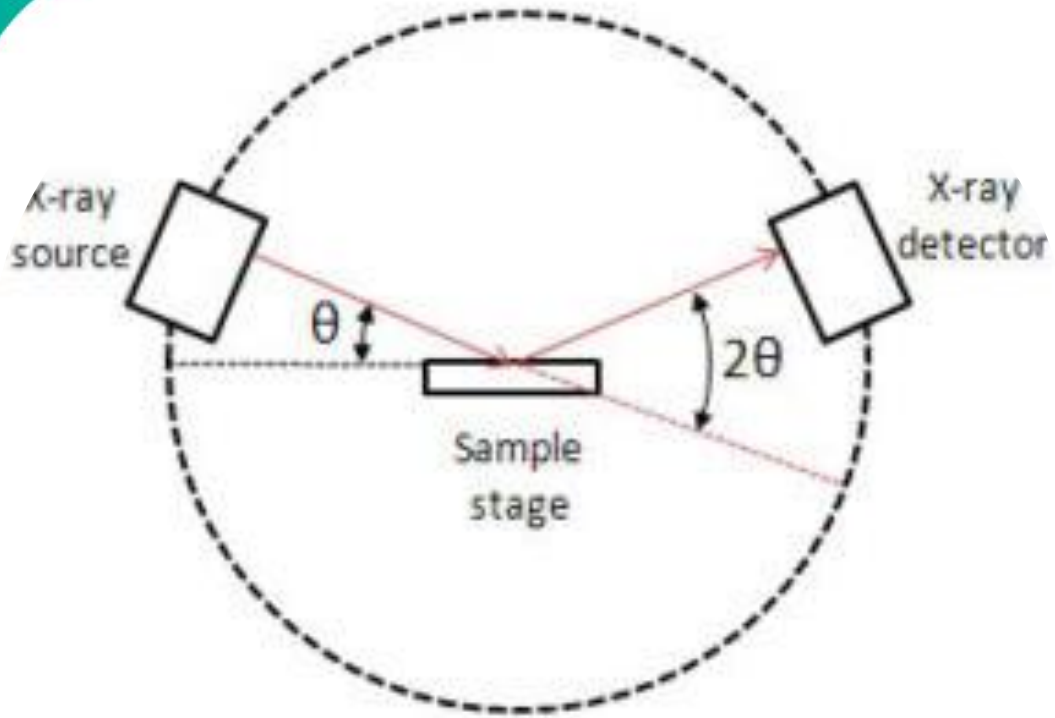

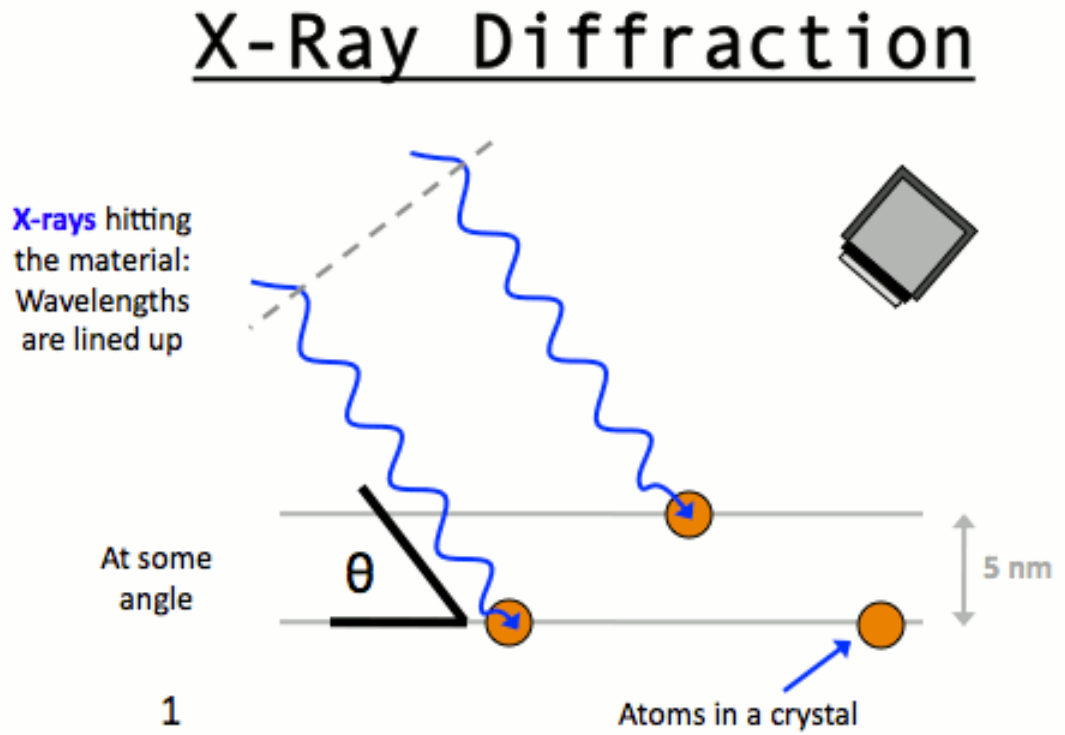

Benefits

- Useful at looking at crystalline material
- Shows phase identification
- Characterise atomic structure
- Non-destructive characterisation technique

Research Councils UK Energy For a Low Carbon Future

DISTINCTIVE

U-oxide Powders Characterisation

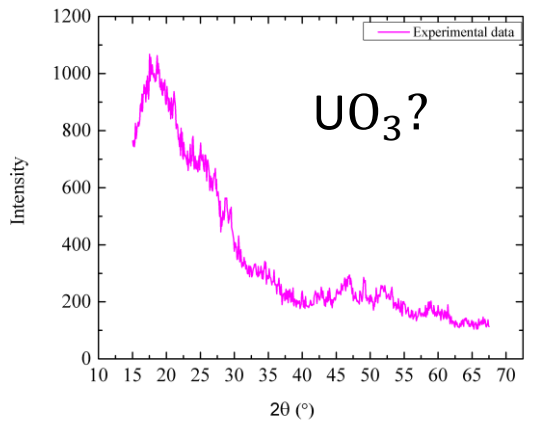

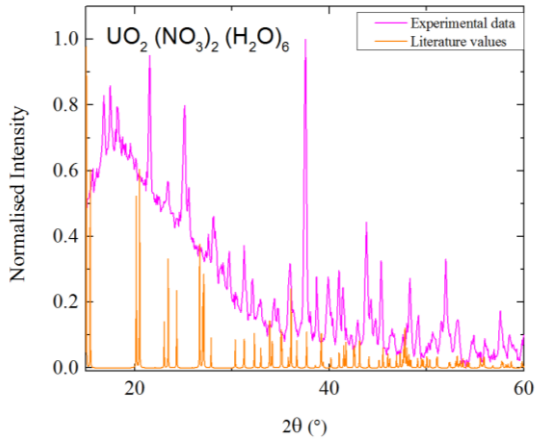

Uranyl Nitrate Hexahydrate

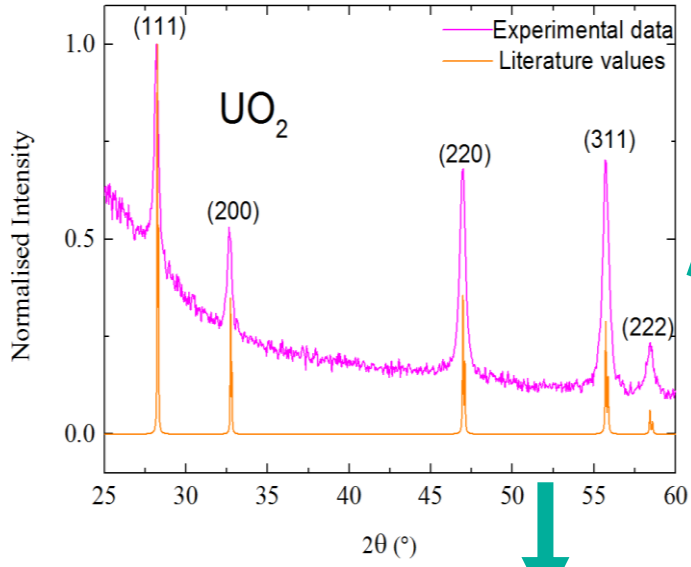

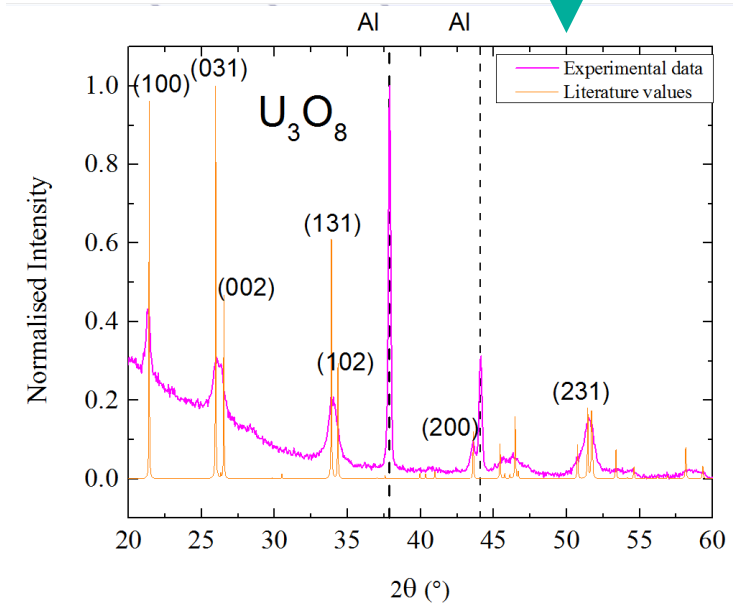

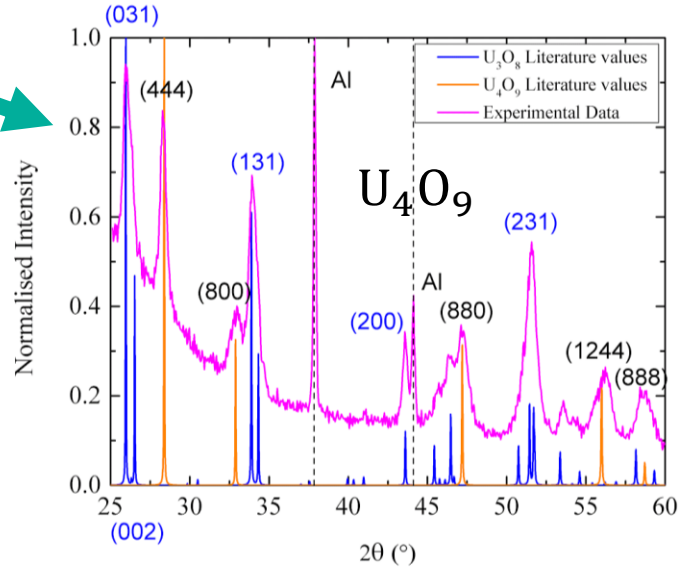

Research Councils UK Energy For a Low Carbon Future

DISTINCTIVE

Raman Scattering and Spectroscopy

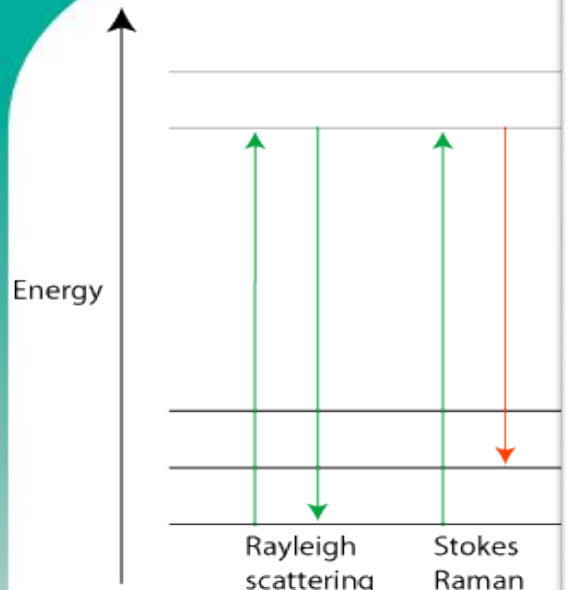

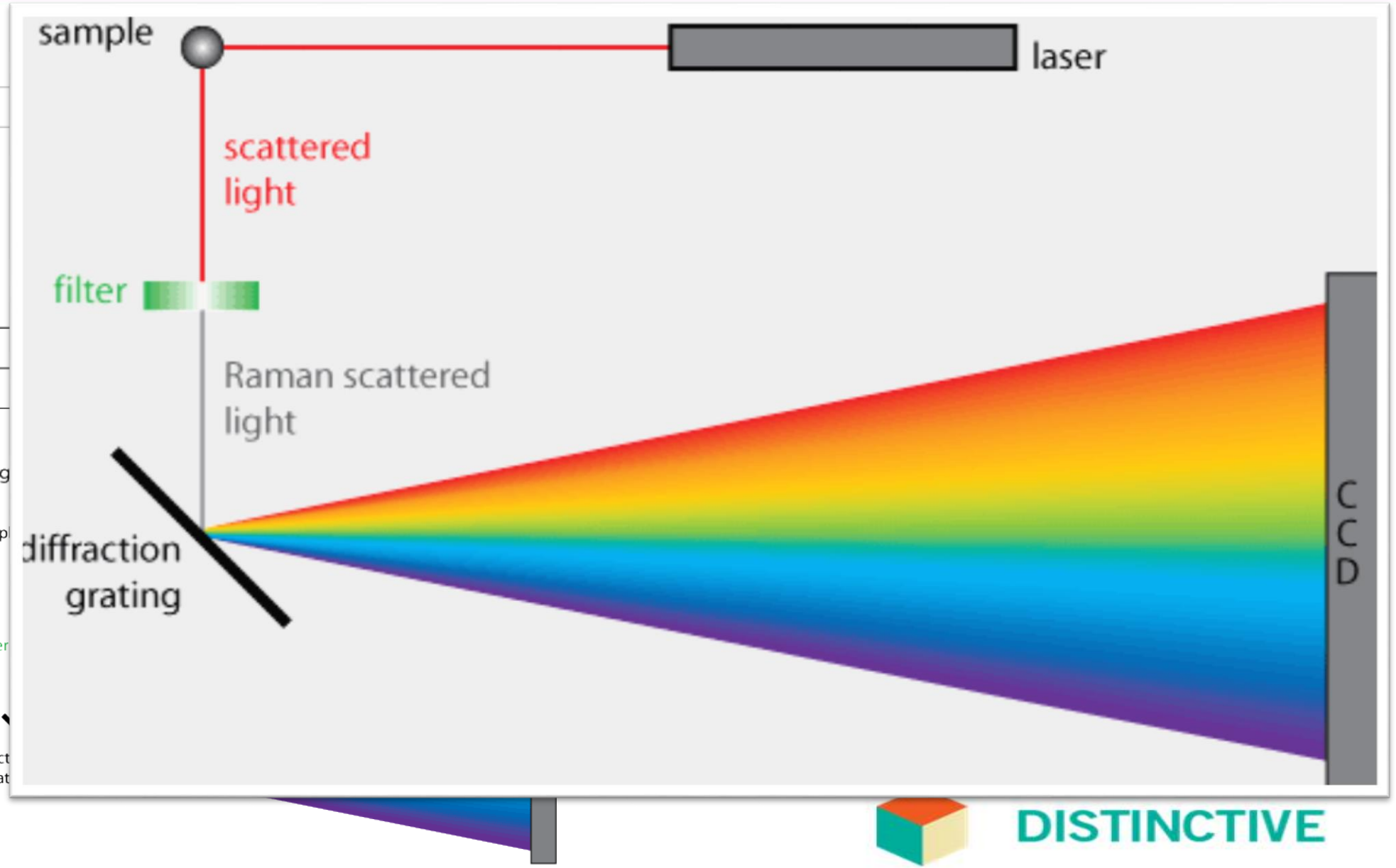

Raman Data

TABLE II. Summary of Raman spectra obtained for UO_2, U_3O_8, and UO_3 using micro-Raman spectroscopy.[a]

UO_2	γ-UO_3	α-U_3O_8	Band assignment
		343 m	U–O stretching vibration
		351 m	
445 s		412 s	U–O stretching vibration
		483 s	
	768 s	738 m	O–U–O–U stretching vibration
	846 m	811 s	U–O stretching vibration

[a] All frequencies in cm^{-1}; s = strong; m = medium.

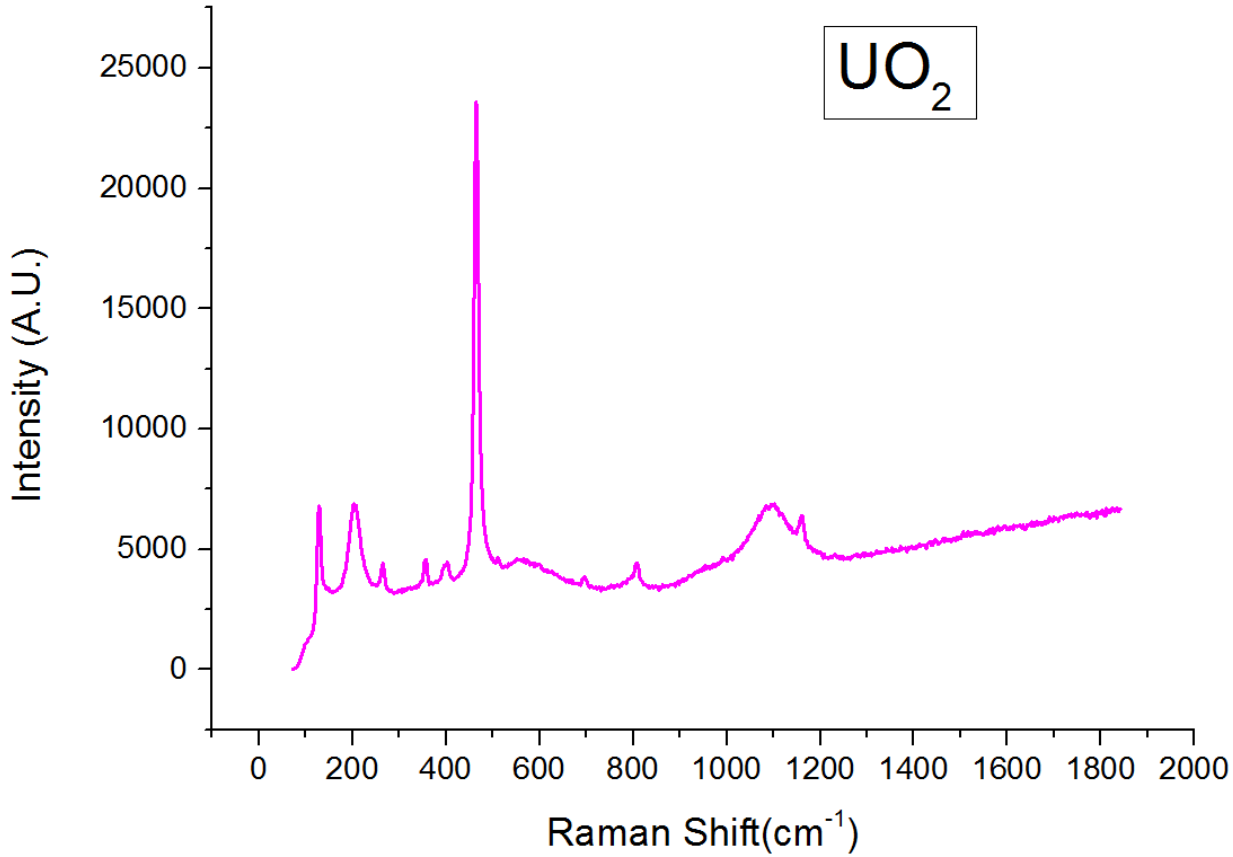

Probe Design

Raman Generation

Light absorption through water

Digital capabilities

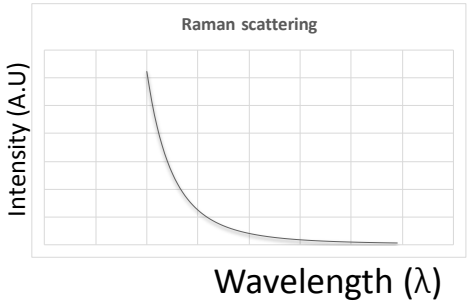

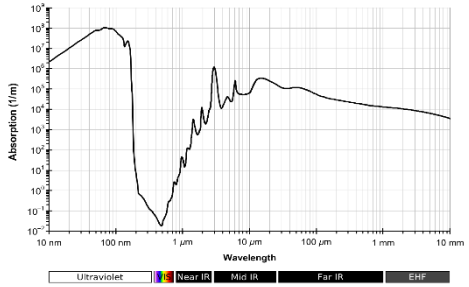

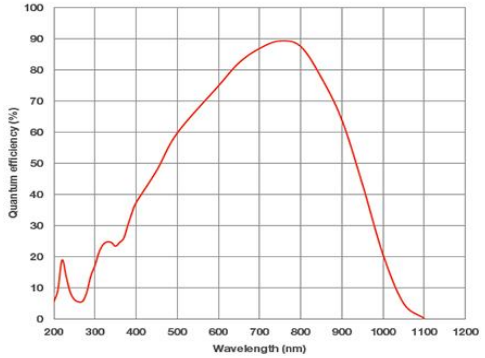

Addition of Reference library

Raman data over a range of wavelengths

Research Councils UK Energy For a Low Carbon Future

DISTINCTIVE

Analysis

Sample fabrication

Successfully manufactured UO_2 & U_3O_8

Made mixed phase U_4O_9

Will need to refine UO_3 synthesis process

XRD Analysis

Successfully showed UO_2 & u_3O_8

Showed the U_4O_9 needs to be repeated at a lower temperature

Confirmed UO_3

Raman Analysis

Fabricate more samples

Perfect sample preparation: thinner sealed glass

The next step…

- Prepare powders for improved Raman data
- Complete Raman Analysis with multiple wavelengths
- Move onto non active samples!

Research Councils UK Energy For a Low Carbon Future

DISTINCTIVE

To Conclude…

- This data will provide a good understanding of any uranium oxides in the sludge matrix
- Synthesis of U-oxides has been a fairly successful venture
- Raman samples needs improvement and then data can be taken
- All non active samples can now go through the same process
- XRD > Raman > addition wavelengths
- With combining all of this information, a new iteration of a probe can be built!

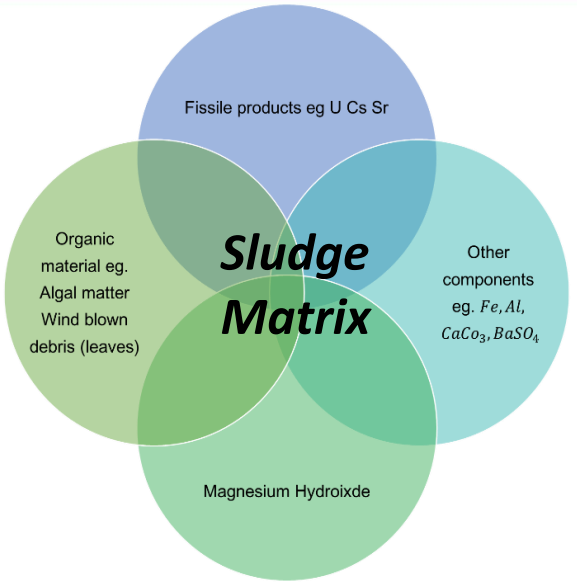

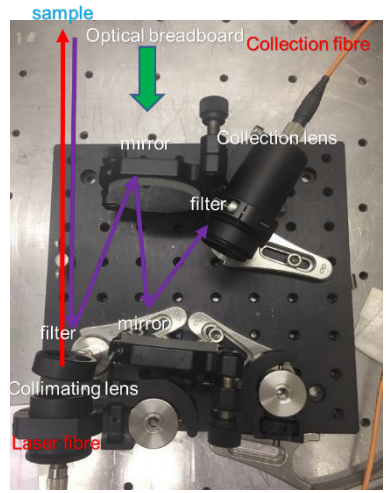

Acknowledgements:

Bill Rogerson, Sellafield Ltd.

Sellafield Ltd

Sophie Rennie, Bristol IAC

Ross Springell, Bristol IAC

Any Questions?

Research Councils UK Energy For a Low Carbon Future

DISTINCTIVE

Simultaneous 3D reconstruction and material/object recognition for nuclear wastes

Henry Cheng Zhao, Kevin Li Sun and Rustam Stolkin
Extreme Robotics Lab, University of Birmingham, UK
Tom Robinson
Sellafield Ltd, Whitehaven, UK

Meeting Title 3rd DISTINCTIVE Annual Meeting
Date 05-06/04/2017
Location York

Research Councils UK Energy For a Low Carbon Future

DISTINCTIVE

Motivation

Decommissioning the UK's 4.9 million tonnes of legacy nuclear waste represents the largest environmental remediation project in the whole of Europe, expected to cost £90-220 billion over the next 100 years.

It is expected that at least 20% of these costs (order £40billion) must be spent on robotic interventions inside radioactive zones which are too hazardous for humans to enter.

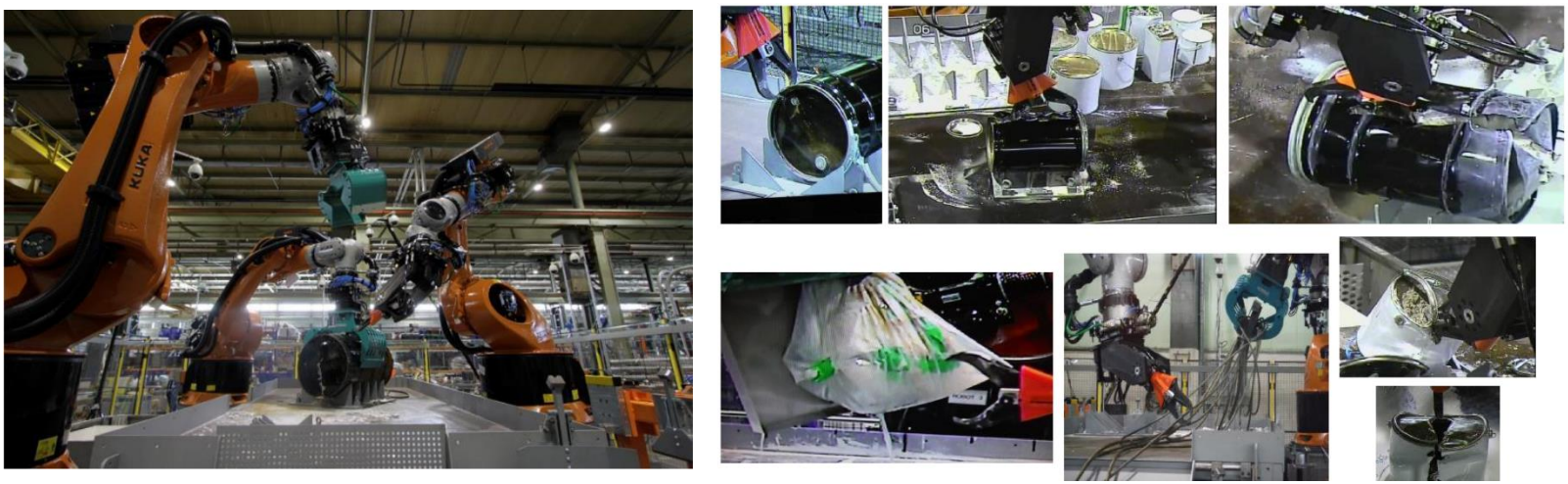

The KUKA robot arm and the nuclear wastes.

Research Councils UK Energy For a Low Carbon Future

DISTINCTIVE

Motivation

My work focuses on the use of advanced computer vision methods for 3D characterization of buildings, scenes or objects, during nuclear decommissioning, especially decommissioning operations which rely on robotic interventions.

A new computer vision methods is developped for real-time, semantic, 3D reconstruction of nuclear waste scenes. This involves real-time 3D reconstruction of a scene, but also involves simultaneously recognising different types of materials or objects that are present in the scene, and using these material/object categories to “semantically” label all parts of the 3D scene model.

I will introduce three pieces of completed work:

1. A 2D-3D nuclear waste database and virtual system for automatically labelling.
2. Real-time RGB-D nuclear object detection and recognition.
3. Real-time simultaneous 3D reconstruction and material recognition.

Research Councils UK Energy For a Low Carbon Future

DISTINCTIVE

2D-3D nuclear dataset

A 2D-3D nuclear waste database has been built. This dataset includes the metal, can, wood, bottle, brick, chain, pipe, sponge, glove, fabric and etc. It contains a large number of RGB images, depth images and 3D point cloud models.

Millions of labelled RGB-D image can be obtained from different viewpoints using our virtual camera system for training a neural network.

Samples of 2D-3D nuclear material database.

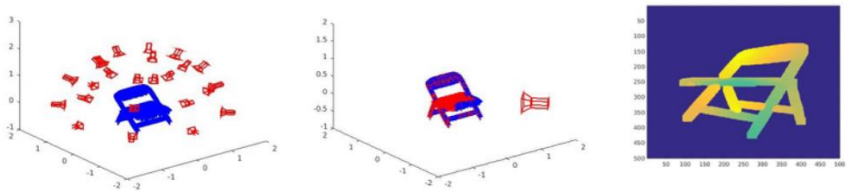

The virtual camera system.

Research Councils UK Energy For a Low Carbon Future

DISTINCTIVE

Real-time RGB-D nuclear object recognition

This work proposed a novel weakly-supervised deep learning approach (DCNN-GPC) for end-to-end learning using minimal annotated data (approximately 50 for each category) by propagating minimal labels to large-scale unlabeled data.

Our proposed pipeline has three steps: (1) a real-time 3D-based object detection approach is proposed to generate high-quality objectness proposals in RGBD video stream; (2) DCNN-GPC is proposed to propagate small-scale labeled data to moderate-scale in order to train the multi-modal DCNN end-to-end; (3) a real-time detection and recognition system is integrated.

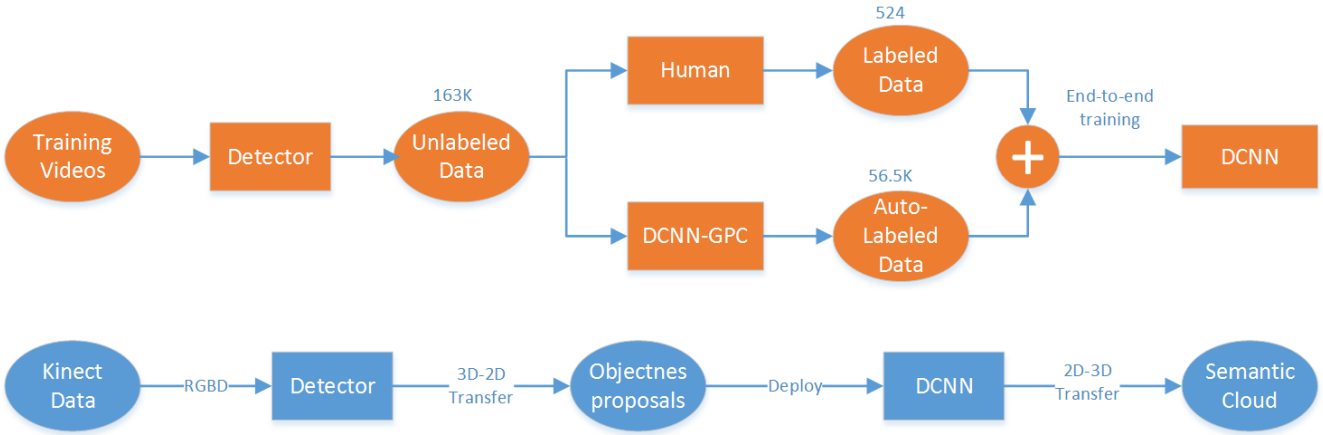

Flow chart of our proposed weakly-supervised DCNN method. Training is shown in orange and deployment in blue.

Research Councils UK Energy For a Low Carbon Future

DISTINCTIVE

Real-time RGB-D nuclear object recognition

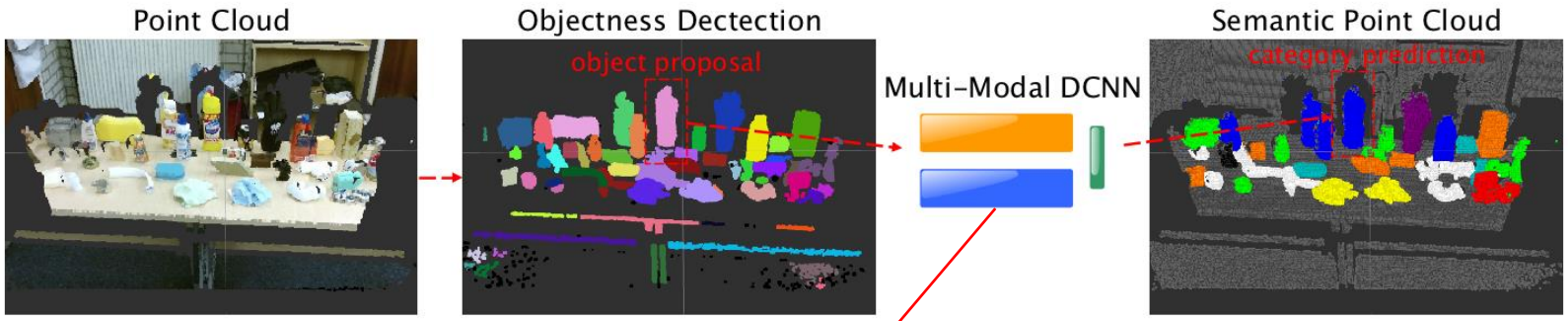

Detection and recognition pipeline of our system. RGBD point cloud (left) yields objectness proposals (middle). For each such proposal, the multi-modal DCNN performs category recognition. The pixel-wise recognition result is projected to obtain a 3D semantic cloud.

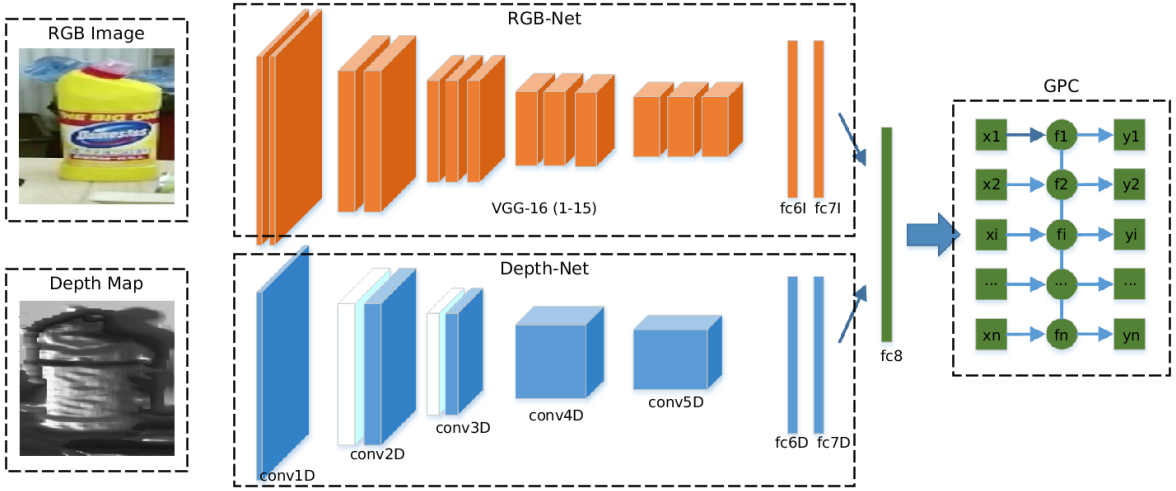

The architecture of proposed multi-modal DCNN-GPC. The inputs of the DCNNs are the raw RGB image and depth map of the object proposal. Our architecture consists of three components: RGB-Net (shown in yellow) Depth-Net (shown in Blue) and non-parametric GPC (shown in Green).

Research Councils UK Energy For a Low Carbon Future

DISTINCTIVE

Real-time RGB-D nuclear object recognition

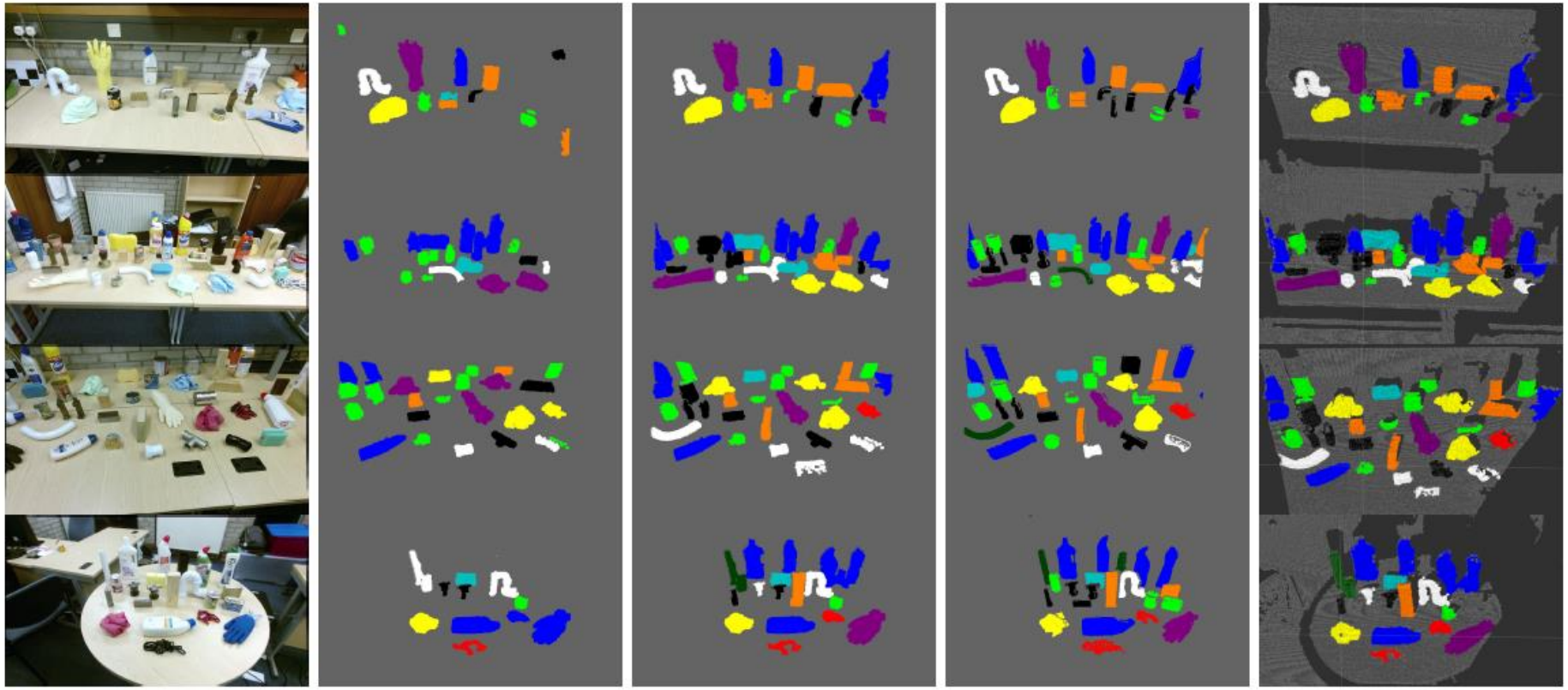

The qualitative results. From left to right: RGB images, 2D semantic maps of R-CNN, 2D semantic maps of our method, the ground truth, and 3D semantic maps of our method.

Research Councils UK Energy For a Low Carbon Future

DISTINCTIVE

Real-time RGB-D nuclear object recognition

Category	bottles	cans	chains	cloth	gloves	metal obj.	pipe join.	plas. pipe	sponges	wood bloc.	overall/ave.
Instance Amount	28 / 12	22 / 15	8 / 3	6 / 3	16 / 5	22 / 10	9 / 5	10 / 4	12 / 6	14 / 7	147 / 70
Videos	4	2	2	4	4	4	2	2	2	3	23
Unlabelled T.E.	20.5K	32.5K	18.3K	13.3K	8.6K	22.1K	21.9K	8.0K	9.0K	14.0K	163K
Labelled T.E.	48	56	26	45	35	48	28	20	32	32	524
GP Labelled T.E.	11436	15525	2322	4606	5298	6101	2287	1037	3223	4734	56.5K
Precise of R-CNN (inst.w.)	68.10%	72.57%	69.77%	62.26%	48.94%	60.00%	44.58%	72.22%	62.26%	67.86%	64.63%
Recall of R-CNN (inst.w.)	53.02%	70.95%	78.95%	70.21%	41.82%	50.85%	45.17%	46.43%	53.52%	16.96%	52.30%
F-Score of R-CNN (inst.w.)	59.62%	71.75%	74.07%	66.00%	45.10%	55.05%	45.02%	56.52%	57.57%	27.14%	57.81%
Precise of Ours (inst.w.)	89.19%	81.82%	79.17%	93.33%	68.25%	75.00%	66.67%	63.16%	92.45%	87.84%	**80.85%**
Recall of Ours (inst.w.)	83.19%	91.84%	95.00%	80.00%	91.49%	64.04%	90.20%	50.00%	87.50%	87.84%	**83.53%**
F-Score of Ours (inst.w.)	86.09%	86.54%	86.36%	86.15%	78.18%	69.09%	76.67%	55.81%	89.91%	87.84%	**82.17%**
Precise of R-CNN (pix.w.)	66.75%	63.55%	68.09%	58.03%	55.24%	45.35%	57.30%	43.81%	55.09%	59.43%	59.46%
Recall of R-CNN (pix.w.)	47.50%	58.85%	48.55%	56.75%	34.99%	36.34%	53.04%	10.21%	45.21%	13.44%	42.06%
F-Score of RCNN (pix.w.)	55.50%	61.11%	56.69%	57.38%	42.84%	40.35%	55.09%	16.57%	49.67%	21.93%	49.27%
Precise of Ours (pix.w.)	83.15%	70.18%	75.97%	89.62%	66.97%	69.96%	61.97%	60.59%	84.27%	86.87%	**75.52%**
Recall of Ours (pix.w.)	75.41%	70.94%	66.21%	70.77%	75.12%	48.58%	85.41%	37.08%	68.44%	72.66%	**70.39%**
F-Score of Ours (pix.w.)	79.09%	70.56%	70.75%	79.09%	70.81%	57.34%	71.83%	46.01%	75.54%	79.13%	**72.87%**

Statistics of our dataset, training examples, and quantitative results of our proposed detection/recognition system. Detection precision rate, recall rate and f-score of each category are given. T.E stands for training examples, inst.w. for instance-wise and pix.w. for pixel-wise.

Research Councils UK Energy For a Low Carbon Future

DISTINCTIVE

Real-time RGB-D nuclear object recognition

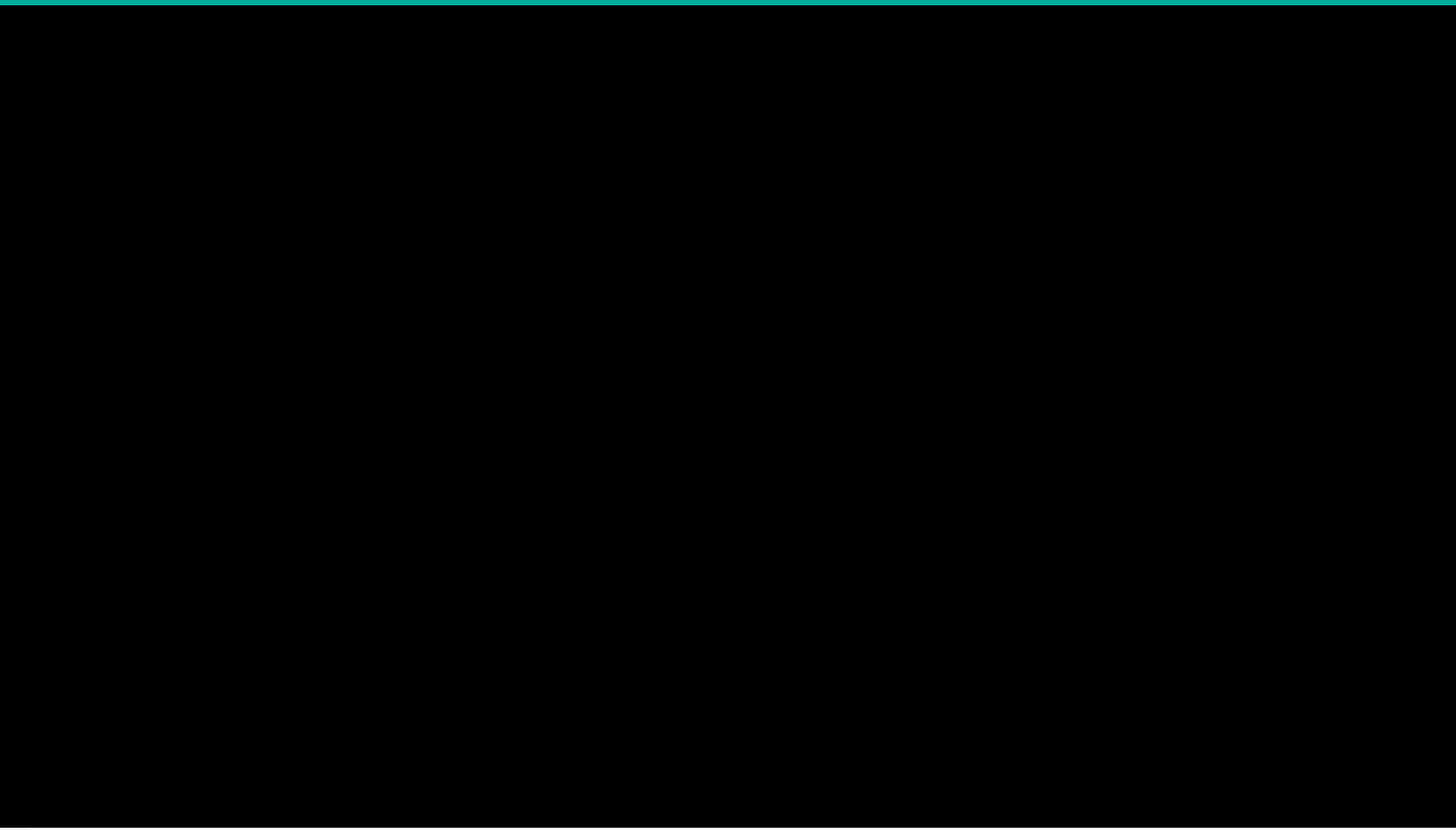

The paper link: [Weakly-supervised DCNN for RGB-D object recognition in real-world applications which lack large-scale annotated training data]

Real-time simultaneous 3D reconstruction and material recognition

This work proposed the first system for simultaneous 3D reconstruction and material recognition. It is a real-time, fully end-to-end system, which does not require hand-crafted features or post-processing CRF optimization. Its run-time performance can be boosted to around 10Hz, enabling real-time 3D semantic reconstruction with a 30fps camera.

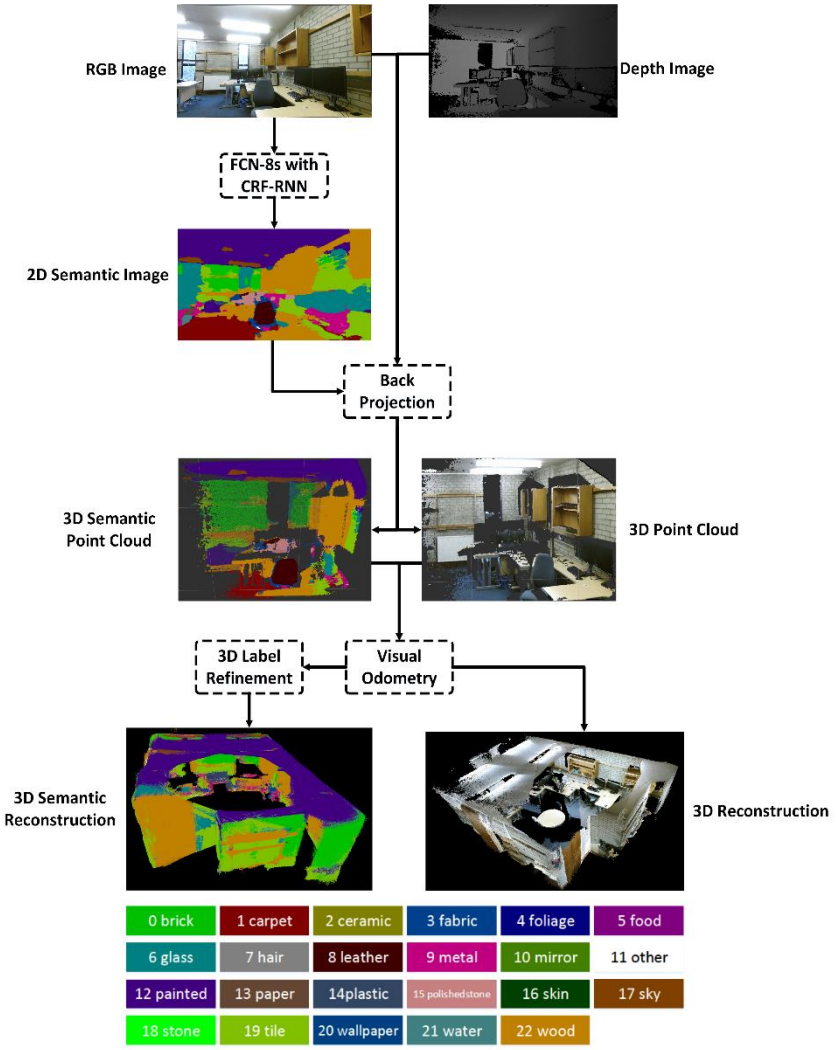

Pipeline of proposed simultaneous 3D reconstruction and material recognition system. Firstly, FCN-8s with CRF-RNN is employed for 2D material recognition using the RGB image from RGB-D camera. Then the semantically labeled RGB image, and the corresponding depth image, are combined together through back-projection to generate a semantic point cloud for each key frame. Finally, all semantic point clouds are combined incrementally using visual odometry, and Bayesian update is employed for label probability refinement.

Research Councils UK Energy For a Low Carbon Future

DISTINCTIVE

Real-time simultaneous 3D reconstruction and material recognition

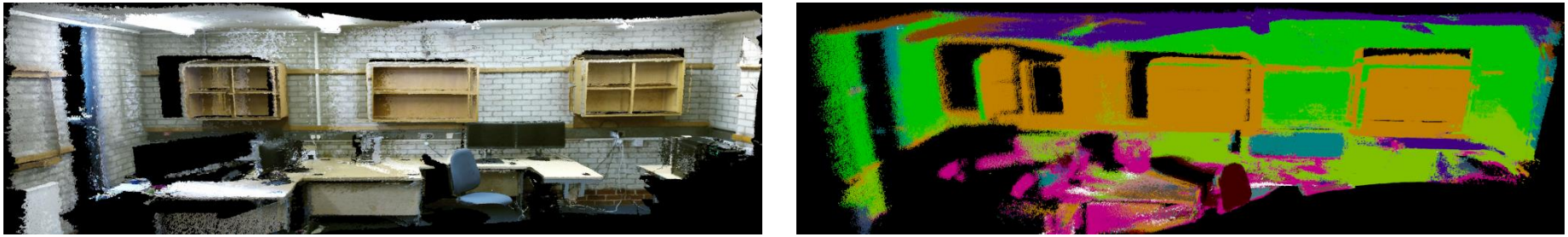

**Qualitative results of 3D semantic reconstruction in a multi-material office:
(a) Local 3D map. (b) Local 3Dsemantic map.**

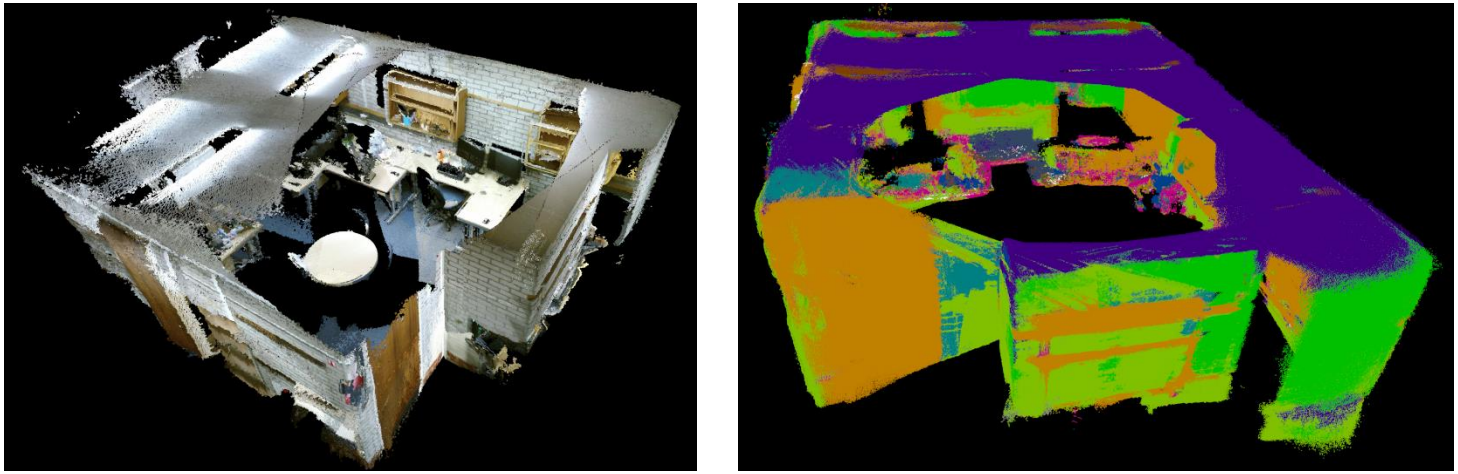

**Qualitative results of 3D semantic reconstruction in a multi-material office:
(a) Global 3D map. (b) Global 3Dsemantic map.**

Research Councils UK Energy For a Low Carbon Future

DISTINCTIVE

Real-time simultaneous 3D reconstruction and material recognition

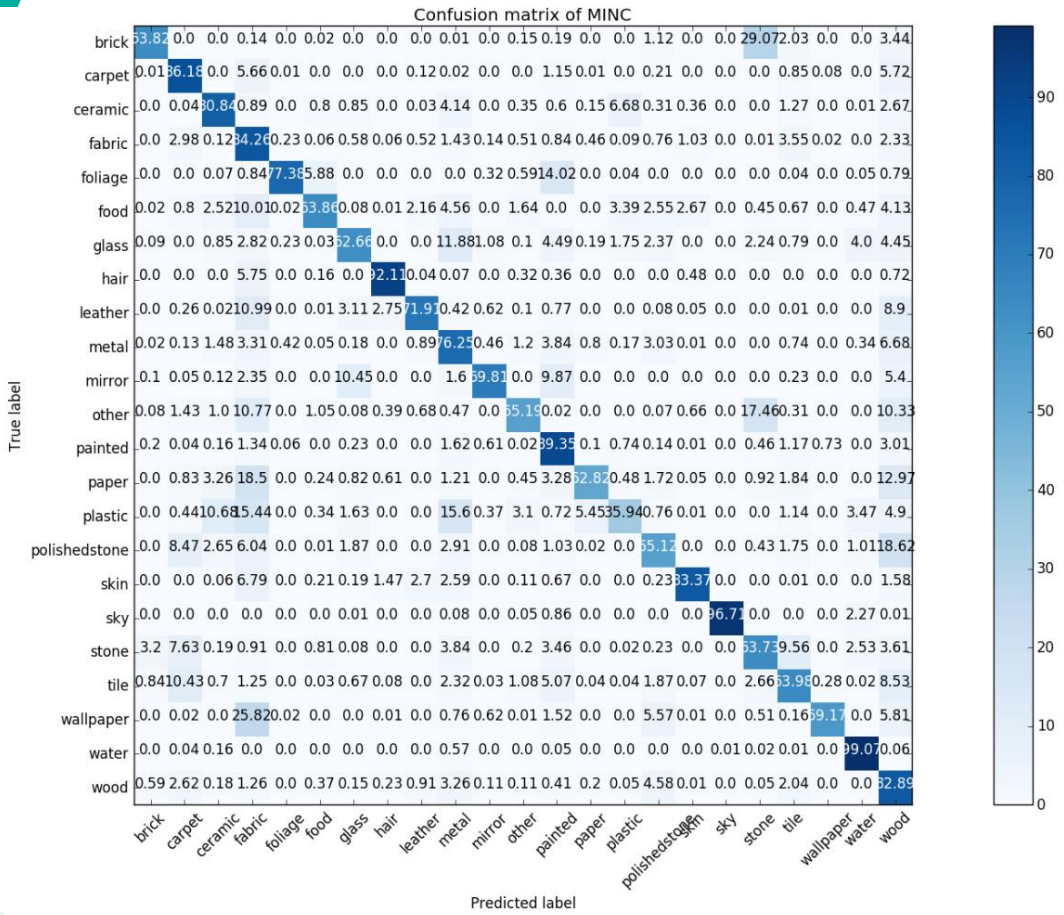

Quantitative results of material recognition: confusion matrices of FCN-8s with CRF-RNN.

	Pixel acc.	Mean acc.	Mean IU	f.w. IU
FCN-8s	78.41%	71.91%	56.51%	66.07%
FCN-8s with CRF-RNN	81.94%	77.07%	61.13%	69.99%

Quantitative results of material recognition. End-to-end FCN-8s with CRF-RNN improve 3.53%, 5.16%, 4.62% and 3.92% for pixel accuracy, mean accuracy, mean IU and frequency weighed IU respectively, compared with FCN-8s alone.

Research Councils UK Energy For a Low Carbon Future

DISTINCTIVE

Real-time simultaneous 3D reconstruction and material recognition

Research Councils UK Energy For a Low Carbon Future

The paper link: [A fully end-to-end deep learning approach for real-time simultaneous 3D reconstruction and material recognition]

DISTINCTIVE

Conclusions

Until now, three pieces of work have been completed:

1. A 2D-3D nuclear dataset and virtual camera system.

2. Weakly-supervised DCNN for RGB-D object recognition in real-world applications which lack large-scale annotated training data.

3. A fully end-to-end deep learning approach for real-time simultaneous 3D reconstruction and material recognition.

Thanks

Any questions?

Research Councils UK Energy For a Low Carbon Future

DISTINCTIVE

Radioactive Waste Management

Geological Disposal: deep down, you know it makes sense.

Dr Amy Shelton
Senior Research Manager

Date: 26/05/2017

Radioactive Waste Management

Radioactive Waste Management (RWM)

Wholly-owned NDA subsidiary (April 2014)

- Current headcount around 120 staff
- Plan for continued development into Site Licence Company

Vision

- A safer future by managing radioactive waste effectively, to protect people and the environment

Mission

- Deliver a geological disposal facility and provide radioactive waste management solutions

Radioactive Waste Management

Why do we need a GDF?

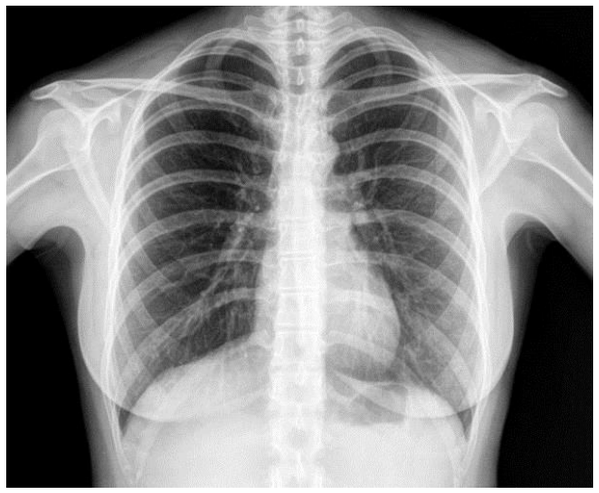

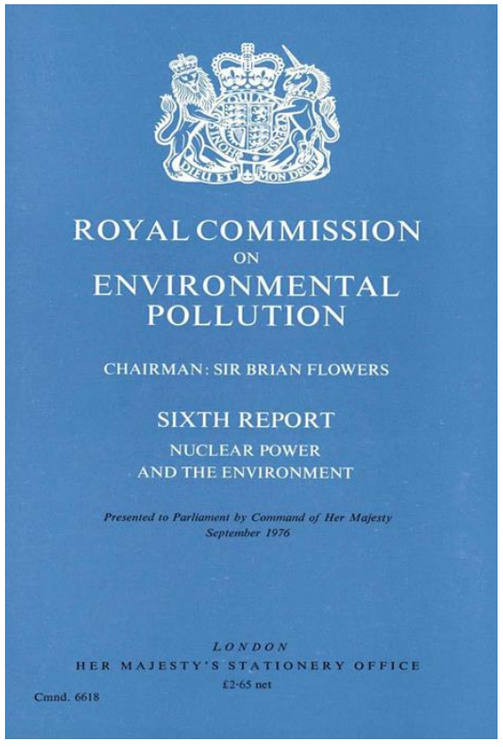

Radioactive Waste Management

Wastes (& potential wastes) for disposal

Low heat generating waste (LHGW)

- Intermediate Level Waste (ILW)

High heat generating waste (HHGW)

- High Level Waste (HLW)
- Spent Fuel (SF)
- Uranium & Plutonium

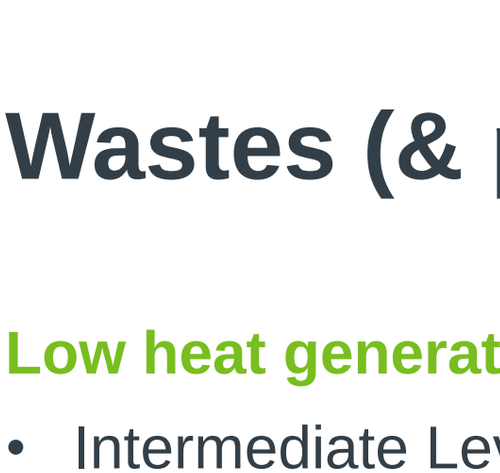

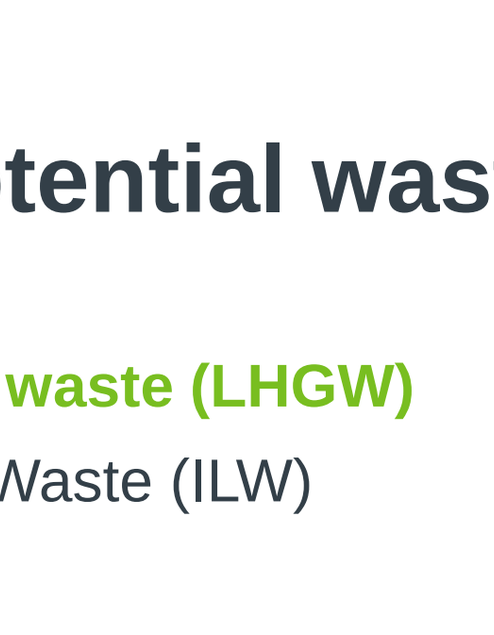

Radioactive Waste Management

What is geological disposal?

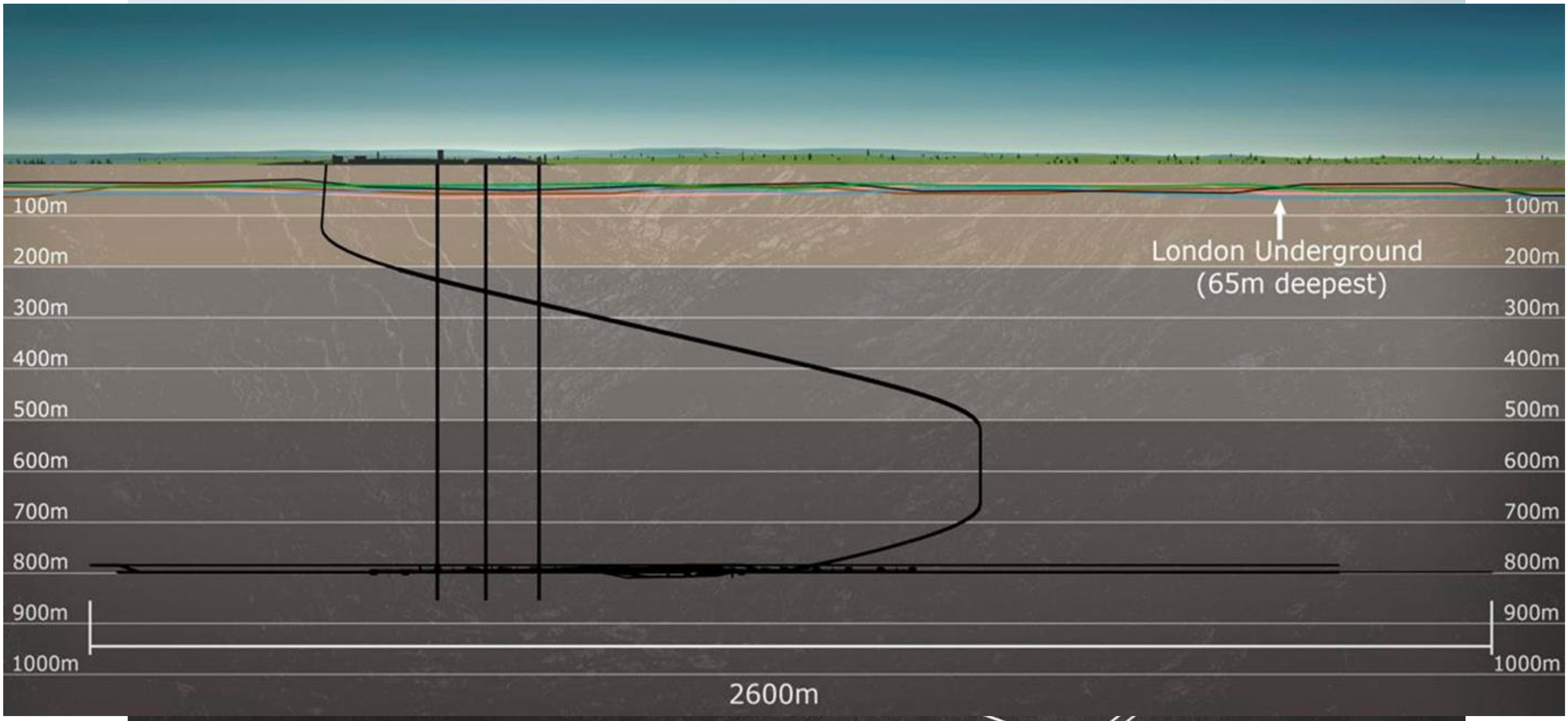

Drawing illustrative only, is not to scale and shows underground disposal tunnels and vaults

Radioactive Waste Management

What is geological disposal?

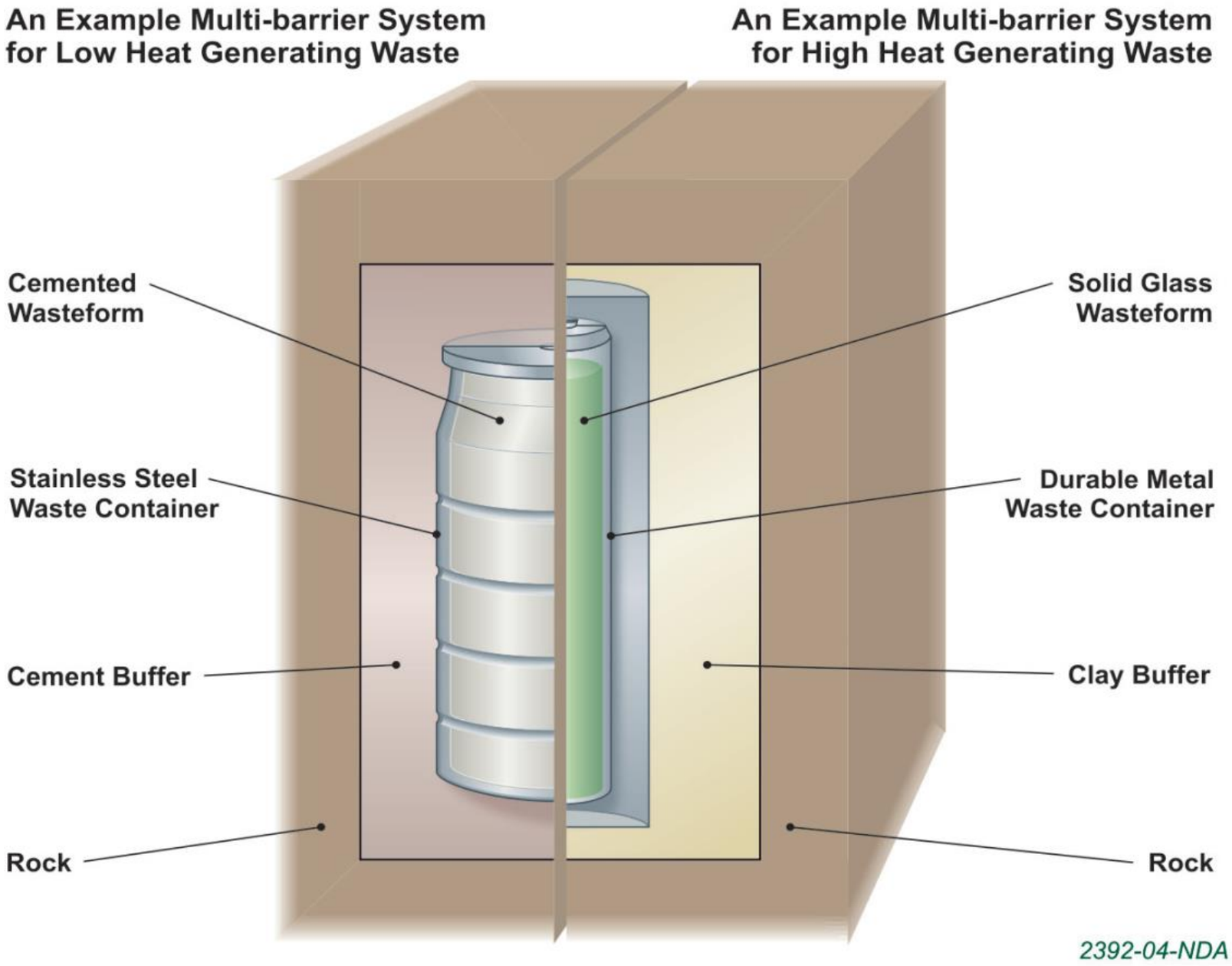

Radioactive Waste Management

What do other countries do?

- Geological disposal is recognised as the safest and most secure option for the long term management of radioactive waste and is therefore being pursued by all major nuclear nations.
- International collaboration offers the opportunity to expand our knowledge base by learning from the experience of others.

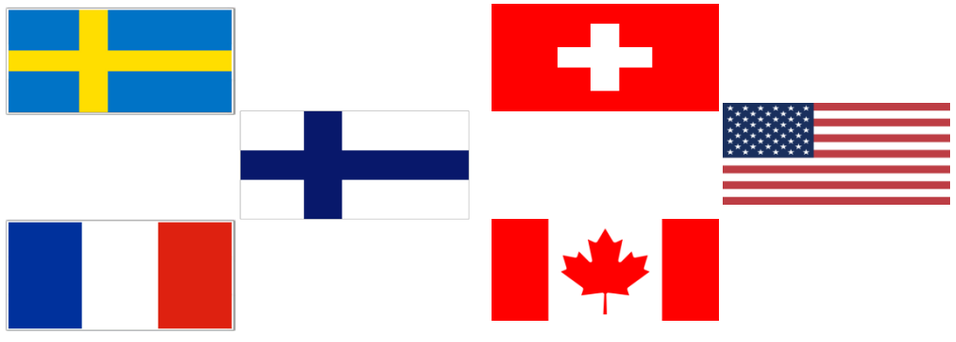

Radioactive Waste Management

Potentially suitable host rock types:

Lower Strength Sedimentary Rocks (e.g. clays, mudstones)

Jurassic mudstone:
Bure, France

Radioactive Waste Management

Potentially suitable rock types:

Higher Strength Rocks (e.g. granite, slate)

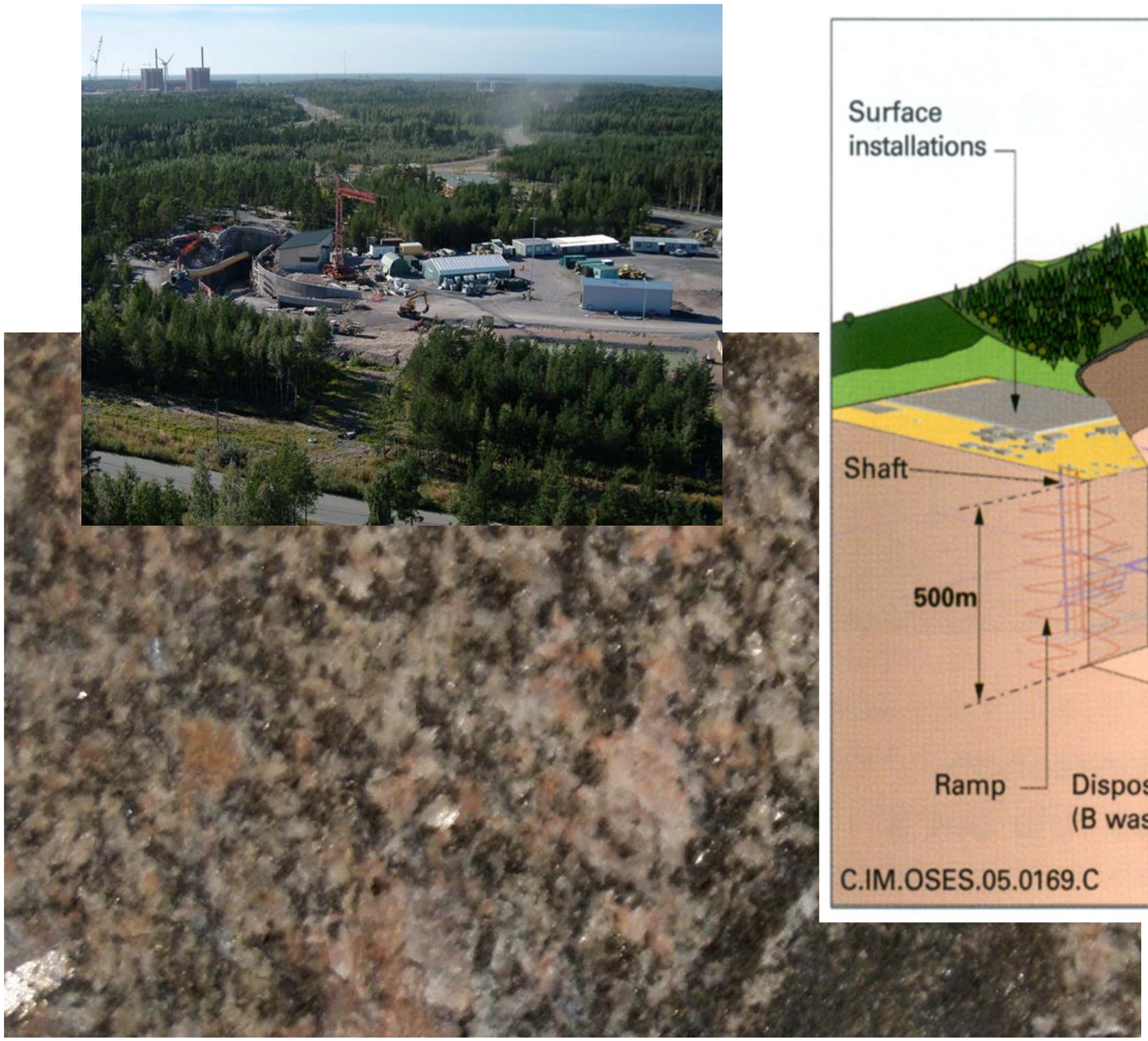

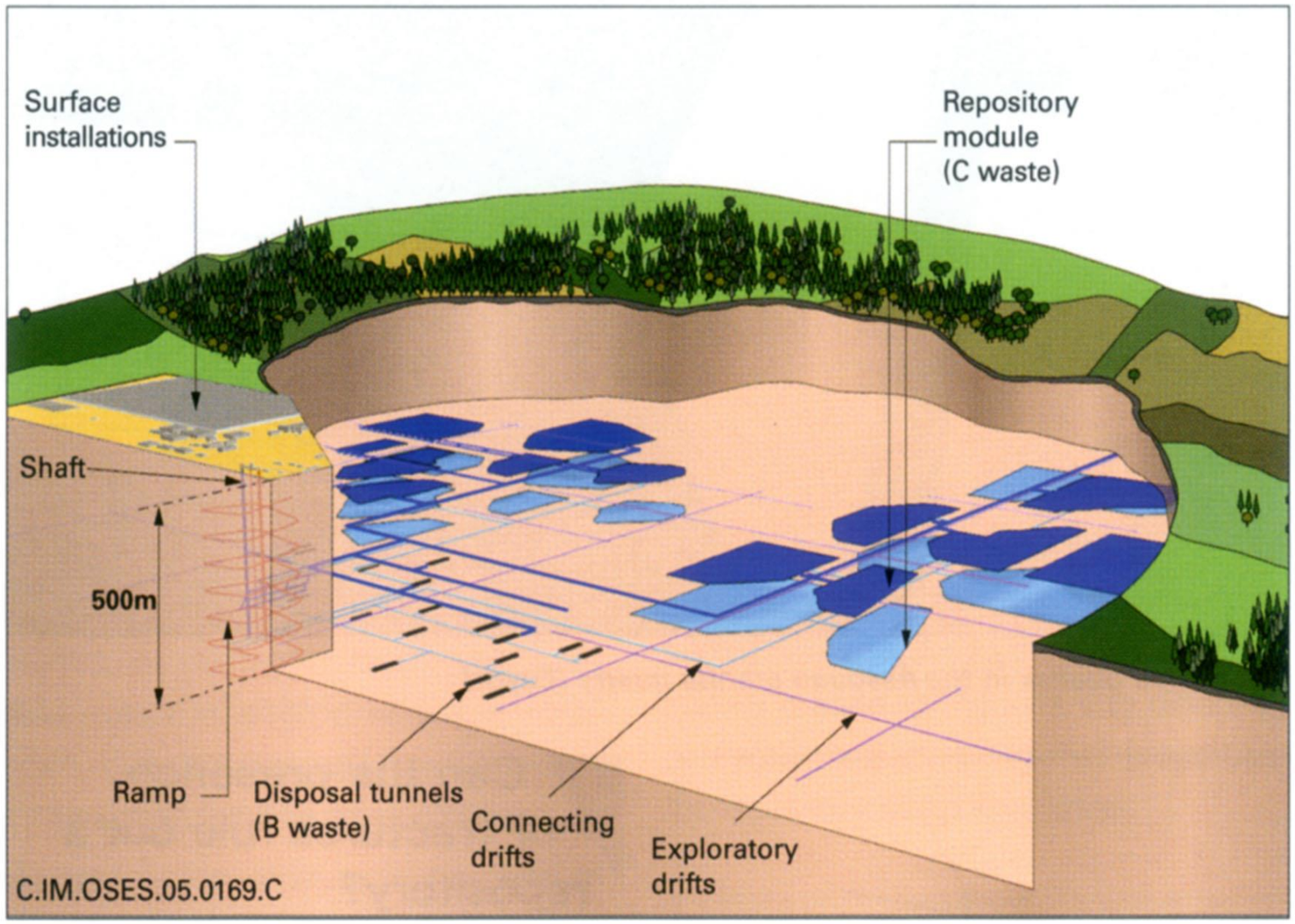

Forsmark granite: Sweden

Radioactive Waste Management

Potentially suitable rock types:

Evaporite (e.g. halite/ rock salt)

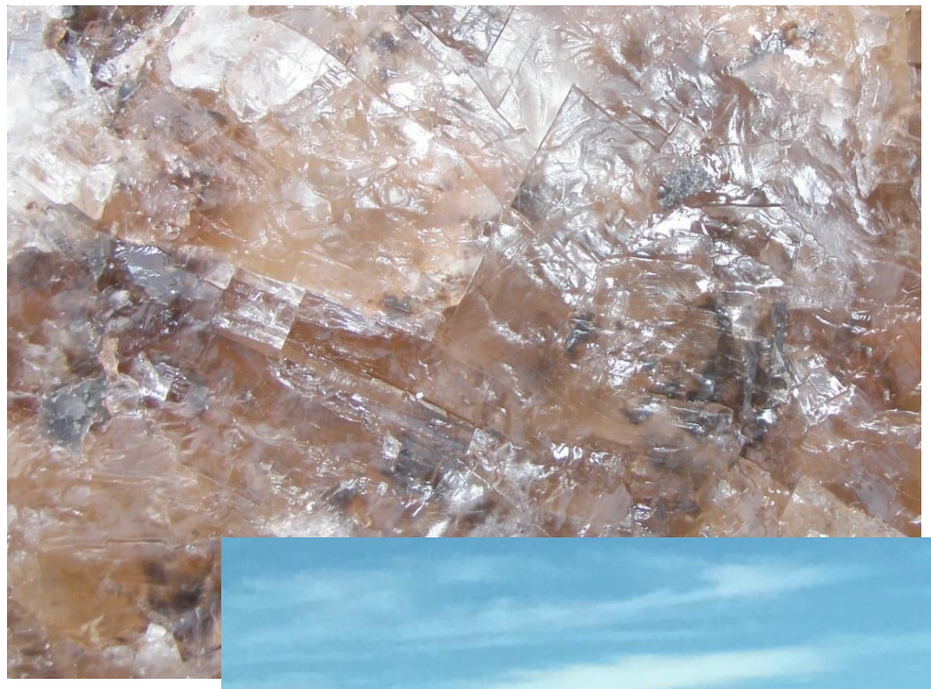

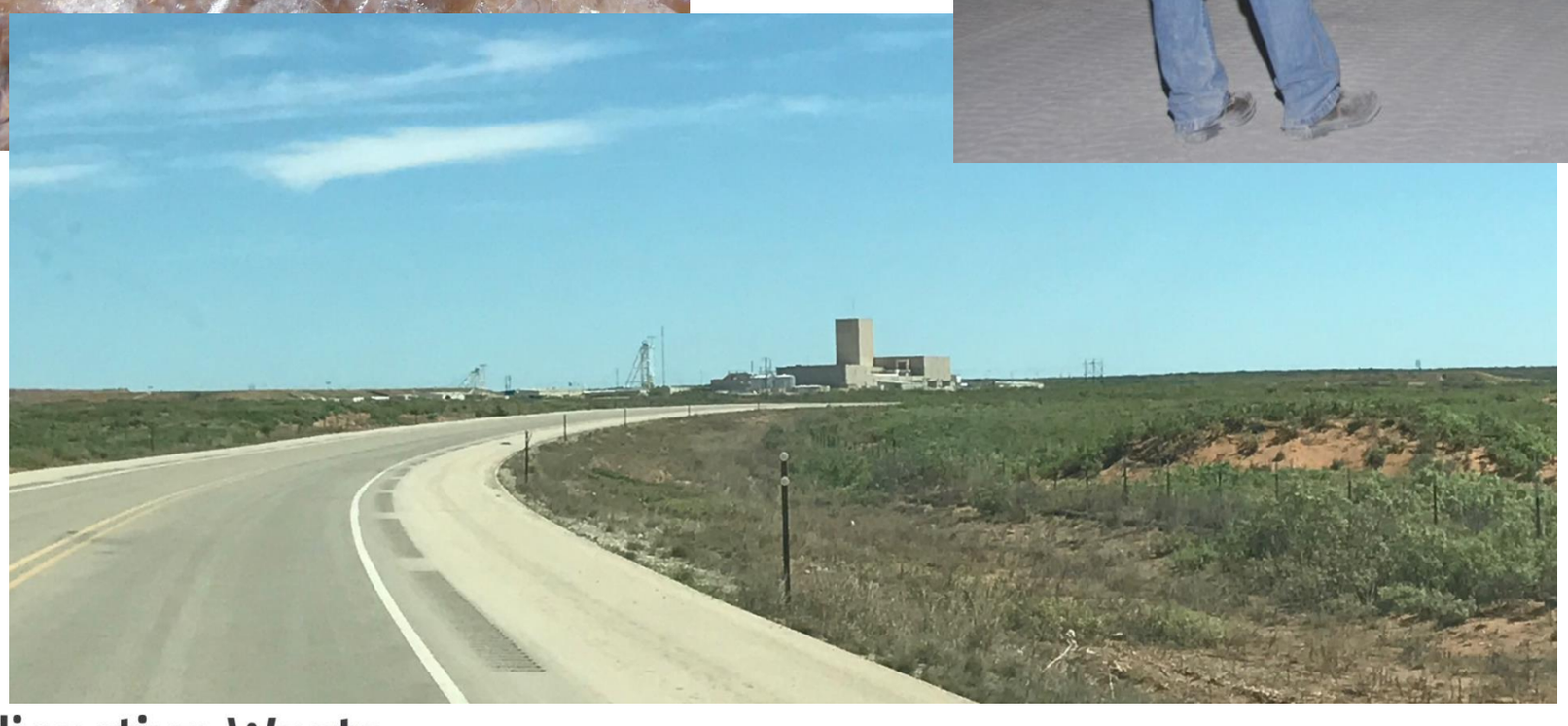

WIPP Site:
USA

Radioactive Waste Management

Generic Disposal System Safety Case

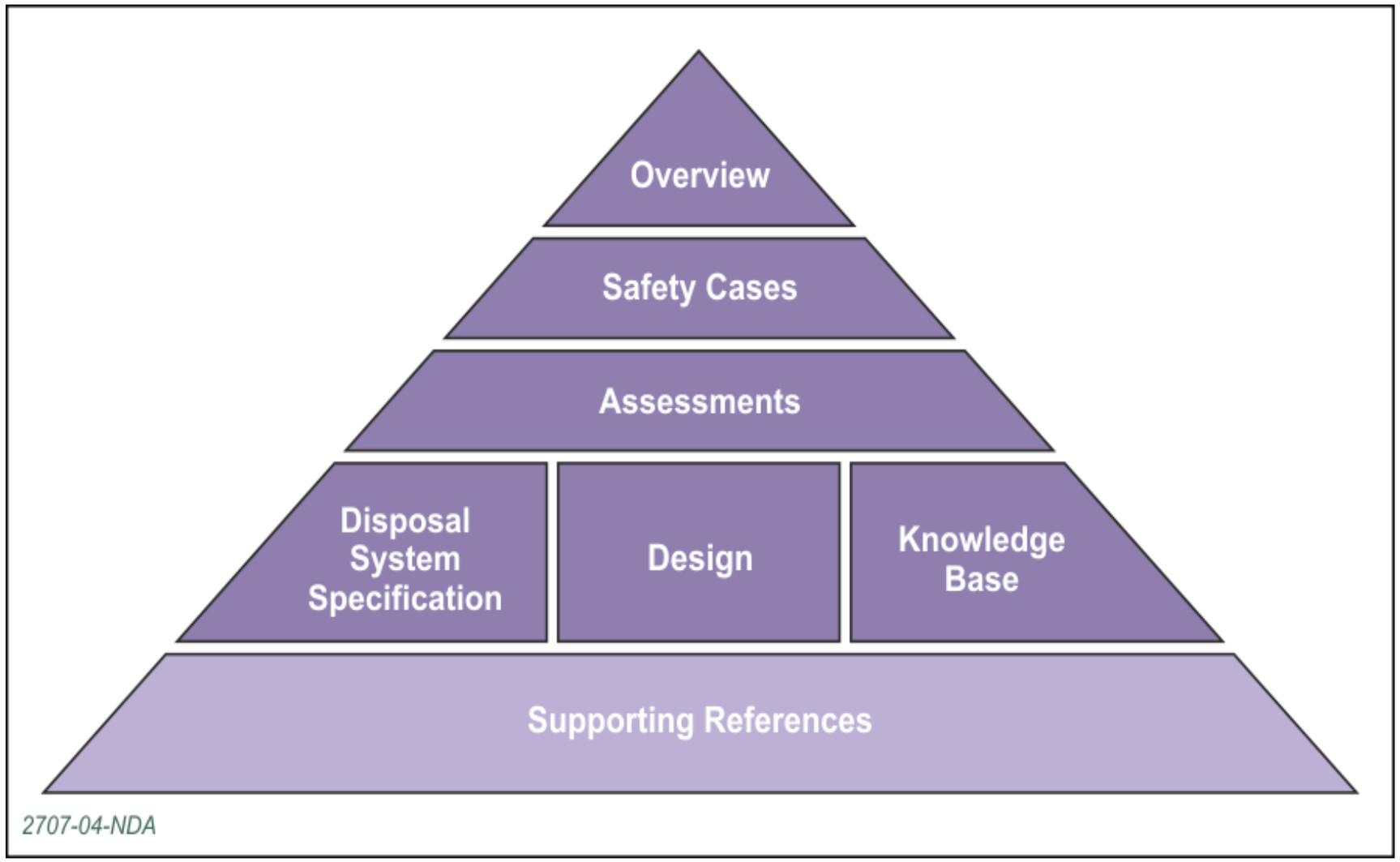

Radioactive Waste Management

Example disposal concept for low heat generating waste

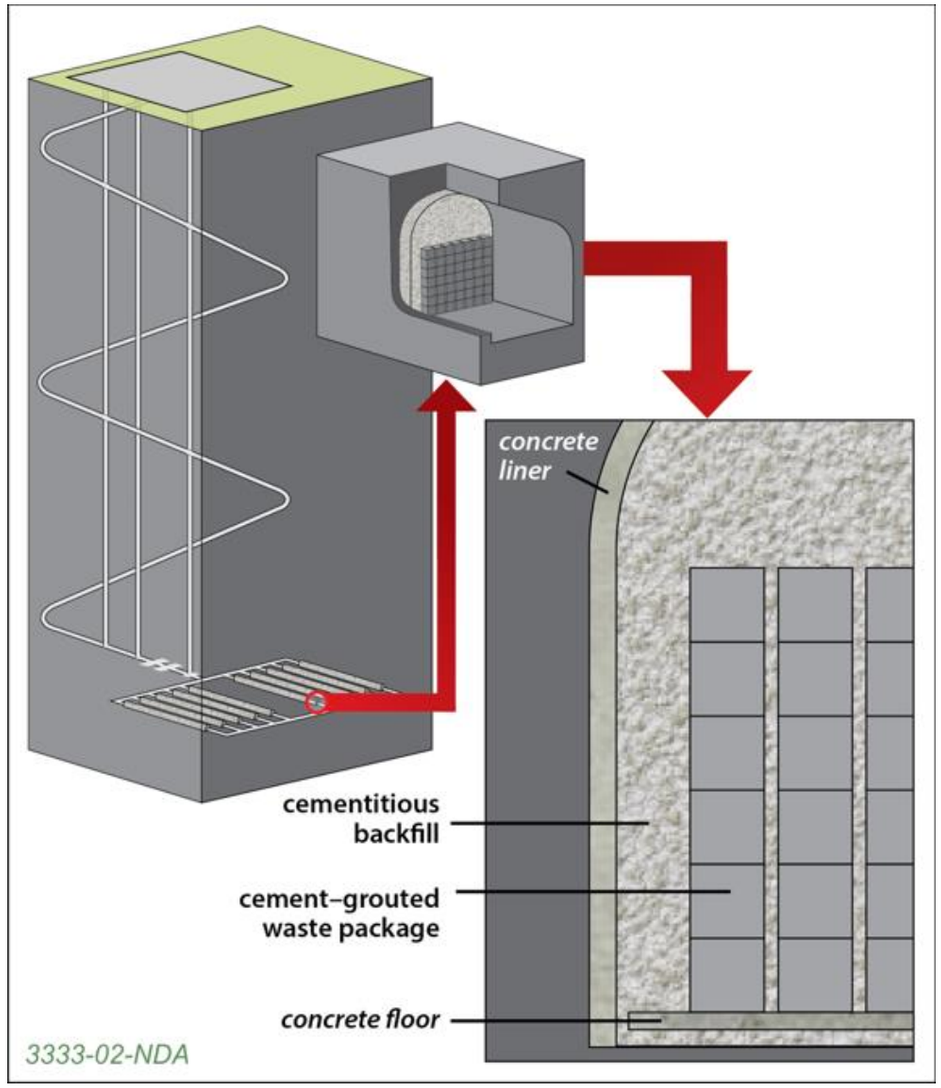

Radioactive Waste Management

Gathering the evidence – Underpinning Science

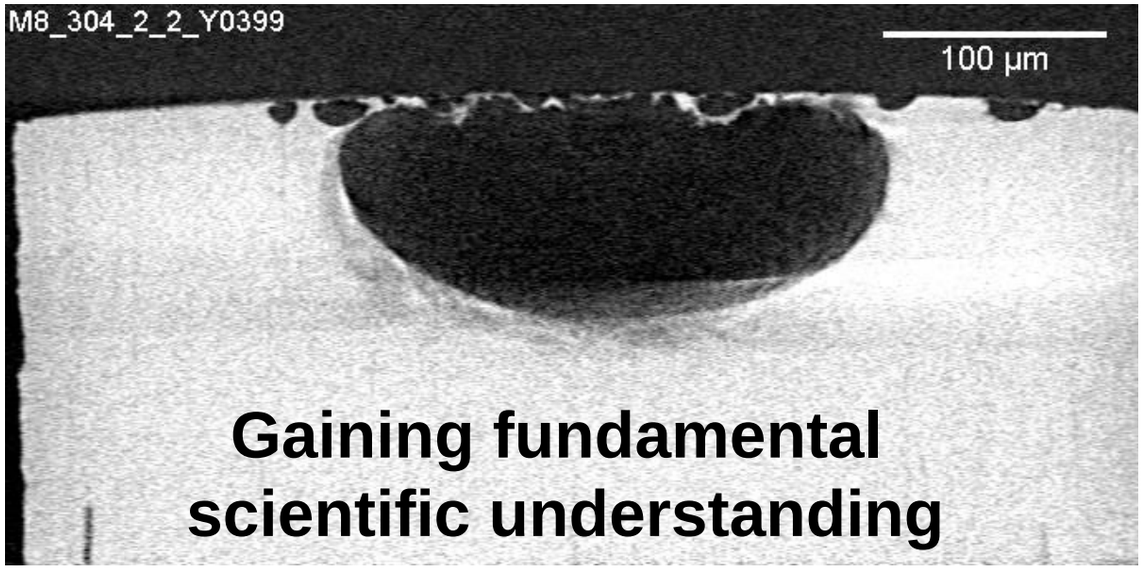

Gaining fundamental scientific understanding

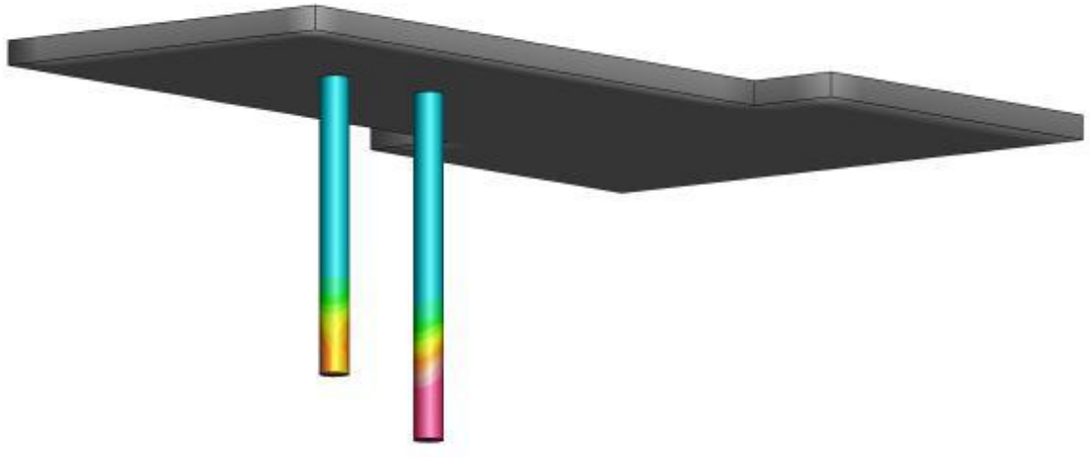

Modelling long-term performance

Testing the real world underground

Validation using natural analogues

Radioactive Waste Management

My Story

- BSc – Chemistry – Loughborough University (2008)
- PhD – Radiochemistry – Loughborough University

Loughborough University

Thesis title:

The Stability of Cement Superplasticiser and its Effect on Radionuclide Behaviour

- RWM – Specification Manager (2012 – 2016)
- RWM – Research Manager (2016 – 2017)
- RWM – Senior Research Manager (2017 – present)

Radioactive Waste Management

PhD Research

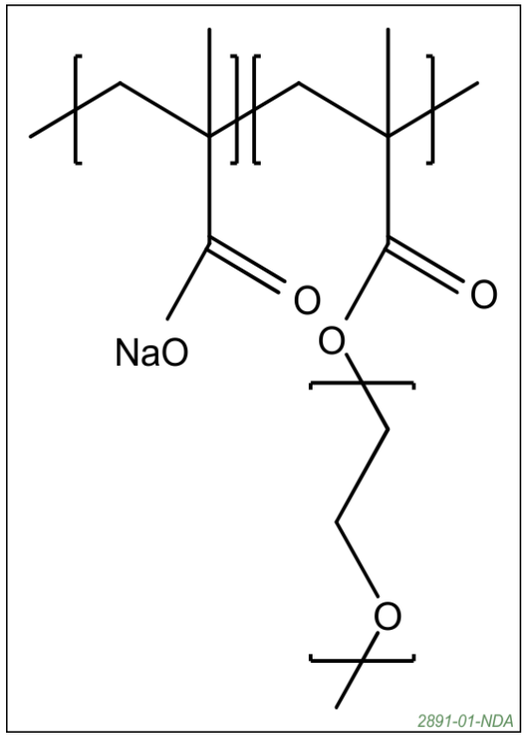

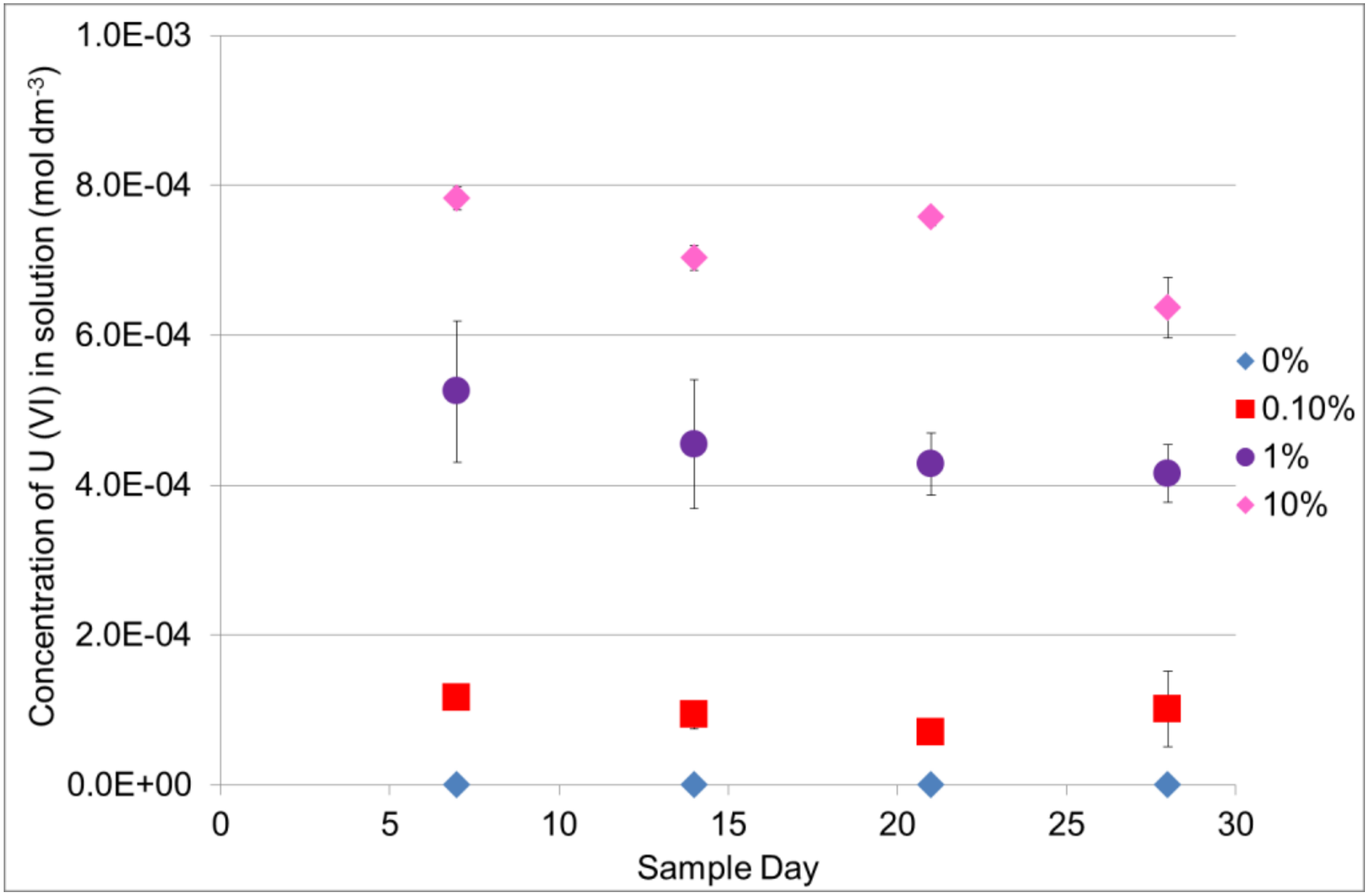

Radioactive Waste Management

PhD Research

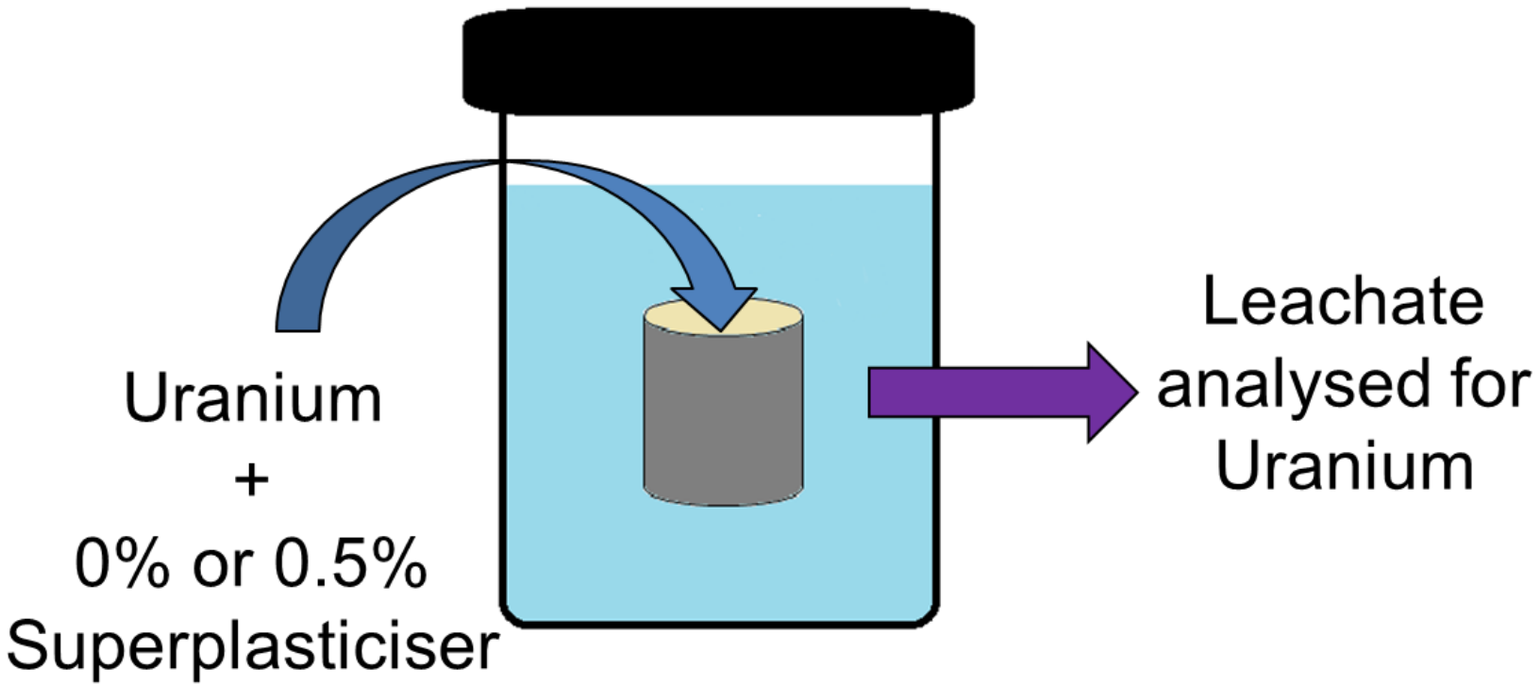

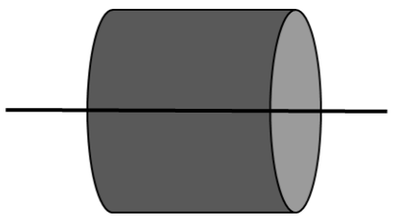

Cement blocks cut
in half lengthways

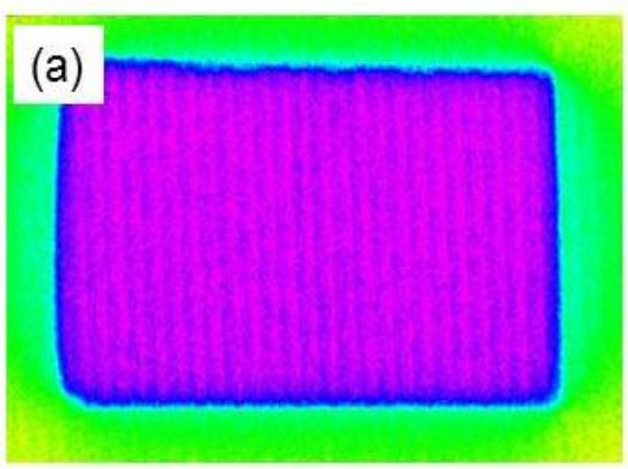

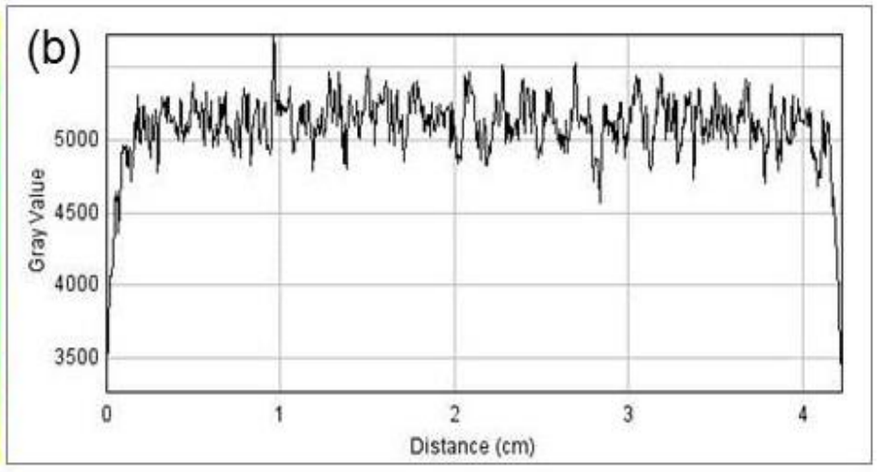

Radioactive Waste Management

How does my PhD research apply to my role?

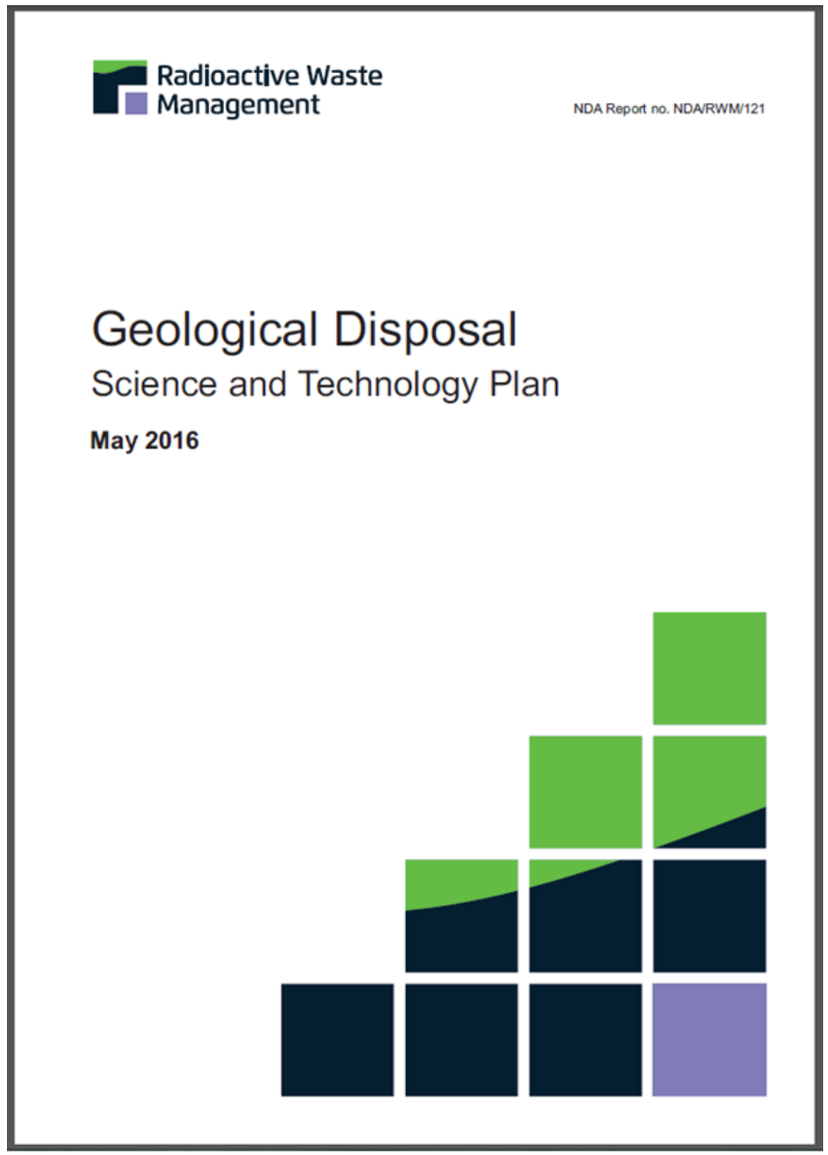

Radioactive Waste Management

Advice?

Keeping in touch

You can contact GDFenquiries@nda.gov.uk or you can reach me directly at: amy.shelton@nda.gov.uk

You can visit our website at: www.nda.gov.uk/rwm

For regular updates please subscribe to our e-bulletin news alerts at: http://www.nda.gov.uk/rwm/subscribe

Radioactive Waste Management

Glass-Ceramics for Pu Disposition: Where are we now?

Stephanie Thornber

Supervisors: Prof Neil Hyatt[1] Dr Martin Stennett[1] Dr Ewan Maddrell[2]

[1] Immobilisation Science Laboratory, Department of Materials Science & Engineering, The University of Sheffield

[2] National Nuclear Laboratory, Sellafield, Seascale, Cumbria, CA20 1PG

sthornber1@Sheffield.ac.uk

DISTINCTIVE consortium annual conference

5-6th April 2017, York, UK

Background

- The UK stores over 120 tonnes of civil separated PuO_2.
- The current policy is to reuse the PuO_2 as MOx fuel. As part of the safety case for this decision, R&D into alternative immobilisation options is underway in-case of any need to dispose of the stockpile in the future.
- Some material is not economically viable for fuel fabrication.

Pu-residues

- Pu-residues are classified as higher activity waste.
- Chemically heterogeneous and physically variable.

Powders

High purity

Fuel pellets

Glass formers

Fuel pins

Sludges

ZrO_2

Cl

Low purity

Solids

Image courtesy of NNL

Previous work developed glass-ceramics for impure Pu-residues and full ceramics for pure waste-streams consolidated by hot isostatic pressing.

Background

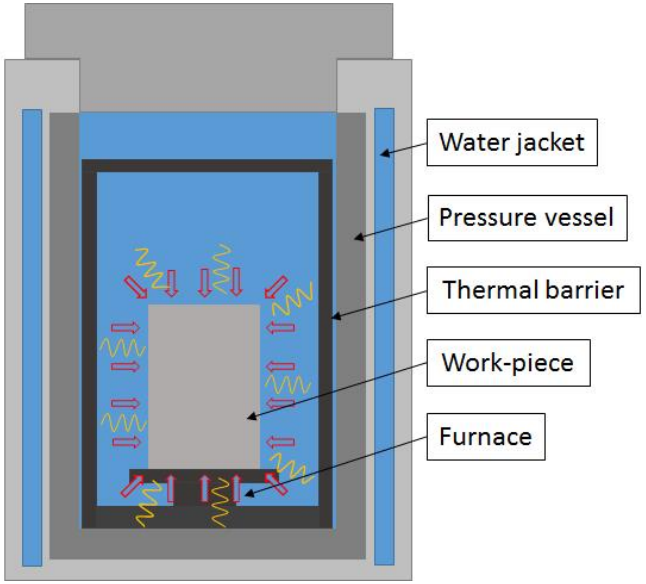

Advantages:
Batch process
Flexible to waste feed and material
Range of processing conditions
Hermetically sealed wasteforms
Significant volume reduction
Uniform incorporation of radionuclides
No off-gas production
No limitations on the wasteform
No secondary waste produced
Significant cost saving

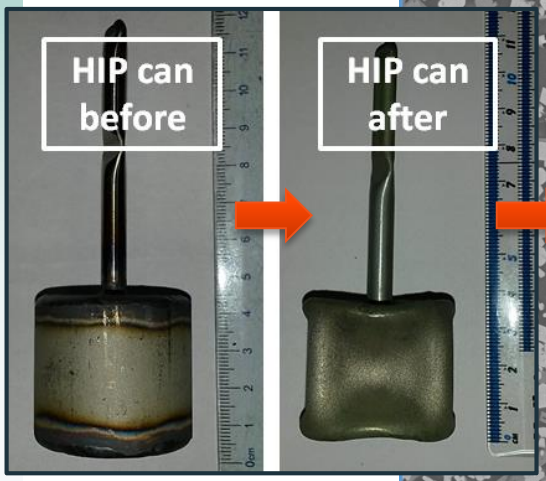

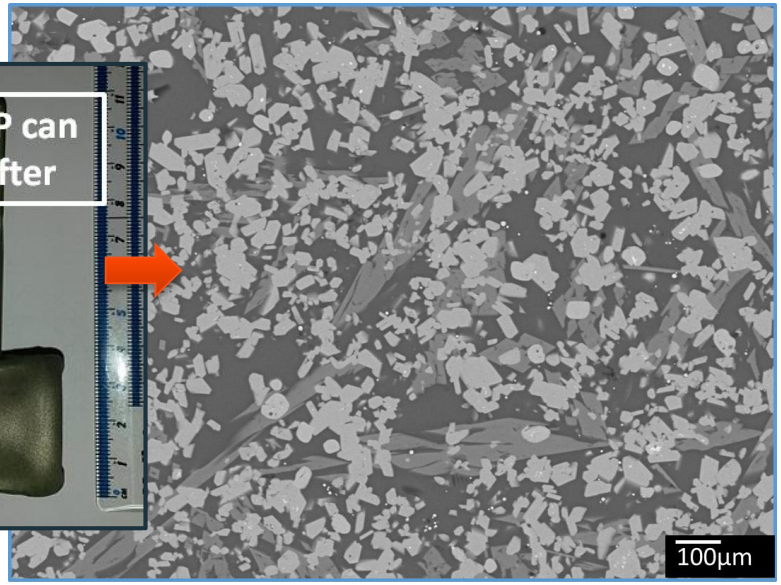

Main advantages:
Proliferation resistance
Chemical durability
Chemical flexibility
Waste loading capacity
Ease of processing
Natural analogues

Process Optimisation

An ex-situ calcination prior to packing the canisters was shown to achieve reproducible high quality samples and increased sample throughput by $^{2}/_{3}$.

Sample	Heat Treatment	
	Calcine (°C)	Bake out (°C)
A	0	300 °C
B	0	600 °C
C	**600 °C**	**300 °C**
D	600 °C	0

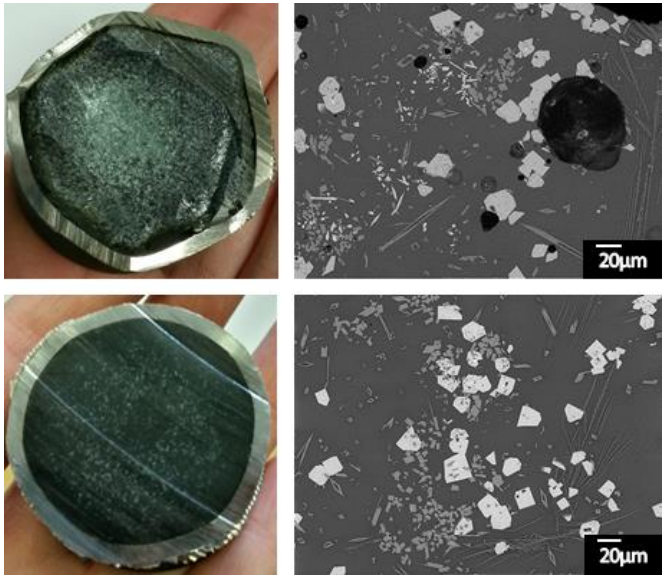

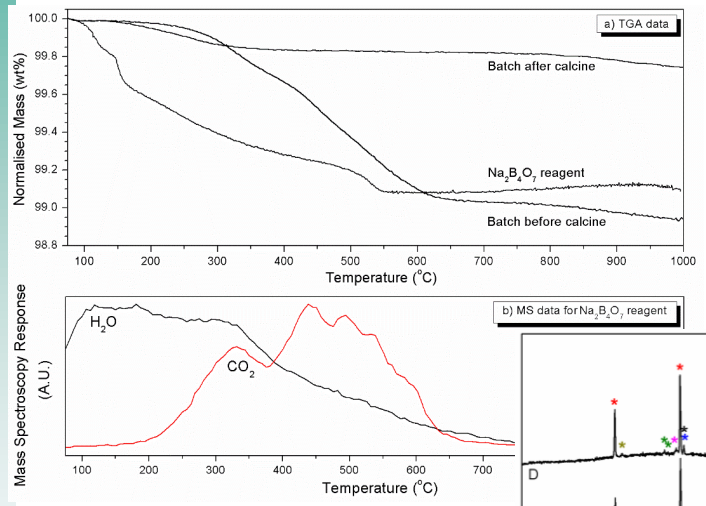

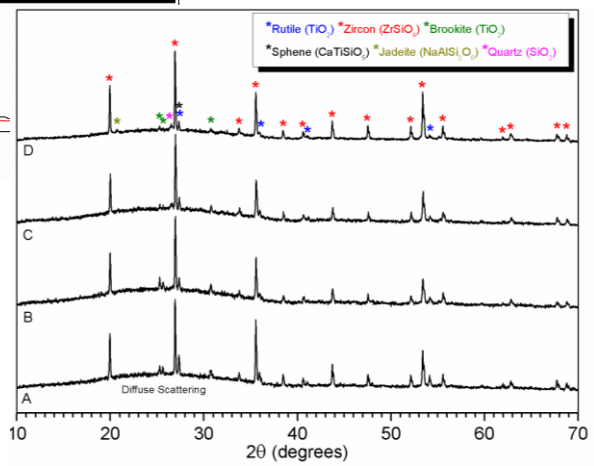

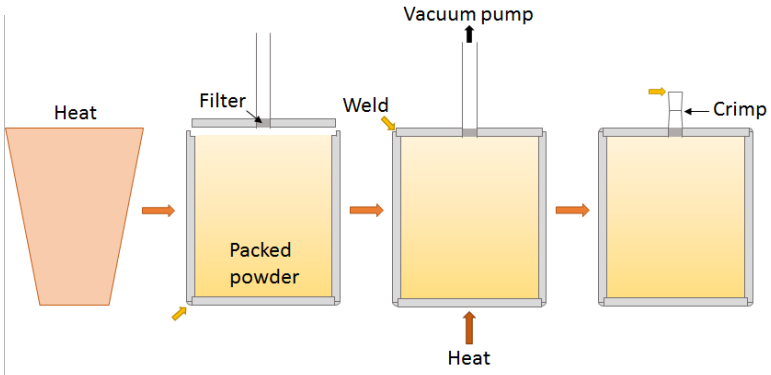

Thornber *et* al. J. Nucl. Mat. 2017

Formulation development

Previous work developed a formulation based on residues containing high CaF_2.

Table I
Model waste composition and the two derivative compositions used to demonstrate the waste form

Simulated waste (Wt%)		Substitute components	U+Th	Pu
		PuO_2		12.1
Pu metal	5.7	U_3O_8	6.5	
PuO_2	5.7	ThO_2	5.5	
CaF_2	50	CaF_2	49.7	49.6
SiO_2	38.6	SiO_2	38.3	38.3

Day *et* al. 2005

EXPERIMENTAL

A precursor formulation was developed for the glass-ceramic waste form and prepared by mixing together oxides, nitrates and hydroxides of the additives/precursor and calcining the batch in alumina crucibles at 750°C. The precursor composition was 26.9 wt% SiO_2 + 24.3 wt% Al_2O_3 + 5.3 wt% B_2O_3 + 6.1 wt% Na_2O + 6.6 wt% CaO + 4.9 wt% Gd_2O_3 + 10.0 wt% TiO_2 + 10.9 wt% ZrO_2 + 5.0 wt% CaF_2. A model waste stream was also developed from data on the Pu-residues wastes [1] and classification of the waste ions present into four categories - actinides, impurity cations, glass formers and anions. In this work the impacts on waste form performance were

2

Stewart *et* al. 2013

CaF_2 is toxic and a problematic neutron source for (α,n)-reactions:

$$^{19}F + \alpha \rightarrow {}^{22}Na^* + n$$
$$^{22}Na^* \rightarrow {}^{22}Na + \gamma(1528\ \text{keV})$$

NNL applied an alkali aluminoborosilicate formulation originally developed for K-basin wastes at Hanford.

Mater. Res. Soc. Symp. Proc. Vol. 1124 © 2009 Materials Research Society 1124-Q04-01

HIPed Tailored Pyrochlore-Rich Glass-Ceramic Waste Forms for the Immobilization of Nuclear Waste

Melody L. Carter, Huijun Li, Yingjie Zhang, Andrew L. Gillen and Eric. R. Vance
Ansto, New Illawarra Rd, Lucas Heights, NSW 2234, Australia.

Carter *et* al. (2009)

2. Experimental

A suite of six samples was prepared based on the glass composition $Na_2Al_{1+x}B_{1-x}Si_6O_{16}$ described above, with $x = 0–1$ in increments of 0.2. The standard batch size comprised nominally 50 g of glass together with 0.25 moles of the zirconolite forming oxides. This blend gives an approximately equivolume mixture of glass and crystalline material if zirconolite forms as the crystalline phase.

Maddrell *et* al. 2015

Formulation development

Glass Fraction (wt%)	Glass Composition: $Na_2Al_{1+x}B_{1-x}Si_6O_{16}$					
	X = 0	X = 0.2	X = 0.4	X = 0.6	X = 0.8	X = 1.0
30	$Na_2AlBSi_6O_{16}$	$Na_2Al_{1.2}B_{0.8}Si_6O_{16}$	$Na_2Al_{1.4}B_{0.6}Si_6O_{16}$	$Na_2Al_{1.6}B_{0.4}Si_6O_{16}$	$Na_2Al_{1.8}B_{0.2}Si_6O_{16}$	$Na_2Al_2Si_6O_{16}$
50	$Na_2AlBSi_6O_{16}$	$Na_2Al_{1.2}B_{0.8}Si_6O_{16}$	$Na_2Al_{1.4}B_{0.6}Si_6O_{16}$	$Na_2Al_{1.6}B_{0.4}Si_6O_{16}$	$Na_2Al_{1.8}B_{0.2}Si_6O_{16}$	$Na_2Al_2Si_6O_{16}$
70	$Na_2AlBSi_6O_{16}$	$Na_2Al_{1.2}B_{0.8}Si_6O_{16}$	$Na_2Al_{1.4}B_{0.6}Si_6O_{16}$	$Na_2Al_{1.6}B_{0.4}Si_6O_{16}$	$Na_2Al_{1.8}B_{0.2}Si_6O_{16}$	$Na_2Al_2Si_6O_{16}$

Increased glass fraction reduced the yield of zirconolite

Increased Al, increased zirconolite

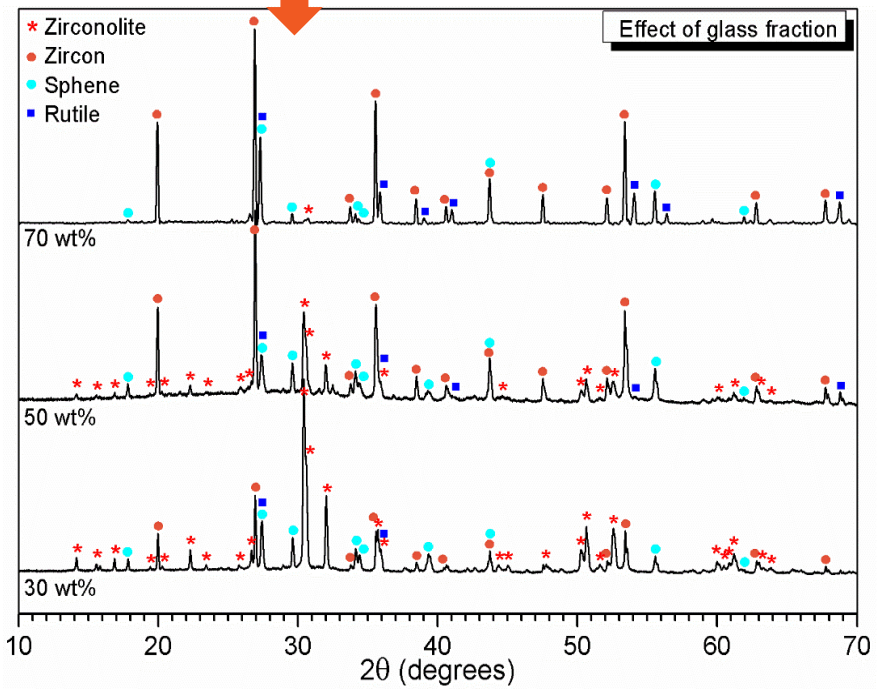

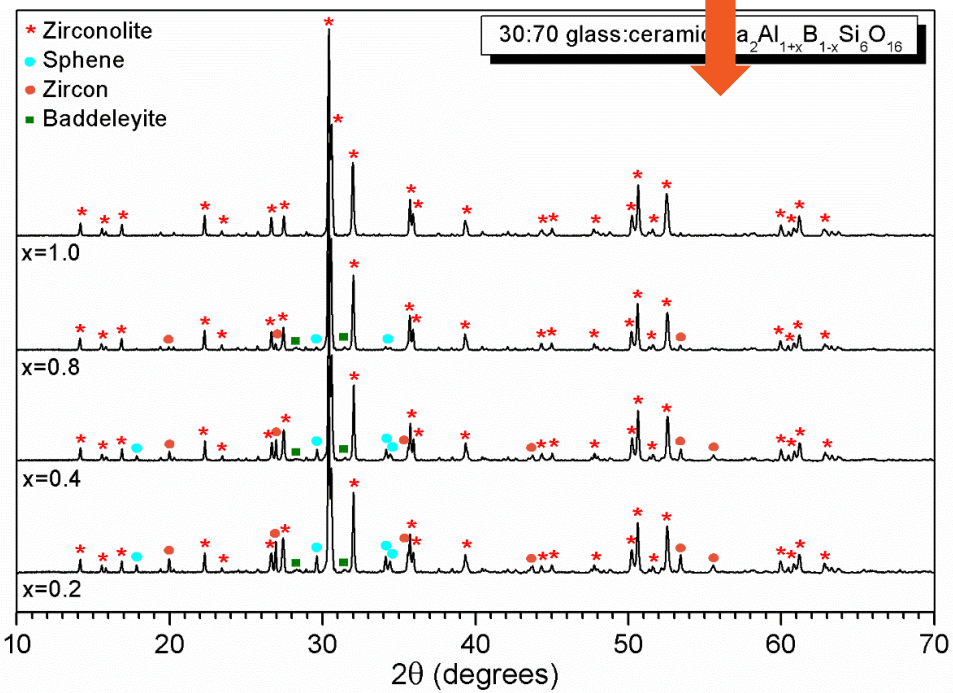

Formulation development

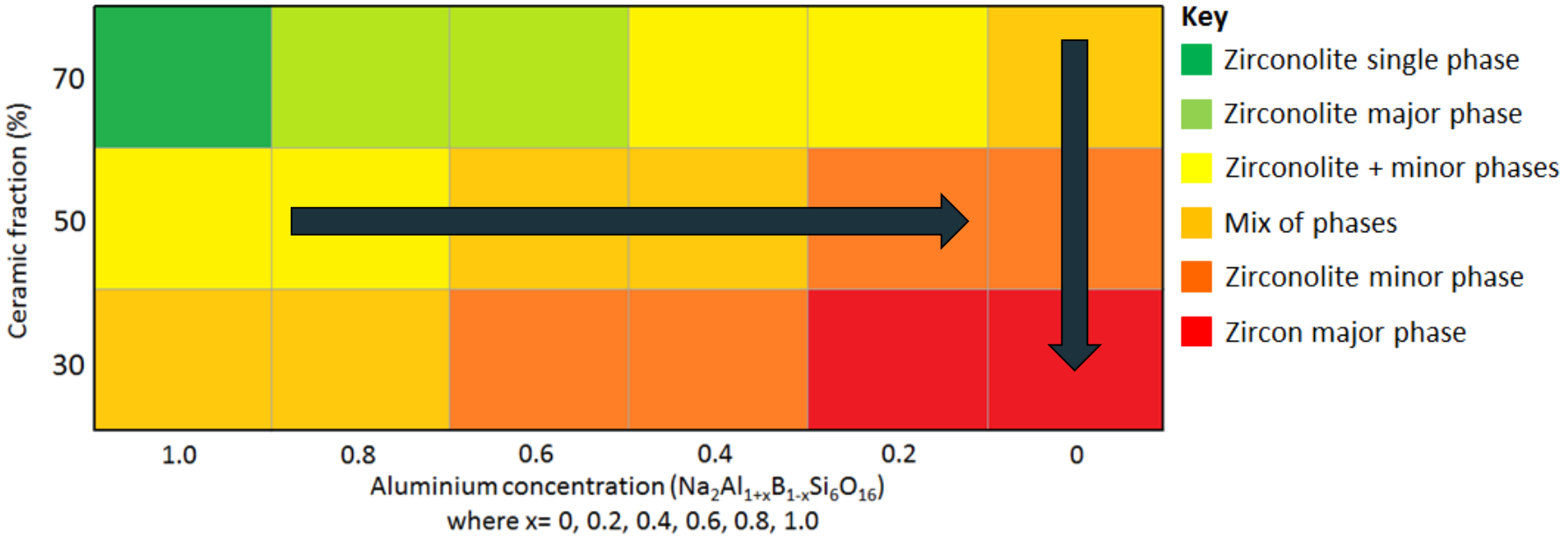

- When $Al_2O_3 \leq Na_2O$ all Al^{3+} is stabilised as tetrahedral units.
- When $Al_2O_3 < Na_2O$ there is excess Na_2O available to stabilise other elemental species and create NBOs.
- Connelly *et* al. predicted the preferential charge compensation of different ions in alkali aluminoborosilicate glasses: **$Al^{3+} > Zr^{4+} > Ti^{4+} > B^{3+} > Si^{4+}$**

↓ Al_2O_3 ↑ Excess Na_2O ↑ Zr^{4+} and Ti^{4+} in glass ↓ Glass connectivity ↑ CaO in glass ↓ $CaZrTi_2O_7$

- SiO_2 acts as the primary glass network former. At low glass fractions all the SiO_2 is consumed within the glass phase, the high glass fraction samples the Si^{4+} is more available to form crystalline phases.

Waste incorporation

Single phase formulation was used for Ce waste incorporation experiments: **30wt% glass phase $Na_2Al_2Si_6O_{16}$**

Sample	Target ceramic composition	Target Ce oxidation state
A	$Ca_{0.8}Ce_{0.2}ZrTi_{1.6}Al_{0.4}O_7$	4+
B	$Ca_{0.9}Ce_{0.1}Zr_{0.9}Ce_{0.1}Ti_2O_7$	3+
C	$CaZr_{0.8}Ce_{0.2}Ti_2O_7$	4+

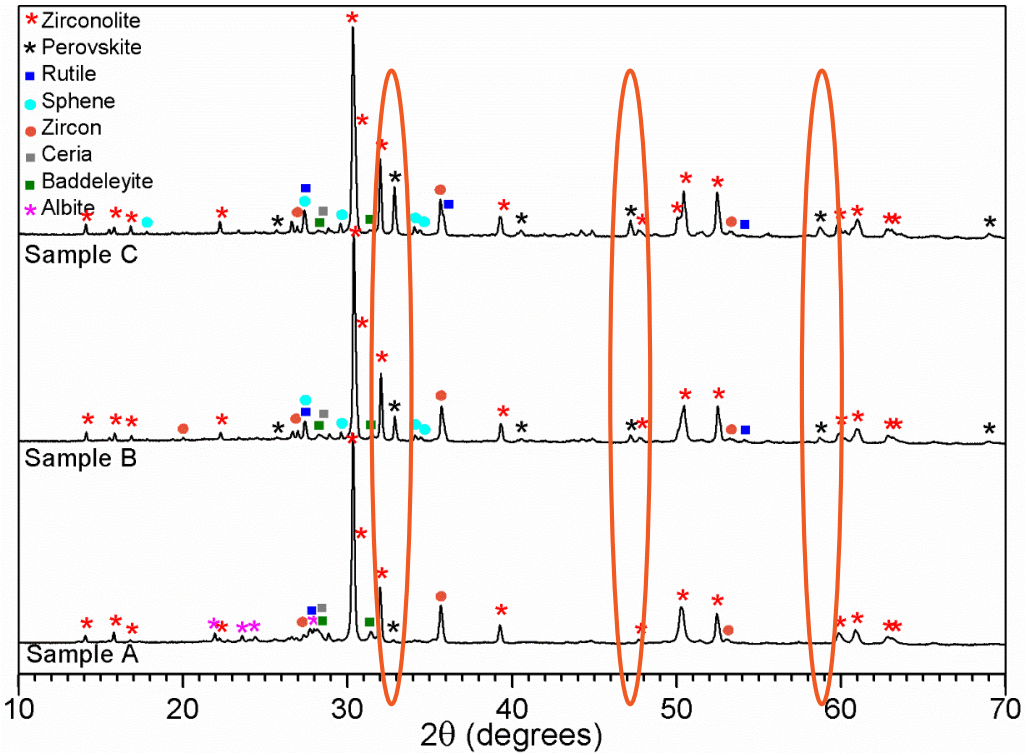

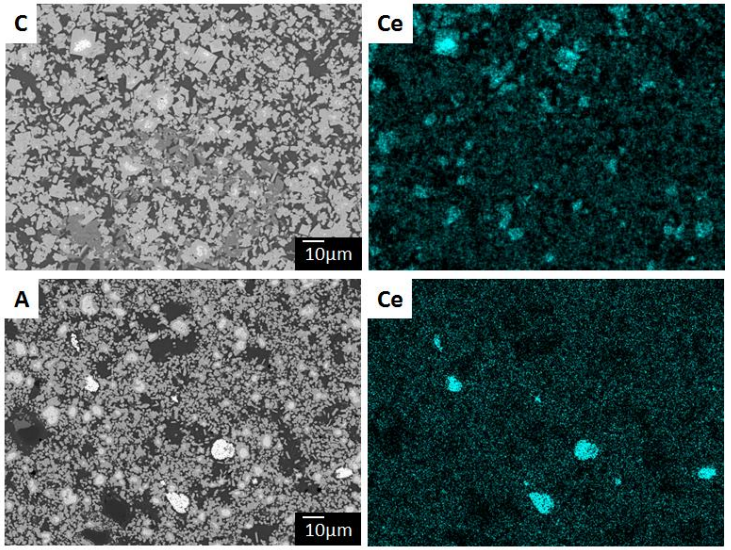

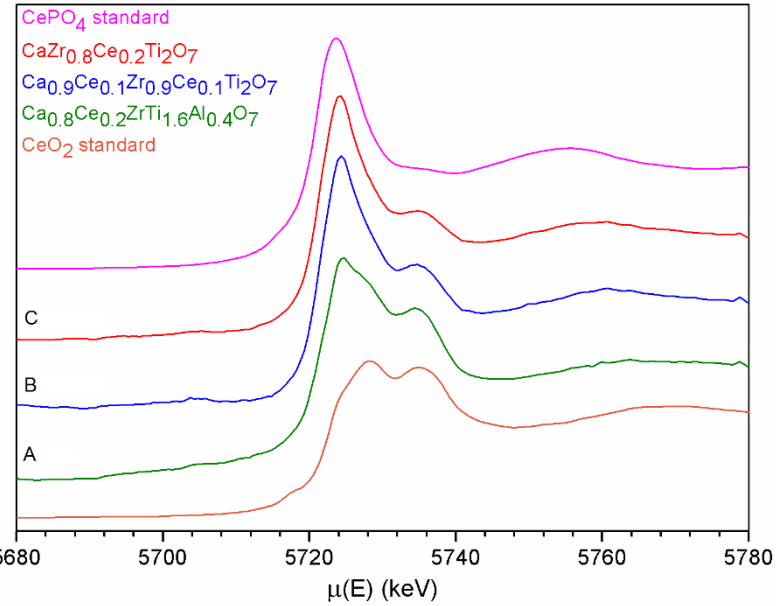

Waste incorporation

Single phase formulation was used for Ce waste incorporation experiments: **30wt% glass phase $Na_2Al_2Si_6O_{16}$**

Sample	Target ceramic composition	Target Ce oxidation state
A	$Ca_{0.8}Ce_{0.2}ZrTi_{1.6}Al_{0.4}O_7$	4+
B	$Ca_{0.9}Ce_{0.1}Zr_{0.9}Ce_{0.1}Ti_2O_7$	3+
C	$CaZr_{0.8}Ce_{0.2}Ti_2O_7$	4+

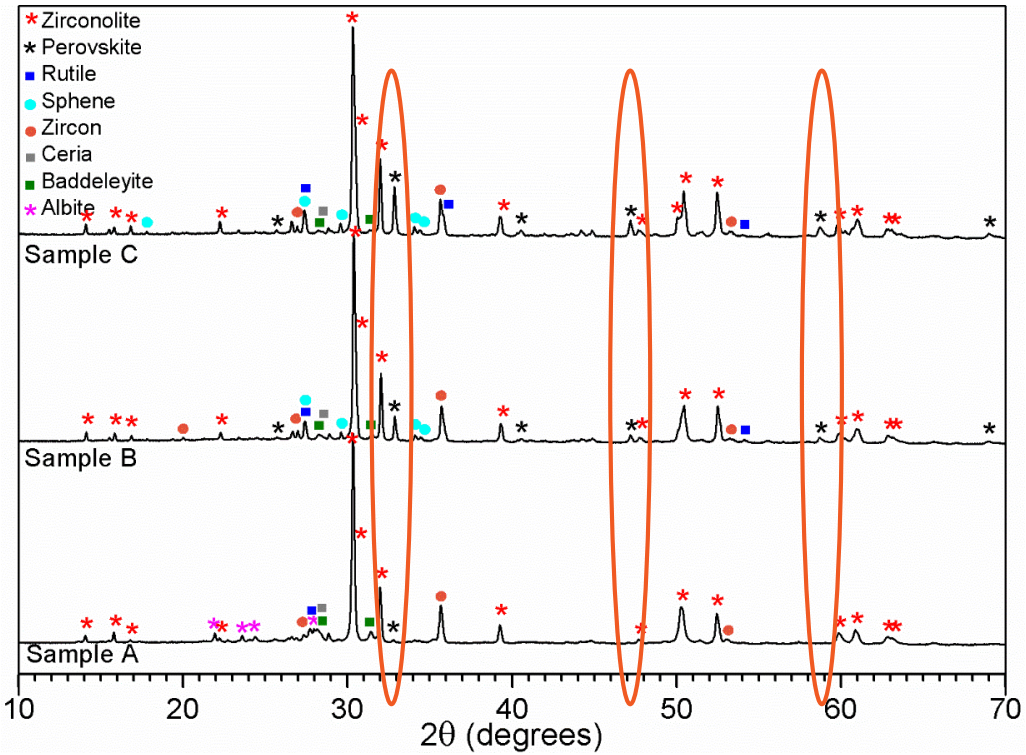

Zirconolite structure:	**Ionic Radii**
Ca^{2+} in 8-fold coordination	1.12Å
Zr^{4+} in 7-fold coordination	**0.78Å**
Ti^{4+} in 5/6- fold coordination	0.51-0.605Å
Perovskite: **Ca^{2+} in 12-fold coordination**	**1.34Å**

Ce^{4+}	**Ionic Radii**
8-fold coordination	0.97Å
7-fold coordination	***0.92Å***
6-fold coordination	0.87Å
Ce^{3+}	
12-fold coordination	**1.34Å**
8-fold coordination	1.14Å
7-fold coordination	1.07Å

Chlorine solubility

Pu-residues stored in PVC packaging are contaminated with Cl.

Can we retain Cl in our HIPed samples?
What is the solubility limit of Cl in our glass-ceramics?
Can we immobilise the Pu (Ce) separately to the Cl?

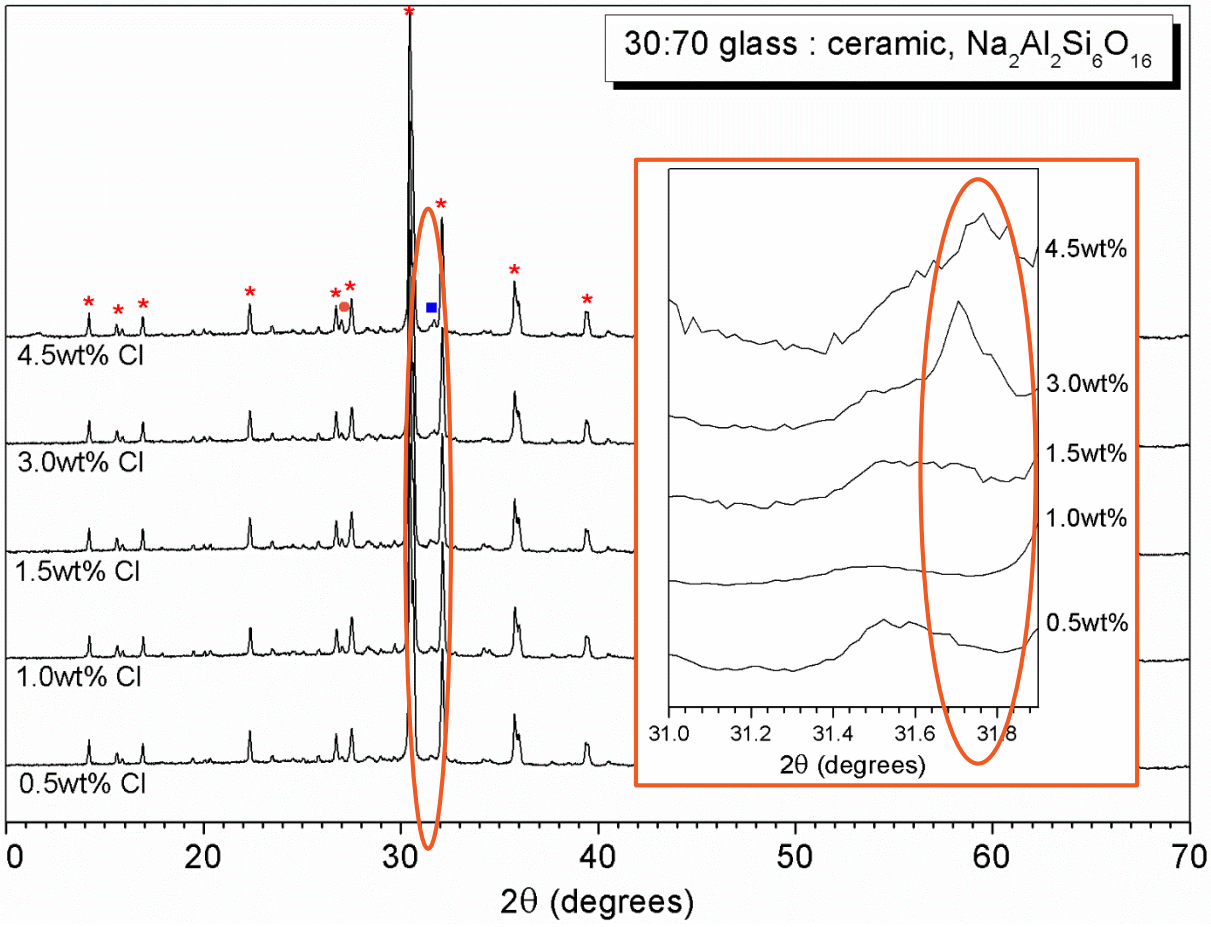

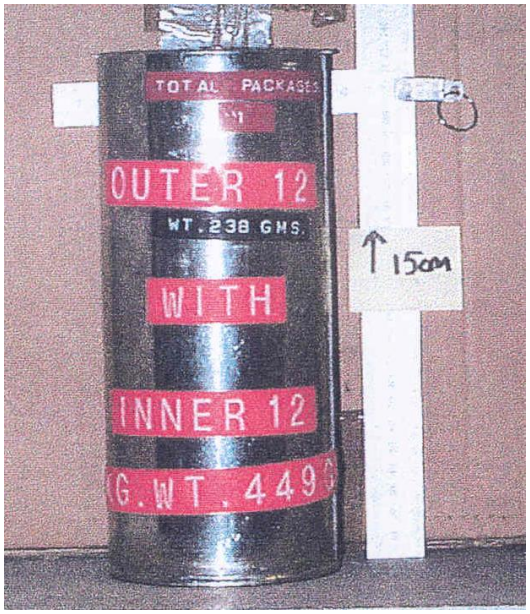

Image courtesy of NNL

Residual NaCl seen between 1.5 – 2.0 wt%

Expected upper limit in Pu-resides is 0.1 wt%.

Stewart *et* al. TMS2013

Chlorine solubility

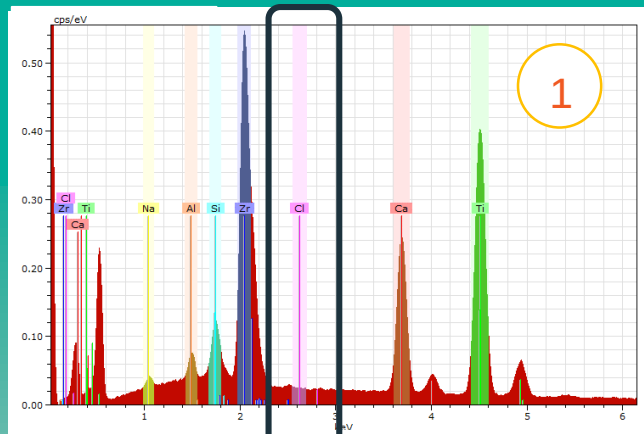

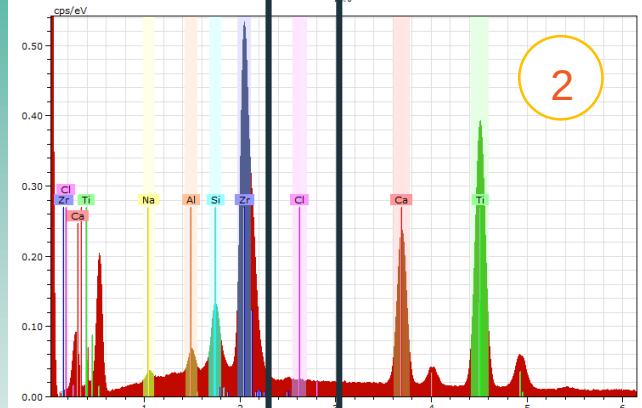

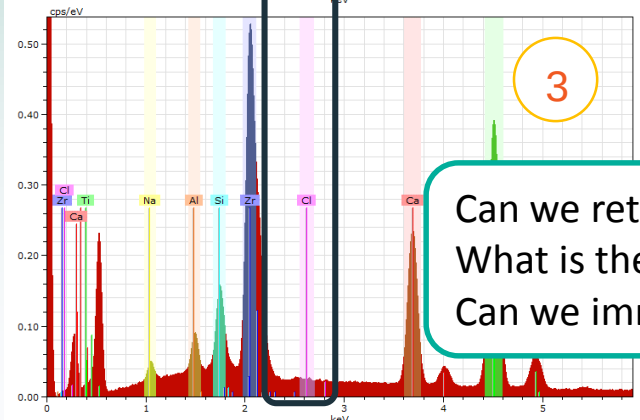

3wt% Cl

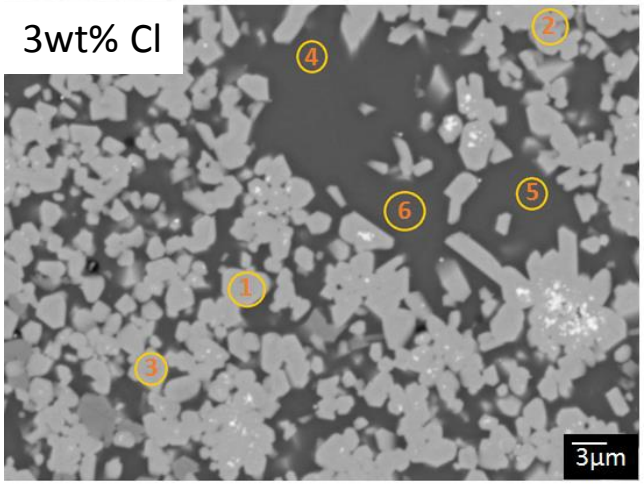

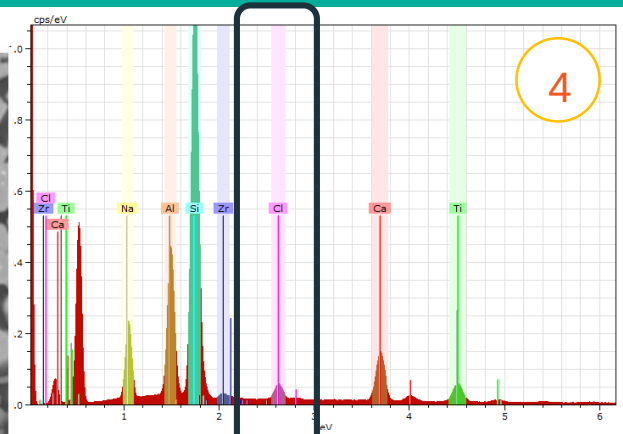

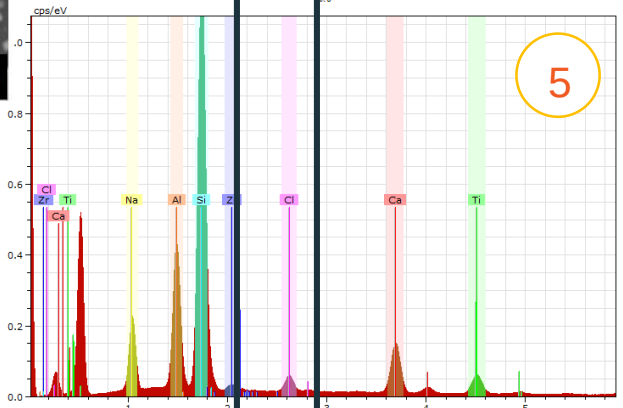

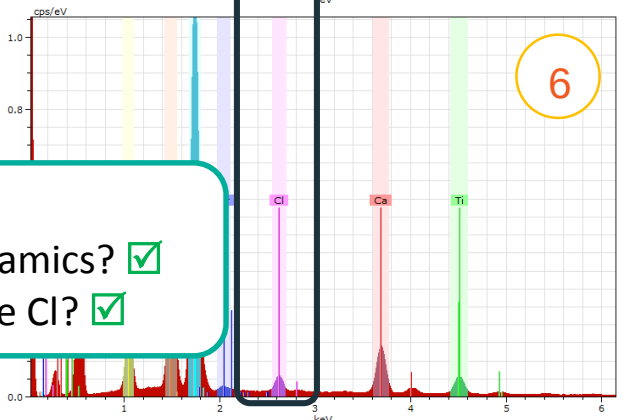

Zirconolite Phase	**Glass Phase**
Cl = 0.03	Cl = 1.37
Cl = 0.05	Cl = 1.52
Cl = 0.00	Cl = 1.45

Cl preferentially partitioned into the glass phase

Can we retain Cl in our HIPed samples? ☑
What is the solubility limit of Cl in our glass-ceramics? ☑
Can we immobilise the Pu (Ce) separately to the Cl? ☑

Still to come…

- Uranium and Plutonium HIP samples at ANSTO

- U-HIP to support our Ce work
- Pu-HIP to investigate the partitioning of Pu with respect to oxygen fugacity

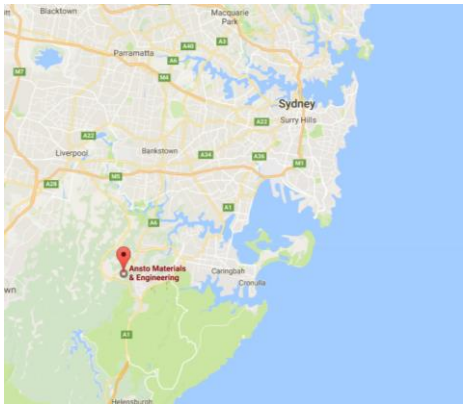

Nuclear Decommissioning Authority

Australian Government

ansto

Active HIP facility at University of Sheffield

AIP AMERICAN ISOSTATIC PRESSES, INC.

DISTINCTIVE

Designed and manufactured by AIP as the first official research active HIP facility in the UK.
The first active containment designed for repeated use.

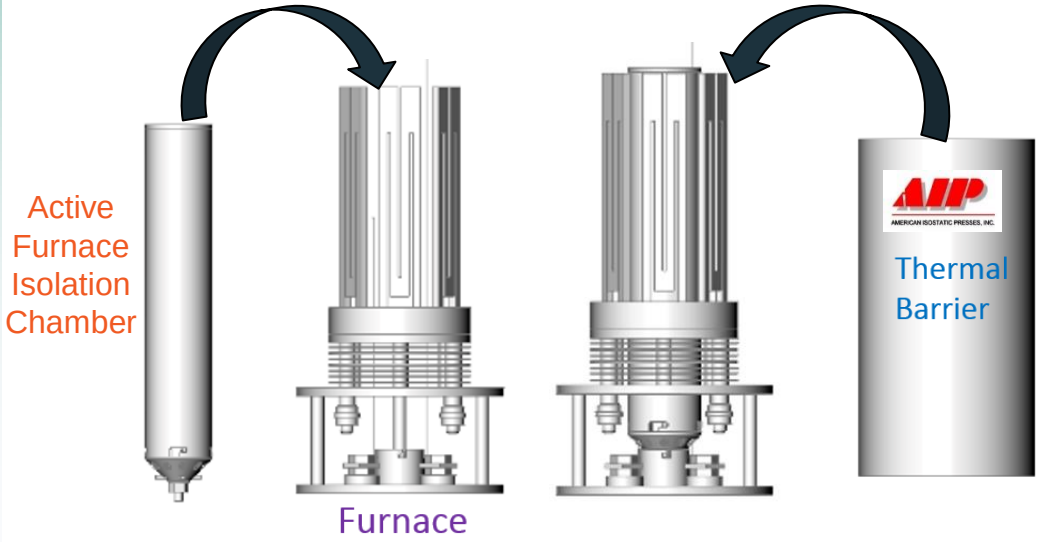

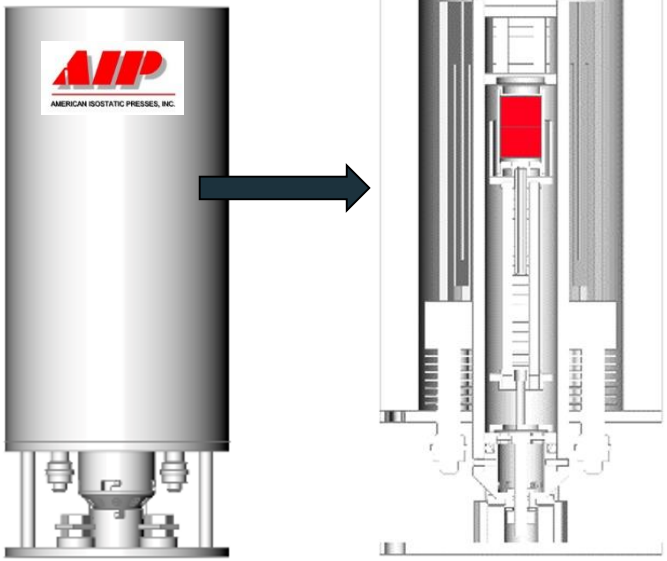

Summary

Process optimisation : the use of a two step heat treatment during sample preparation ensures high quality and reproducible HIPed wasteforms.

Formulation optimisation : a single phase zirconolite glass-ceramic formulation was determined. Increasing Al_2O_3 favours the formation of zirconolite. Changes to the glass composition and fraction effect the glass structure such that a less polymerised glass stabilises more Zr^{4+} and Ti^{4+} in the glass.

Ce incorporation : Ce substitution on either the Ca and / Zr sites showed a limitation of Ce^{4+} on the Zr site resulting in the formation of a Ce-bearing perovskite. When targeting Ce on the Ca site the perovskite yield was reduced and XANES showed better retention of Ce^{4+} in the Al charge compensated sample.

Cl contamination : Cl was successfully retained and incorporated into our HIP glass-ceramics. The Cl was preferentially incorporated in the glass phase therefore separate to Ce / Pu in the wasteform. The solubility limit of Cl in the glass was around 1.5 wt%, which is far above the expected contamination levels in Pu-residues.

Still to come…. U and Pu HIP samples at ANSTO.
Installation of AIP's active furnace isolation chamber at Sheffield's HIP facility.

Acknowledgements

Prof Neil Hyatt

Dr Martin Stennett

Dr Ewan Maddrell

Dr Paul Heath

Sam Moricca – AIP

References

Nuclear Decommissioning Authority, Conditioning of Plutonium Residues by Hot Isostatic Pressing and Options for packaging and Disposal (pre-conceptual stage) Summary of Assessment Report. (2009).

C.R.Scales, E.R.Maddrell, N.Gawthorpe, B.D.Begg, S.Moricca, R.A.Day, M.W.A.Stewart, "Development of a process for the immobilization of actinide containing residues on the Sellafield site," International conference of environmental remediation and radioactive waste management, (2005).

B. D. Begg, E. R. Vance, The incorporation of cerium in zirconolite, Mat. Res. Soc. Symp. **465, (**1997).

B. D. Begg, R. A. Day, A. Brownscombe, Structural effect of Pu substitutions on the Zr-site in zirconolite, Mat. Res. Soc. Symp. **663**, (2001).

M. Gilbert, J. H. Harding, Energetics of Ce and Pu incorporation into zirconolite waste-forms, Phys. Chem. Phys. **13, (**2011).

E.R. Vance, M.W.A. Stewart, and S.A. Moricca, "Progress at ANSTO on SYNROC," J. Aust. Ceram. Soc., **50** [1] 38–48 (2014).

E. Maddrell, S. Thornber, and N. Hyatt, "The influence of glass composition on crystalline phase stability in glass-ceramic wasteforms," J. Nucl. Mater., (2014).

https://www.csun.edu/~hcchm003/321/Ered.pdf accessed on 10/11/2016

M. Carter et al., HIPed Tailored Pyrochlore-rich Glass-ceramic wasteforms for the immobilisation of Nuclear waste, 2009

Stewart *et* al, Glass-Ceramic Waste Forms for Uranium and Plutonium Residues Wastes, WM2013, 2013

Day et. Technical Demonstration of Zirconolite Glass-Ceramics Processed in a Hot Isostatic Press: An Option for Immobilisation of Actinide Containing Residues at Sellafield, ICEM05, 2005

AGR cladding corrosion: Investigation of the behaviour of heat treated and unsensitised steel under pond water conditions

06/04/2017

Elizabeth Howett
Supervisors: Prof Colin Boxall and Dr David Hambley (NNL)

Contents

- *Introduction*
- *Unsensitised and heat treated 20/25/Nb SS*
  - *Linear sweep voltammetry*
  - *Electrochemical impedance spectroscopy studies*
- *Unsensitised and heat treated 304H SS*
  - *Linear sweep voltammetry*
  - *Electrochemical impedance spectroscopy studies*

Purpose of AGR Stainless Steel Cladding Experiments

- Fuel has been successfully stored for period of 10-20yrs however may extend to 100yrs
- Assess the validity of extended storage periods without extra containment
- Cladding can be breached due to stress corrosion cracking or damaged during dismantling, evolution of the cladding and fuel surfaces on exposure to pond water are considered corrosion processes
- Currently, pond water temperature 30^{o}C; pond water chemistry dominated by NaOH corrosion inhibitor at pH 11.4
- Thorp R&S pond will have a new racking system which will give an increase in the operating temperature of the ponds
- New racks, with higher, post-dismantling packing density, will lead to higher pond water temperatures of ~45^{o}C under normal pond conditions, leading to a pH change to 10.79 at current NaOH loadings; peak normal operating temperature of 60^{o}C leads to pH of 10.66
- Loss of cooling may lead to pond water temperatures of ~90^{o}C, leading to a pH change to 9.8 at current NaOH loadings

Materials and experimental conditions

- Thermally sensitised 304H and 20/25/Nb stainless steel in simulant pond water
- Sample Composition:

	Cr	Ni	N	C	Mn	Si	S	Nb	P	Co	Fe
304H	18-20	8-10.5	0	0.04-0.1	2	0.75	0.03	0	0.045	0	Balance
20/25/Nb	20	25	0.016	0.049	0.7	0.57	0.007	0.7	0.006	0.0025	Balance

- Pond chemistry: pH≈11.4

Na^+	Ca^+	Cl^-	SO_4^{2-}	K^+	OH^-
5.4mM	2µM	30µM	2µM	5µM	Balance

- Varying temperature: Room temperature, 45°C (normal operating conditions), 60°C (peak operating conditions) and 90°C (LOCA/malfunction)

Degree of sensitisation: Etching 20/25/Nb SS with 10wt% oxalic acid

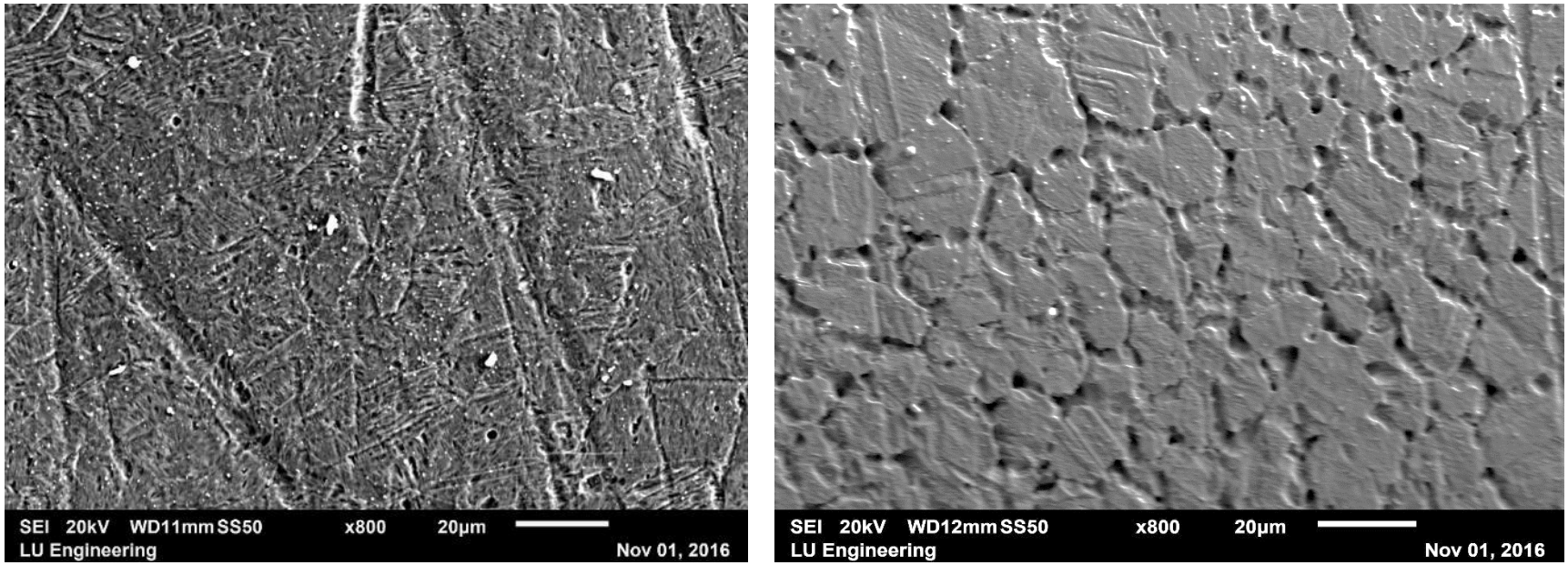

Figure 1: Etched surfaces of 20/25/Nb SS, unsensitised (left) and heat treated (right)

Effect of dosing pond water with NaOH to a pH≈11.4 on the corrosion behaviour of 20/25/Nb

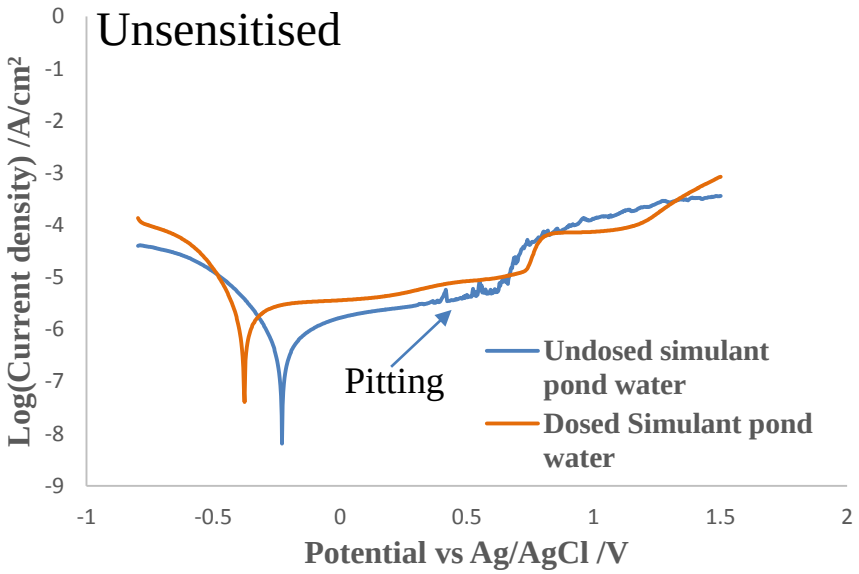

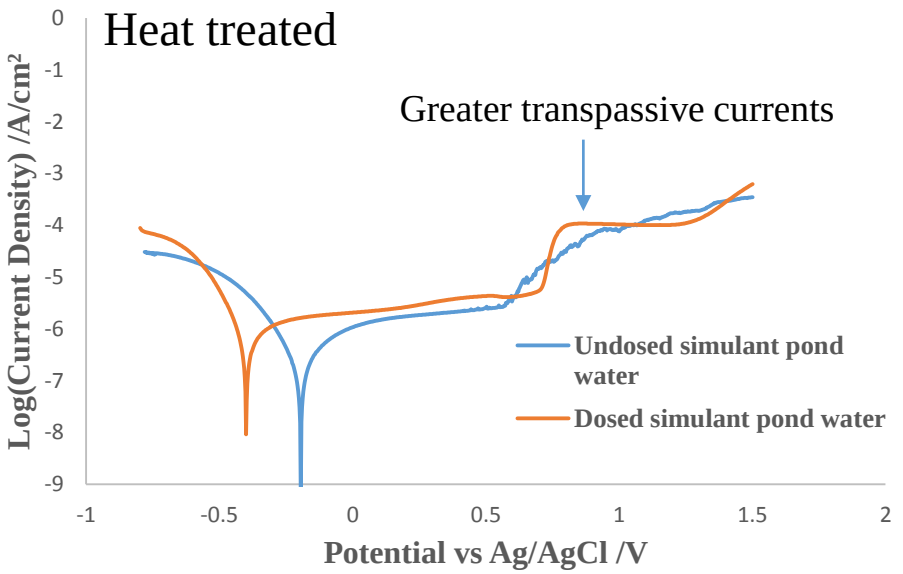

Figure 2: Effect of dosing pond water to a pH≈11.4, unsensitised (left) and heat treated (right) 20/25/Nb SS

Electrochemical impedance spectroscopy

- Measure of the resistance and capacitance developed on the electrode system due to the formation of an oxide layer on the electrode surface
- The lower the resistance the more susceptible to corrosion the electrode i.e. the surface is not being block
- A small sinusoidal potential is applied to the working electrode and the frequency is scanned between 10,000 and 0Hz
- Nyquist plots – show the frequency response of the system, give information on the stability of a system. It is a plot of the real versus imaginary components of the impedance
- Equivalent circuit models are used to extract information on the resistance and capacitance of a system from the Nyquist plot

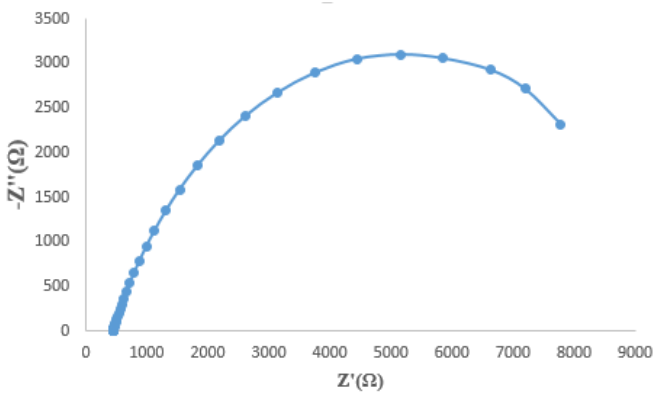

Figure 3: Example of a Nyquist plot

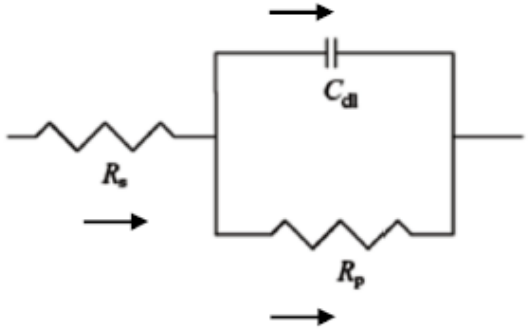

Figure 4: Electrical equivalent circuit model used to represent an electrochemical interface undergoing corrosion in the absence of diffusion control (Randle cell)

Electrochemical impedance Spectroscopy of unsensitised and heat treated 20/25/Nb, pH≈11.4

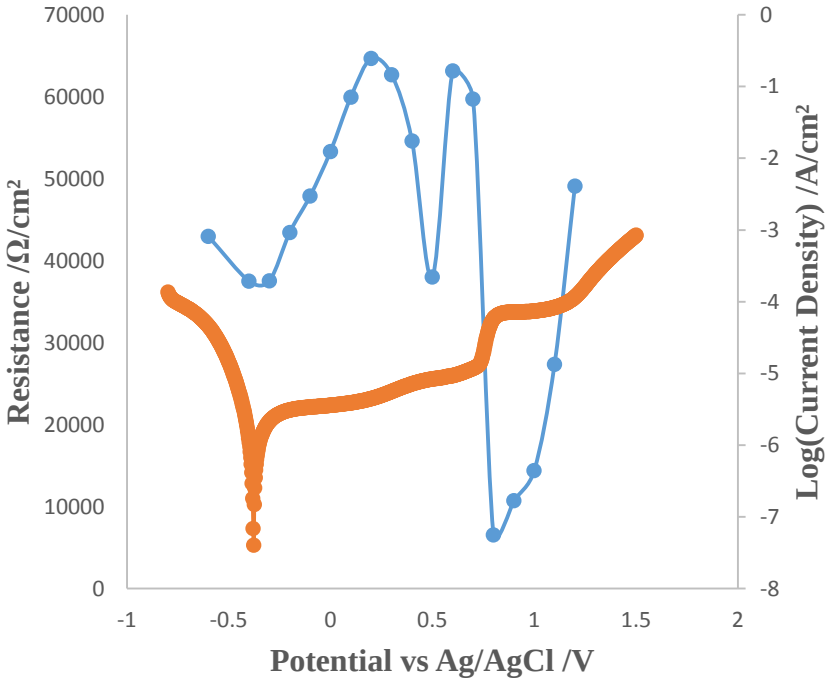

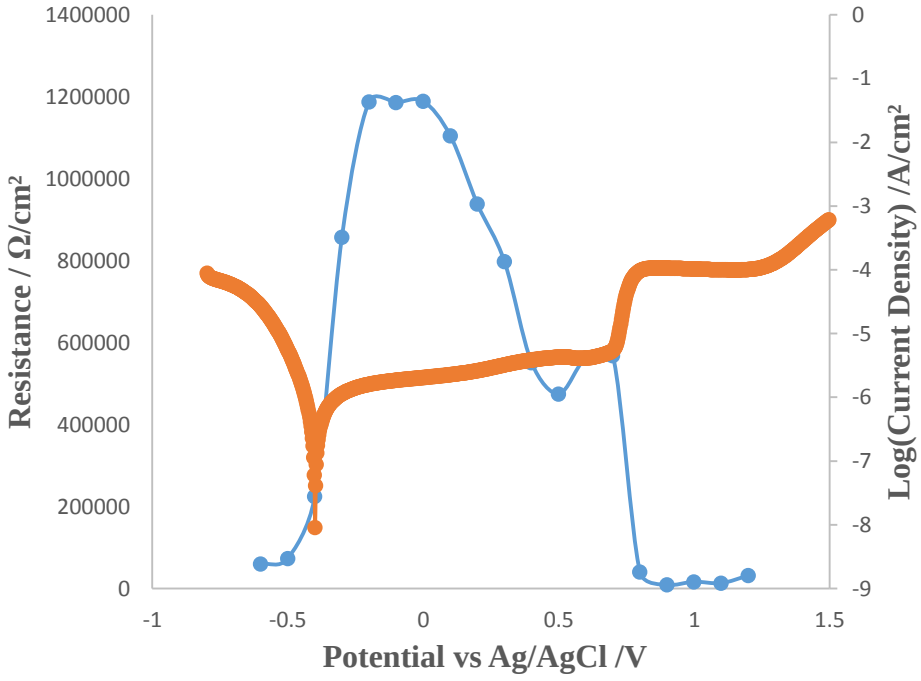

Figure 5: Resistance obtained from electrochemical impedance spectroscopy experiments for unsensitised (left) and heat treated (right) 20/25/Nb SS

Electrochemical impedance Spectroscopy of iron and chromium, pH≈11.4

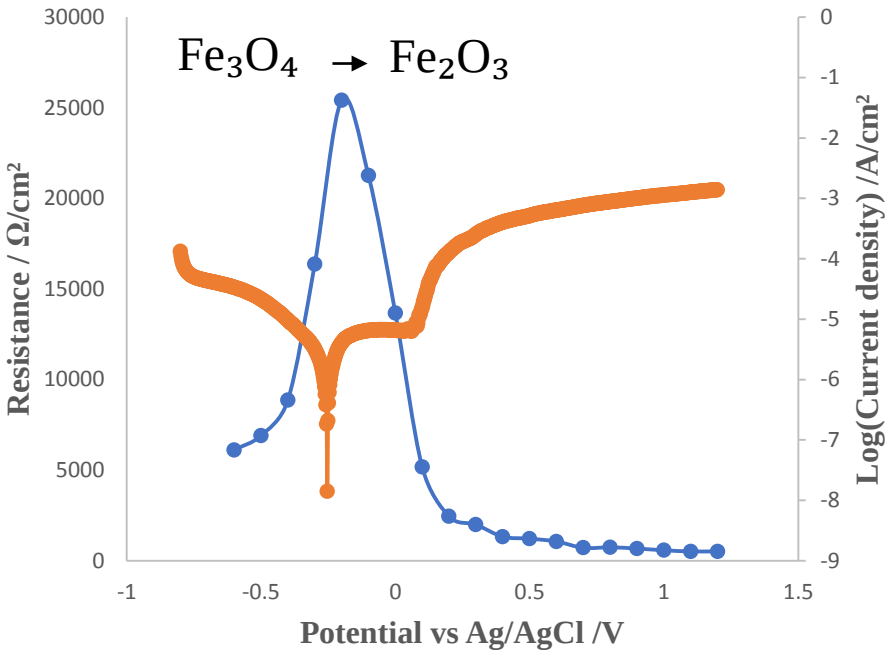

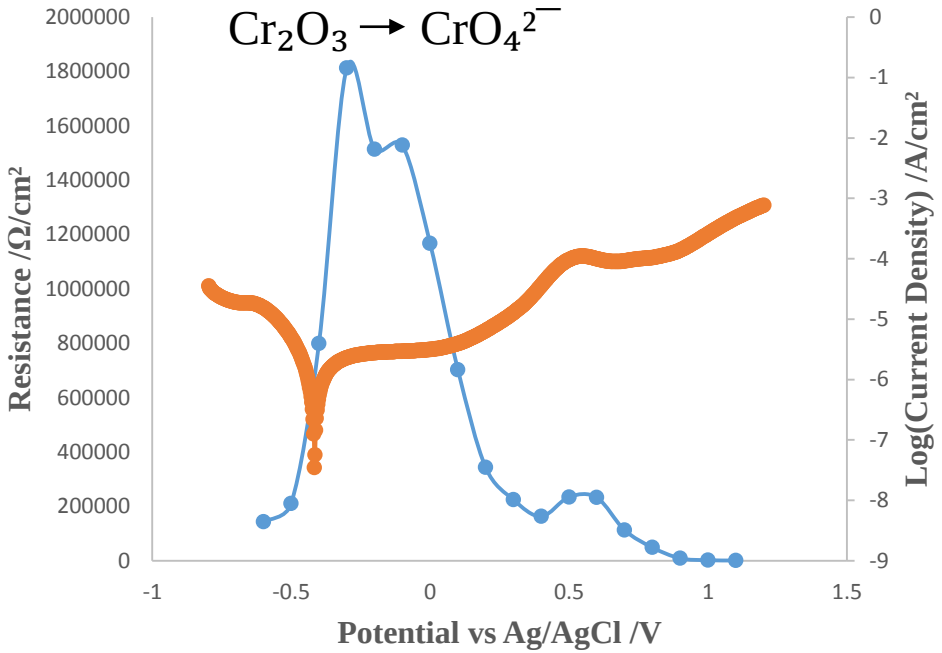

Figure 6: Resistance obtained from electrochemical impedance spectroscopy experiments for pure iron (left) and pure chromium (right)

Electrochemical impedance Spectroscopy of nickel, pH≈11.4

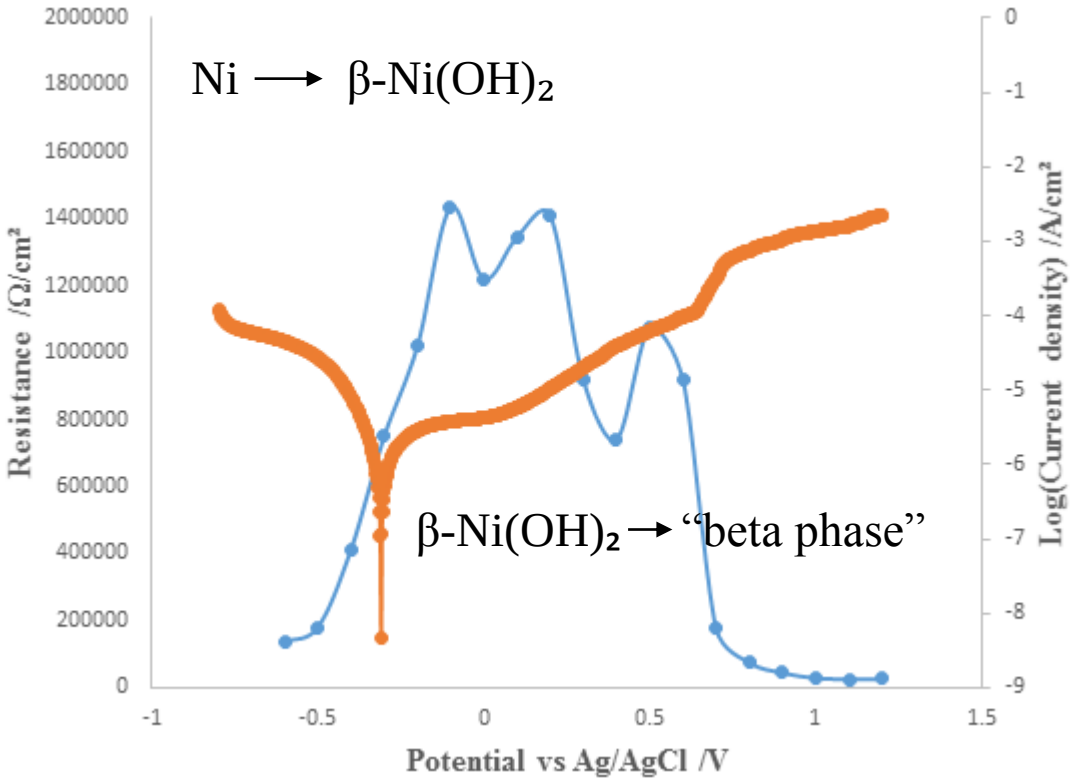

Figure 7: Resistance obtained from electrochemical impedance spectroscopy experiments for pure nickel

Electrochemical impedance Spectroscopy of unsensitised and heat treated 20/25/Nb, pH≈11.4

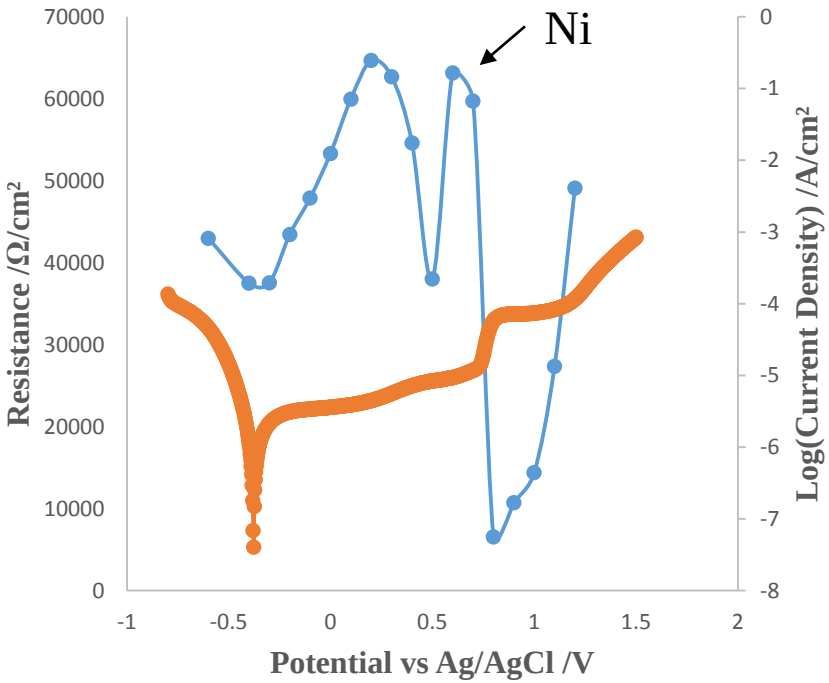

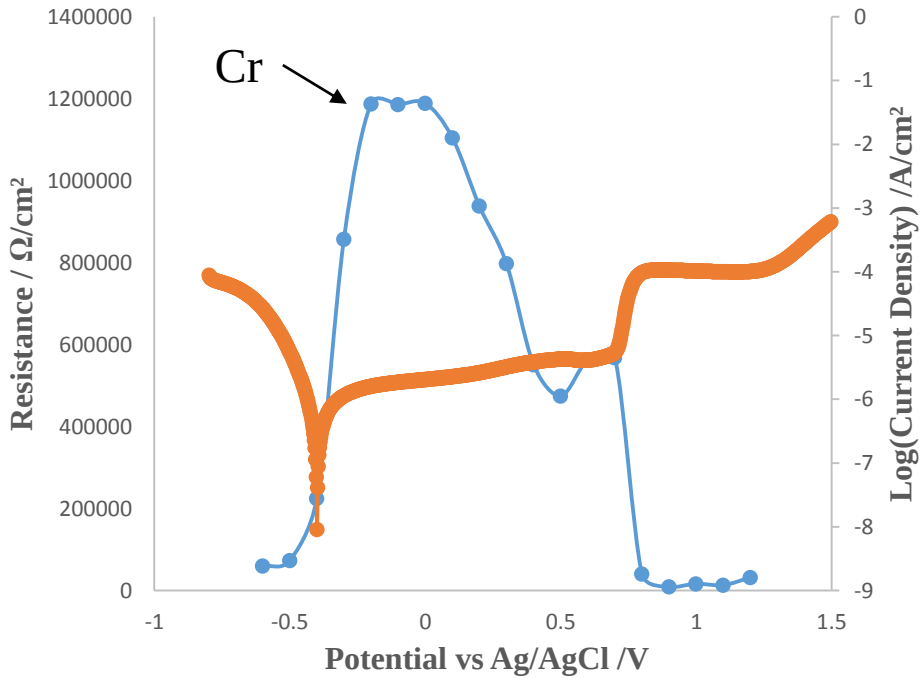

Figure 8: Resistance obtained from electrochemical impedance spectroscopy experiments for unsensitised (left) and heat treated (right) 20/25/Nb SS

Surface XPS of 20/25/Nb SS

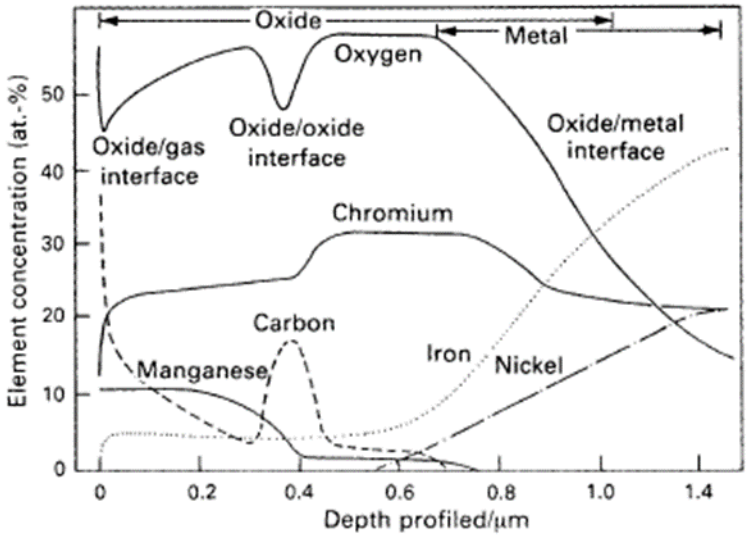

Figure 9: XPS depth profile through oxide formed on 20/25/Nb SS in CO_2 environment. Ref. ***Anal. Proc.***, 1993,**30**, 19-27

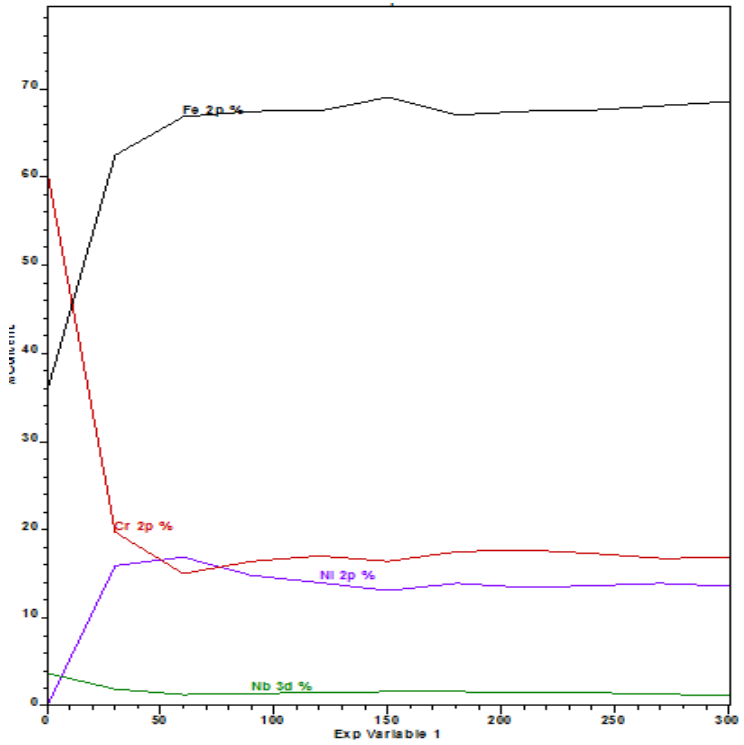

Figure10: XPS of unsensitised 20/25/Nb exposed to air

Effect of temperature on the corrosion behaviour of 20/25/Nb, pH≈11.4

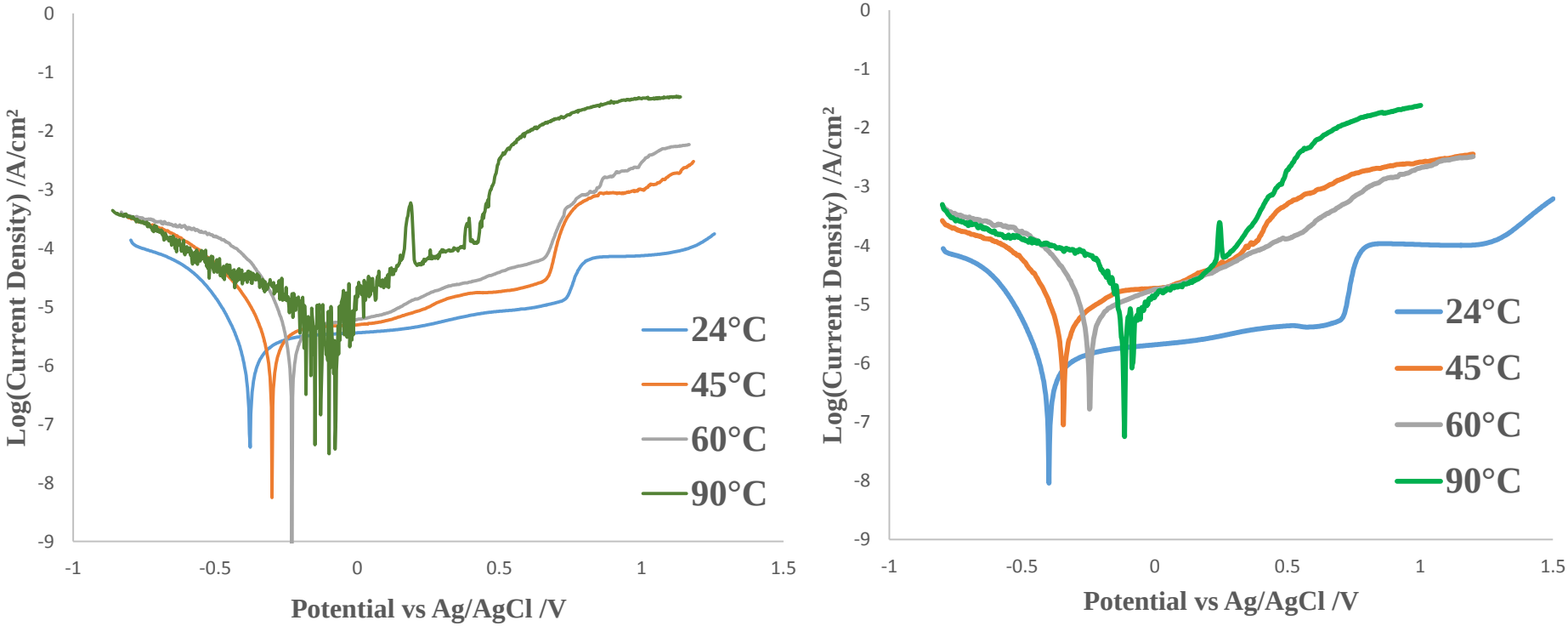

Figure 11: Effect of increasing the pond water (pH≈11.4 at 24°C) temperature, unsensitised (left) and heat treated (right) 20/25/Nb SS

Effect of [H2O2] on OCP of unsensitised 20/25/Nb SS, pH≈11.4

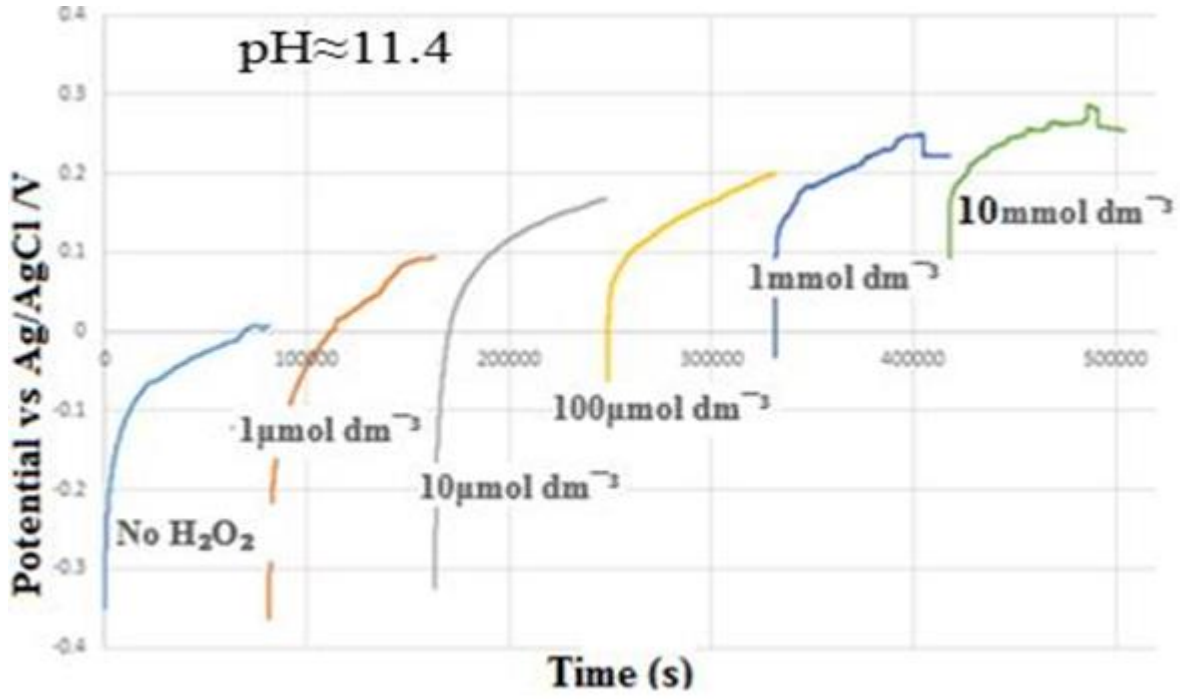

Figure 12: Open circuit potential of unsensitised 20/25/Nb with varying concentration of hydrogen peroxide at pH ≈11.4

Degree of sensitisation: Etching 304H SS with 10wt% oxalic acid

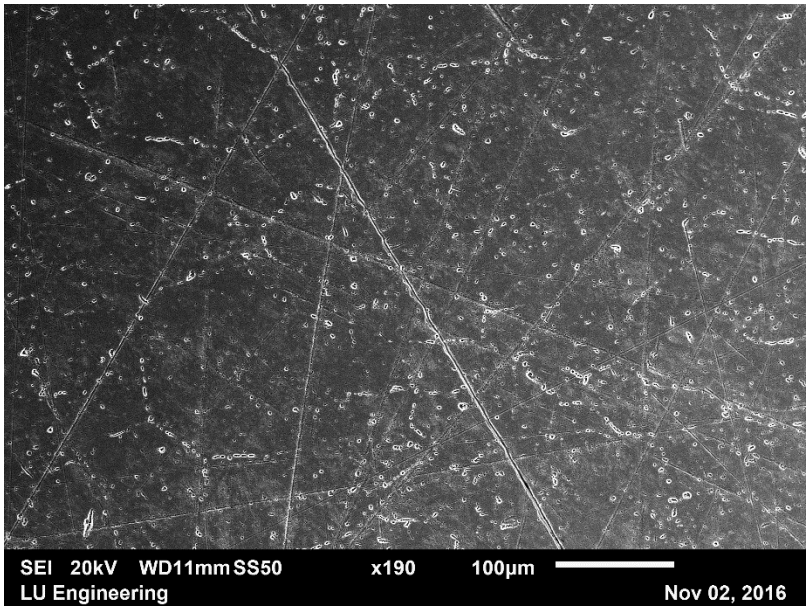

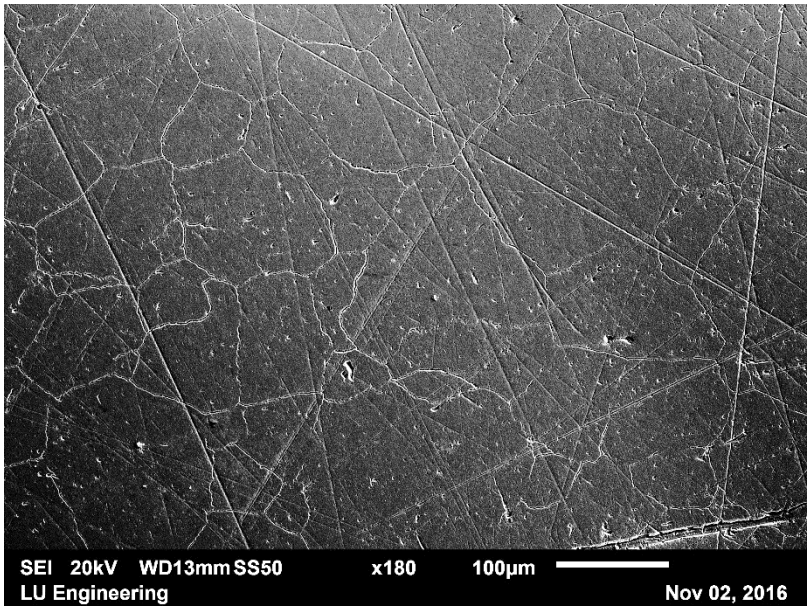

Figure 13: Etched surfaces of 304H SS, unsensitised (left) and heat treated (right)

Effect of dosing pond water with NaOH to a pH≈11.4 on the corrosion behaviour of 304H

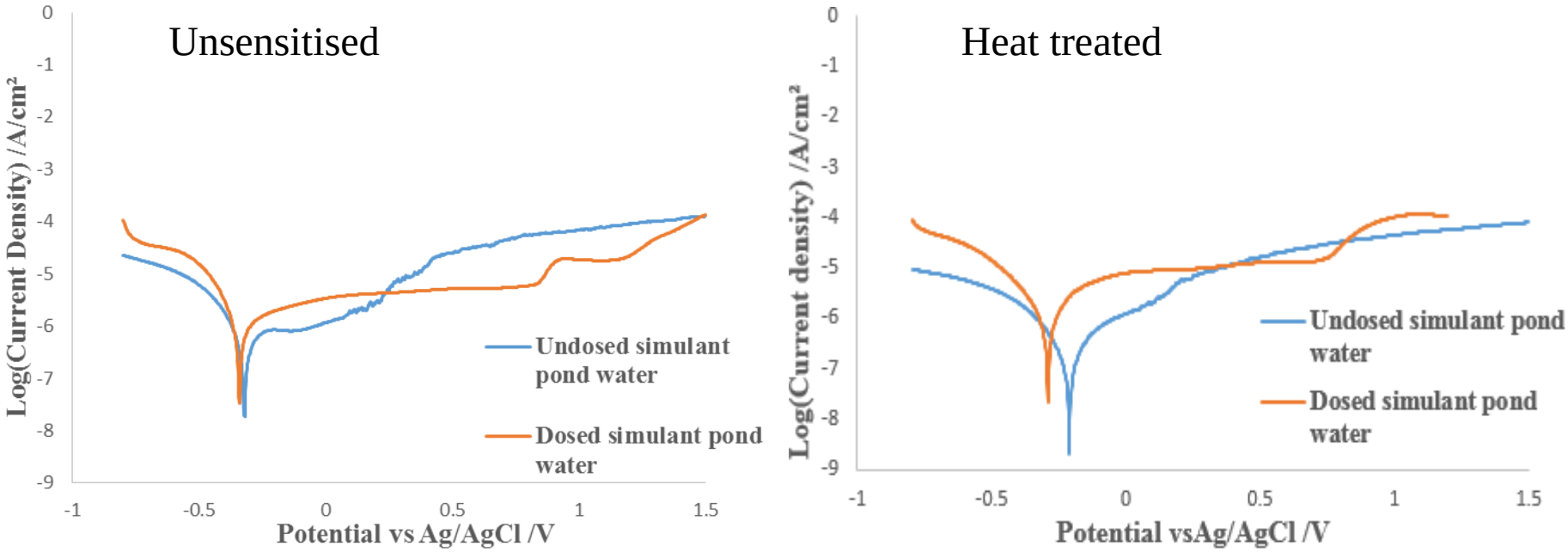

Figure 14: Effect of dosing pond water to a pH≈11.4, unsensitised (left) and heat treated (right) 304H SS

Electrochemical impedance Spectroscopy of unsensitised and heat treated 304H, pH≈11.4

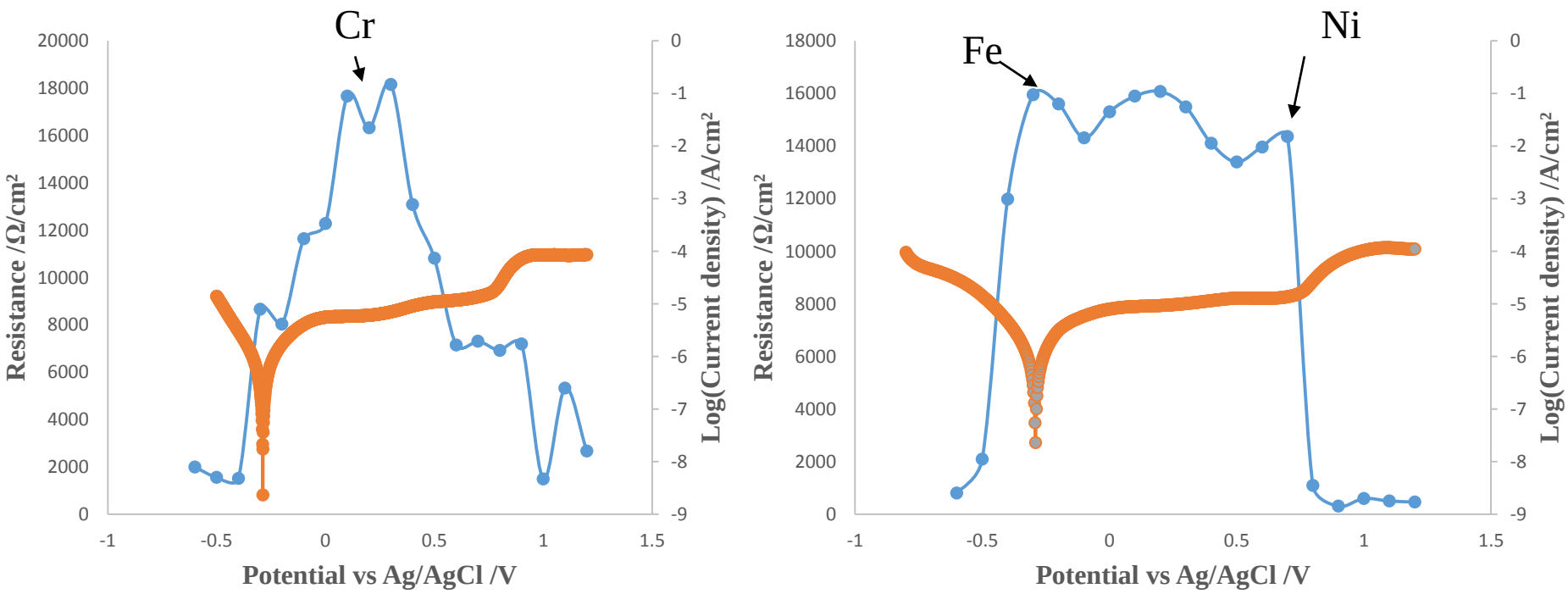

Figure 15: Resistance obtained from electrochemical impedance spectroscopy experiments for unsensitised (left) and heat treated (right) 304H SS

Effect of temperature on the corrosion behaviour of 304H, pH≈11.4

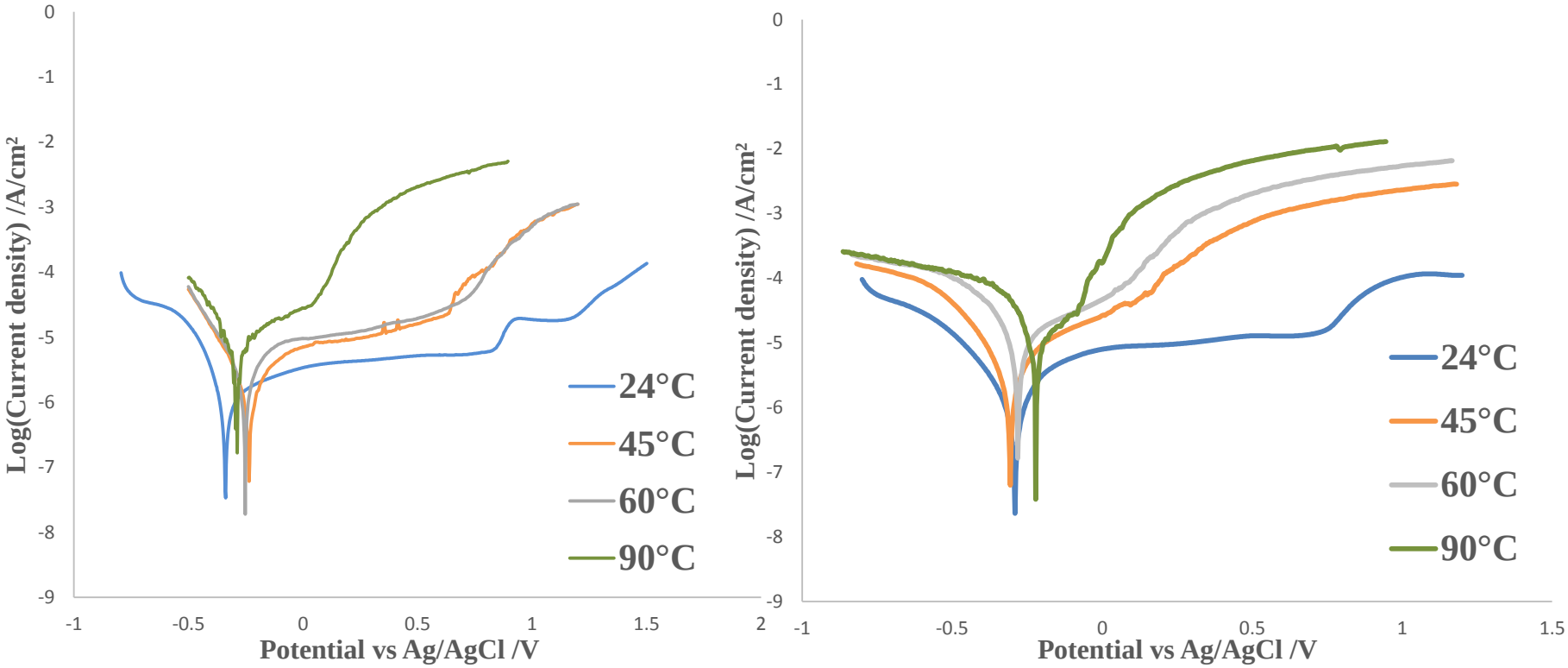

Figure 16: Effect of increasing the pond water (pH≈11.4 at 24°C) temperature, unsensitised (left) and heat treated (right) 304H SS

Conclusions

- It is advantageous in terms of minimising corrosion to dose the ponds to pH≈11.4. In most cases, at pH ≈ 7 the initiation of pitting is observed ~0.4V vs Ag/AgCl, pits are considered to be initiators of stress corrosion cracking (SCC).

- Heat treatment of 20/25/Nb causes an increase in passivation attributed to Cr, sample has most likely been effectively sensitised

- Opposite effect is seen for 304H stainless steels – Cr doesn't offer the same protection for the heat treated sample

- There generally appears to be no localised corrosion threat to unsensitised fuel cladding as the electrolyte temperature is increased in the range 24°C-60°C, in the absence of peroxide, assuming that the fuel has not undergone SSC or intergranular attack before submersion in the ponds.

Future Work

- Surface analysis of passive layers
- Analogous experiments on real irradiated cladding
- OCPs of 304H samples at higher temperatures
- Continuation of uranium work including electrochemical studies and raman spectroscopy

- The NNL have been developing a non-active analogue of AGR cladding to use in testing corrosion inhibitor experiments at the higher temperatures predicted for the new storage regime. In an attempt to create such an analogue 20/25/Nb and 304H stainless steels (SS) have been heat treated. 20/25/Nb SS is the AGR cladding material. 304H has been selected as an analogue as it has similar carbon and chromium concentrations to 20/25/Nb but much lower Ni and zero Nb content. It is being used because it is easier to sensitise (i.e. become chromium depleted at the grain boundaries owing to the precipitation of chromium carbides) because there is no Nb to lock-up the C that would otherwise be available to precipitate as chromium carbides when heat treated. It is, however, recognised that the process by which sensitisation is created is different from RIS and the resulting Cr profiles in thermal and irradiation sensitised material are different.